Aus der Abteilung für Strahlenzytogenetik

Leiter Prof. Dr. rer. nat. Horst Zitzelsberger

Helmholtz Zentrum München

Validation and functional characterization of a prognostic 4-miRNA signature in Glioblastoma

Dissertation

zum Erwerb des Doktorgrades der Naturwissenschaften

an der Medizinischen Fakultät der

Ludwig-Maximilians-Universität zu München

vorgelegt von

Daniel Piehlmaier

aus München

2020

Mit Genehmigung der Medizinischen Fakultät
der Universität München

Betreuer:	Prof. Dr. rer. nat. Horst Zitzelsberger
Zweitgutachter:	Prof. Dr. Peter Jon Nelson, Ph.D.
Dekan:	Prof. Dr. med. dent. Reinhard Hickel
Tag der mündlichen Prüfung:	25.09.2020

Eidesstattliche Versicherung

Ich erkläre hiermit an Eides statt, dass ich die vorliegende Dissertation mit dem Thema

Validation and functional characterization of a prognostic 4-miRNA signature in Glioblastoma

selbstständig verfasst, mich außer der angegebenen keiner weiteren Hilfsmittel bedient und alle Erkenntnisse, die aus dem Schrifttum ganz oder annähernd übernommen sind, als solche kenntlich gemacht und nach ihrer Herkunft unter Bezeichnung der Fundstelle einzeln nachgewiesen habe.

Ich erkläre des Weiteren, dass die hier vorgelegte Dissertation nicht in gleicher oder in ähnlicher Form bei einer anderen Stelle zur Erlangung eines akademischen Grades eingereicht wurde.

München, 12.10.2020

_____	_____
Ort, Datum	**Daniel Piehlmaier**

Table of Contents

List of figures

List of tables

A Introduction

A.1 Background

Glioblastoma multiforme (GBM) is the most common type of primary brain tumors in adults (Wen and Kesari, 2008). Tumors classified into GBM make up the majority of malignant gliomas (60-70%), other high-grade gliomas consist of anaplastic astrocytomas (10-15%), anaplastic oligodendrogliomas (10%) and less frequent subtypes (Ostrom et al., 2014). GBM is more common in males compared to females with an overall incident rate of 3-5/100,000 people per year. The overall median age at time of diagnosis is 64 years (Wen and Kesari, 2008).

The survival of the patients is poor and inversely correlated with age, ranging from a median survival of 8.8 months in the group of patients younger than 50 to a survival of only 1.6 months in the group of patients older than 80 (Ohgaki and Kleihues, 2007). In the early 2000s, a phase II study showed that a combination of radiotherapy and concomitant chemotherapy using temozolomide (TMZ) followed by adjuvant TMZ therapy could increase the median survival to 16 months, whereby patients under 50 years old and those who underwent surgery had the best survival outcome (Stupp et al., 2002). The subsequent study by Stupp et al. (2005) led to the current standard protocol of GBM treatment that consists of radiotherapy (60 Gray (Gy) in 30x 2 Gy fractions) concomitantly with daily TMZ chemotherapy (75 mg/m^2 per m^2) for 42 days, followed by a maintenance TMZ treatment. Five years later, the authors reported an overall survival of 27.2% at 2 years, 16% at 3 years versus a respective survival of 10.9% and 4.4% with radiotherapy alone (Stupp et al., 2005, 2009).

Surgical resection is generally performed prior radiochemotherapy except for the very elderly or with poor performance status (Wen and Kesari, 2008). It provides an immediate mass effect relief for the patients and is used for pathological analysis of

the tumor. Usually, gross total resection of the contrast-enhancing mass, without provoking neurological deterioration, should be attained (Delgado-López and Corrales-García, 2016). Aggressive extent of resection improves overall survival of the patients even at the highest levels of resection (Sanai et al., 2011). Although, if gross total resection is not possible, even partial resection with thresholds of >70% resection and residual tumor volume of <5 cm^3 could be associated with higher survival of GBM patients (Chaichana et al., 2014). Despite this treatment, even complete resection is associated with recurrence of the tumor within 2 cm of the resection margins (Wallner et al., 1989). Even today, only complete removal of the complete tumor was related with survival bonus (Quick et al., 2014). The prognosis for patients who develop recurrent GBM is poor with a median survival of 12-15 months (Stupp et al., 2009). Treatment options for recurrent GBM are limited and no universally standard of care protocol is available so far (van Linde et al., 2017), thus, representing a need for alternative treatment options.

A study conducted in the frame of The Cancer Genome Atlas (TCGA) classified four molecular subtypes in GBM: classical, mesenchymal, proneural and neural subtypes (Verhaak et al., 2010). Recently, the authors retracted the neural subtype due to possible contamination with non-tumor tissue (Wang et al., 2017). The three remaining subtypes differ in clinical prognosis while patients with tumors of the classical and mesenchymal subtype have a significantly reduced overall survival, which was not observed for the proneural subtype (Verhaak et al., 2010). The characteristic alterations in the subgroups were mainly based on the expression of EGFR (classical), NF1 (mesenchymal) and PDGFRA/IDH1 (proneural).

A.1.1 Biomarkers in GBM

Generally, biomarkers are defined as biological molecules detected in body fluids or tissue that are a sign for a normal or abnormal process, of a condition or disease (NCI Dictionary of Cancer Terms). Biomarkers can be diagnostic, prognostic or predictive, while prognostic biomarkers predict the outcome of a disease regardless of a

treatment and predictive biomarkers are associated with the outcome of a specific therapy. Biomarkers may also fit into more than one category, so that a biomarker can be prognostic and predictive at the same time (Kang et al., 2015). Biomarkers require robust clinical performance in terms of high specificity and sensitivity and prognostic value (Kang et al., 2015).

Currently, the strongest biomarker for outcome and benefit of TMZ chemotherapy in GBM is methylation of the O^6-methylguanine-DNA methyltransferase (MGMT) promoter (Stupp et al., 2009). TMZ is a DNA methylating agent most commonly modifying N^7-methylguanine and N^3-methyladenine (Trivedi et al., 2005). Methylation events which yield O^6-methylguanine are highly cytotoxic if the methyl group is not removed before cell division (Liu et al., 2002). MGMT is a cellular DNA repair protein that reverses methylation at the O^6 position of guanine, thereby neutralizing the effects of TMZ (Hegi et al., 2008). Thus, clinical outcome of patients treated with alkylating agents such as TMZ in combination with radiotherapy is significantly improved in the presence of a MGMT promoter methylation. The 18-month survival rate of patients with MGMT promoter methylation was 62% compared to a survival of 8% in the absence of the promoter methylation (Hegi et al., 2004).

Additionally several prognostic biomarkers have been identified with regard to overall survival of GBM patients: these include age at diagnosis, the Karnofsky performance score, resection status and presence of particular molecular aberrations (Laws et al., 2003; Delgado-López and Corrales-García, 2016). Important molecular genetic alterations are MGMT promoter methylation, 1p/19q co-deletion and mutations in *IDH1*/*IDH2* (isocitrate dehydrogenase) gene. The *IDH1* enzyme is part of the citric acid cycle and catalyzes the reaction of isocitrate to α-ketoglutarate yielding nicotinamide adenine dinucleotide phosphate (NADPH). *IDH1* serves as a major source for NADPH production in the cytoplasm. *IDH1* mutation is commonly found in secondary GBM but rarely present in primary GBM (Sanson et al., 2009). 1p/19q co-deletions are common in oligodendrogliomas and are correlating with a significantly higher overall survival (median survival 14.9 years versus 4.7 years)

(Fallon et al., 2004). 1p/19q co-deletions are rare in GBM (von Deimling et al., 2000) but it could be shown that GBM patients with oligodentric tumor areas exhibit a beneficial prognosis (He et al., 2001).

A.1.2 MicroRNA (miRNA) biogenesis and function

As described above, the outcome of GBM patients strongly differs based on the individual biologic background and prognosis. Therefore, for individualized treatment of the patients the definition of subgroups is a prerequisite. For this purpose, miRNAs can be utilized for stratification of patient groups. MiRNAs are a large family of small non-coding RNA that regulate mRNA expression on a post-transcriptional level. During the last decade, there was a significant gain of knowledge on the function and role of miRNAs. In mammals, miRNA are thought to control the majority of all protein-coding genes (Friedman et al., 2009) and miRNAs play a role in every cellular process investigated so far (Bartel, 2009; Carthew and Sontheimer, 2009; Krol et al., 2010). The history of miRNAs started early 2000s with only a handful miRNAs known (Bartel, 2004) and developed to currently 38589 entries listed in www.mirbase.org (Griffiths-Jones, 2004).

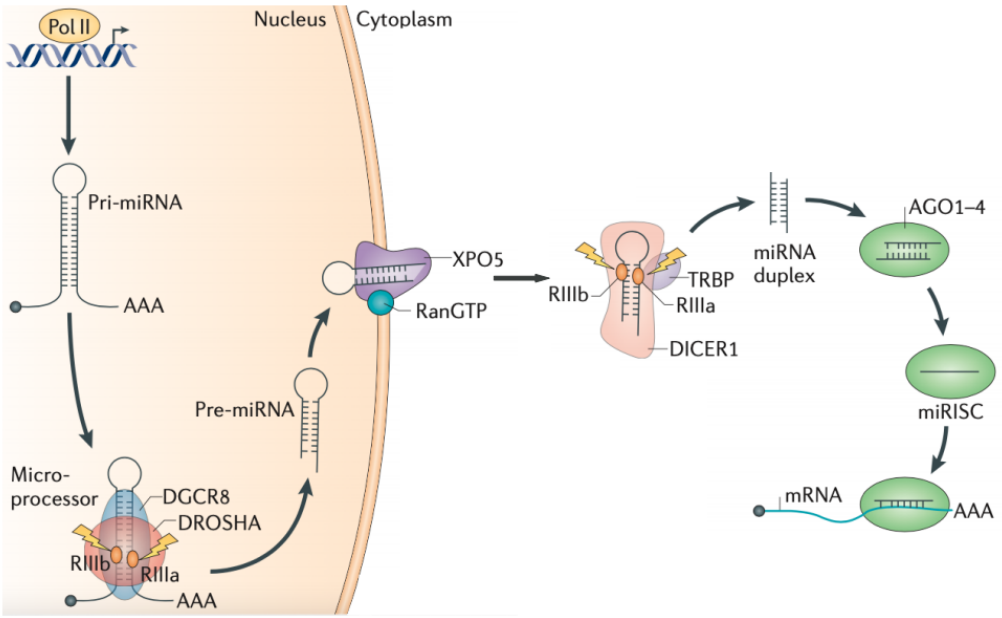

Figure 1: Overview of miRNA biogenesis pathway

MicroRNA genes are transcribed by RNA polymerase II as primary miRNAs (pri-miRNAs). The long pri-miRNAs are processed by DROSHA to generate precursor miRNAs (pre-miRNAs). The pre-miRNAs are transported into the cytoplasm by exportin 5 (XPO5). Afterwards, the pre-miRNAs are loaded into the DICER complex to form miRNA duplexes that are processed by Argonaute (AGO) proteins to create mature miRNAs. The mature miRNAs are incorporated into a miRISC complex for silencing of mRNA. (adapted from Lin and Gregory, 2015)

MiRNAs are transcribed by RNA polymerase II (Figure 1) as primary miRNAs (pri-miRNAs). Those long transcripts may inherit multiple miRNA loci and are further processed in the nucleus by the DROSHA protein complex. The regulation of miRNA expression is complex and the presence and the locations of most miRNA promoters are still under investigation. Localization of the promoters was performed by analyzing CpG Islands, RNA sequencing and Chromatin Immuno-precipitation DNA-Sequencing (ChIP-seq) data (Ozsolak et al., 2008). Additionally, some miRNAs are encoded on introns of protein-coding genes and share the promoter of the host gene (Ha and Kim, 2014). Furthermore, it has been speculated that intronic miRNAs may also have promoters distinct from their host genes (Monteys et al., 2010). After

transcription, the pri-miRNAs undergo several steps of maturation. Generally, pri-miRNAs consist of multiple stem-loop structures in which the mature miRNAs are located (Lee et al., 2002). The pri-miRNAs are processed by DROSHA that crops the stem-loops and hairpin-like precursor miRNAs (pre-miRNAs) are formed (Ha and Kim, 2014). Intronic miRNAs form precursor structures independent from DROSHA. Thereby, hairpin structures are created directly after splicing from host mRNA (Ruby et al., 2007).

Further processing of the miRNAs is completed in the cytoplasm. Therefore, the pre-miRNAs are transported into the cytoplasm by a transport protein complex XPO5 (Exportin 5) (Bohnsack et al., 2004). Afterwards, DICER cleaves the pre-miRNAs and small RNA duplexes are formed (Ketting et al., 2001). For creation of the mature miRNAs, the RNA duplexes are loaded into Argonaute (AGO) proteins. In humans, multiple AGO proteins exist (Dueck et al., 2012) which unwind the double stranded RNA and create mature single stranded miRNA. In combination with the AGO proteins, miRNAs form RNA-induced silencing complexes (RISC) that bind to mRNA and induce silencing of the targets (Kawamata and Tomari, 2010). Generally, miRNA target inhibition is either achieved by repression of translation or by target degradation (Huntzinger and Izaurralde, 2011).

In this study, the function of the human miRNAs, let-7a-5p, let-7b-5p, miR-125a-5p and miR-615-5p was analyzed. The miRNAs let-7a and let-7b belong to the same miRNA family (called lethal-7) that was one of the first discovered miRNAs. The let-7 miRNA plays an important role in the developmental timing in *Caenorhabditis elegans* since mutants carrying an altered let-7 miRNA die during development (Reinhart et al., 2000). The let-7 family consists of multiple miRNAs (distinguished by letters) that all carry the same seed sequence. This highly preserved sequence spans from nucleotide 2 through 8 and is an essential part for target recognition of the RISC complex (Brennecke et al., 2005). Lower developed organisms like *Caenorhabditis elegans* or *Drosophila melanogaster* only have one let-7 miRNA while higher developed animals have multiple let-7 family members. Usually, each let-7 family member is present in multiple copies across the genome. Let-7a has three

different precursor sequences let-7a-1 (human chromosome 9), let-7a-2 (human chromosome 11) and let-7a-3 (human chromosome 22). All of these precursors encode the same mature miRNA let-7a-5p (Lee et al., 2016). Additionally, all of the let-7a precursors are encoded on polycistronic miRNA clusters. Notably, let-7a-3 is on a miRNA cluster on chromosome 22 that also contains the only copy of let-7b, suggesting that the regulation of these miRNAs is linked. The let-7 miRNA family is well-investigated and is believed to promote differentiation during development and let-7 is supposed to be a tumor suppressor in various cancers (Lee et al., 2016).

The human miRNA family miR-125 consists of only three family members, miR-125a (human chromosome 19), miR-125b-1 (human chromosome 11) and miR-125b-2 (human chromosome 21). It has been reported, that the miR-125 family members play an important role in differentiation of cells, proliferation and apoptosis (Bousquet et al., 2012). Furthermore, miR-125 acts as tumor suppressor in various cancers. In lung cancers, miR-125a suppresses cell migration and invasion. It could be shown that the expression of miR-125a in lung tumor and lymph node metastasis was much lower than in adjacent normal lung tissues (Jiang et al., 2010). Similar observations were made in ovarian cancer cells (Cowden Dahl et al., 2009). It could be shown, that the oncogene epidermal growth factor receptor (EGFR) signaling leads to translational repression of miR-125a.

In contrary to the other miRNAs of the signature, much less is known about the human miR-615. Unlike the other miRNAs, miR-615 is an intronic miRNA, located in a homeobox gene *Hoxc5* (Quah and Holland, 2015). Thus, transcription of the host gene also generates miR-615. Notably, it could be shown that miR-615 may also be generated independently, suggesting that the miRNA possesses its own promoter (Quah and Holland, 2015). The role of intronic miRNAs is sparsely investigated, yet it could be shown that intronic miRNAs perform complementary functions with its host gene (Quah et al., 2015).

A.1.3 A 4-miRNA signature predicts the clinical outcome in GBM

Only few prognostic factors have been identified in GBM and novel markers for stratifying patients into specific prognosis and treatment groups are needed. One approach utilizes miRNAs for predicting the clinical survival of GBM patients. In an own study we identified a 4-miRNA signature that predicts overall survival in GBM and allows to the stratification into high- and low-risk GBM patients Niyazi et al., (2016). The risk groups can be considered for the development of alternative therapeutic approaches including radiochemotherapy escalation/de-escalation strategies. We discovered the signature in GBM patients retrospectively collected at the Frankfurt University clinics. Applying machine learning methodology on miRNA microarray profiles of resectates or biopsies from these patients we identified a prognostic model including the four miRNAs hsa-let-7a-5p, hsa-let-7b-5p, hsa-miR-125a-5p and hsa-miR-615-5p. The model significantly predicted overall survival of standard-of-care treated GBM patients and was validated in a carefully matched (therapy, sex and age) matched subset of GBM patients of the TCGA GBM cohort. The signature is independent of sex, age and MGMT promoter methylation status and we recently were able to validate it in a pooled multicenter cohort of 106 patients (data unpublished). Furthermore, the median risk score of the patients was calculated from the cumulative expression levels of the four miRNAs that assigns individual patients to either high- or low-risk groups. The median survival of the patients of the high-risk group was 13.5 months and the survival of the low-risk group was 18.4 months. The signature was discovered using global miRNA expression from 36 GBM patients. A forward selection approach was utilized to unveil differentially expressed miRNAs. We discovered that high expression of let-7a-5p, let-7b-5p and miR-125a-5p correlated positively with overall survival while the expression of miR-615-5p correlated negatively with outcome. In combination with the MGMT promoter methylation status, the subgroups could further be split into four risk strata that further increased the prognostic accuracy in comparison to the strata defined by MGMT promoter methylation or by the miRNA signature alone. These findings proposed further investigation of the biologic function of the

signature miRNAs. Little is known about the functional role of the four miRNAs in GBM. This demands for further investigation of the biologic role of the miRNAs and the potential mRNA targets. In this thesis, the 4-miRNA signature was validated and a translational approach was followed to characterize the 4-miRNA signature as described below.

A.1.4 Genome editing using site specific nucleases

For the analysis of the functional impact of miRNAs in model systems, one approach is to modulate the expression of the miRNAs by stable knockouts or transient transfections. Transient modulation of miRNA expression is usually performed by transfection of small RNA molecules that either mimic the miRNA function or reduce the amount of available miRNAs in the cell. Like natural miRNAs, mimics are double stranded RNAs that inherit an active forward strand, which can be incorporated in the AGO complex. The reverse strand is non-functional and gets degraded in this process. Anti-miRNA oligonucleotides are reverse-complementary to the target miRNAs which bind to the miRNA and thereby block their function (Lennox and Behlke, 2011). In this study, we investigated the use of CRISPR (clustered regularly interspaced short palindromic repeats)/Cas9 (CRISPR-associated protein) system for stable knockout of the miRNAs.

CRISPR is originating from bacteria (Jansen et al., 2002) and represent an important tool for simple and efficient genome editing (Wang et al., 2016). Unlike other sequence specific genome editing tools like zinc finger nucleases (ZNFs) or transcriptor activator-like nucleases (TALENs) (Figure 2), CRISPR mediated genome editing does not need specifically engineered proteins for target recognition. Generation of genetic mutations by CRISPR requires a 20-nuclease long guide RNA that utilizes base pairing to recognize and bind to the target site. The Cas9 nuclease interacts with a short protospacer-adjacent motif (PAM) directly next to the guide sequence (Jinek et al., 2012; Gasiunas et al., 2012; Garneau et al., 2010; Marraffini and Sontheimer, 2008; Bolotin et al., 2005). Cas9 can be used to target any DNA sequence by simply changing the guide RNA sequence, making it a versatile tool for genome editing. The mechanism of genome editing occurs in a multiple-step

process: Cas9 introduces double strand breaks (Jinek et al., 2012) that are repaired by the cell afterwards. Two different repair pathways exist, nonhomologous end joining (NHEJ) and homology-directed repair (HDR).

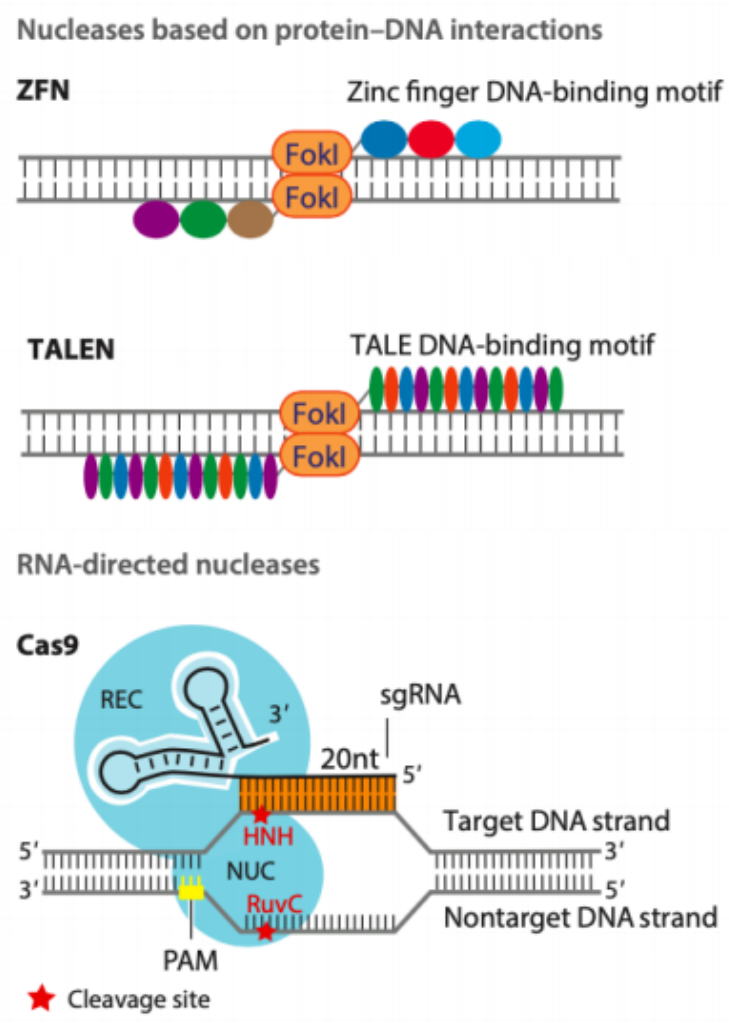

Figure 2: Overview of sequence-specific tools for genome editing

Comparison of programmable sequence-specific genome editing nucleases. Zinc-finger nucleases (ZFNs) and transcriptional activator-like effector nucleases (TALENs) utilize DNA-binding domains fused to FokI nucleases to recognize and cut DNA. Cas9 is a RNA-guided nuclease that recognizes its target DNA using 20 nucleotide guide RNAs that interact with the DNA. (adapted from Wang et al., 2016)

NHEJ introduces random deletions and insertions at the DNA double-strand break that may cause frame-shifts in protein coding sequences or alter critical regions in regulatory elements (Lieber, 2010). Double-strand breaks can also be utilized by HDR to introduce donor DNA at the CRISPR target site. Therefore, constructs harboring homologous regions flanking the upstream and downstream regions, are designed to insert novel DNA sequences at the break (Choulika et al., 1995). Various gene modifications can be introduced by HDR: targeted gene deletion, mutation or insertion (Wang et al., 2016).

Mutations caused by the CRISPR/Cas9 technology generally require transfection of multiple plasmids followed by screening and selection of mutants and are quite time intensive. Less time consuming knockdown (and overexpression) of miRNAs can also be achieved by transfection of small interfering RNA (siRNA) that either inhibit (or mimic) miRNA function (Lam et al., 2015). A major disadvantage of this method is the short-term effect by the transfected siRNAs that usually lasts 5-7 days. These synthetic miRNAs (also known as miRNA mimics) are short RNA duplexes that can be used to target and silence mRNA. Similar to miRNAs, synthetic mimics are processed in the DICER complex that trims the double stranded RNA. Afterwards, the mimics are incorporated in the RISC/AGO protein complex that allows inhibition of the target mRNA (Agrawal et al., 2003, Lam et al., 2015). Furthermore, miRNA function can be suppressed by transfection of synthetic miRNA inhibitors. These molecules consist of single-stranded RNA that resemble the reverse complement of the mature miRNA (Robertson et al., 2010). Additionally, miRNA inhibitors are chemically modified in order to prevent RISC-induced cleavage of the inhibitor/miRNA duplex. The modifications also grant enhanced binding affinity and make the inhibitors resistant to nucleolytic degradation (Esau, 2008).

A.2 Aims

The overall aims of my study were the validation of the four signature miRNAs and the elucidation of the molecular impact of these miRNAs in GBM *in vitro* models. As for this purpose, the secondary aim was the identification of suitable *in vitro* tumor

model systems. Thus, a panel of seven established GBM cell lines was characterized with respect to cytogenetic, transcriptomic and DNA methylation properties.
The first step was to authenticate the cell lines using STR-typing in combination with cytogenetic analysis by spectral karyotyping in order to characterize chromosomal aberrations, ploidy and clonality of cell lines. A further aim was to validate the signature in the analyzed cell line panel and in GBM patient samples using qRT-PCR. Moreover, the cell lines were analyzed for resistance towards ionizing radiation and TMZ. Additionally, I analyzed the expression of the GBM risk signature miRNAs and associations between phenotypic properties and miRNA expression. Moreover, the global gene expression profiles of the cell lines were generated and analyzed including molecular subtyping. These data were supposed the basis for the selection of cell lines to be used in miRNA modulation experiments.

In the selected cell culture models the expression of the 4-miRNAs was modified by CRISPR knockout and transient transfection of miRNA mimics and inhibitors. A specific aim was to introduce a CRISPR/Cas9 knockout system in specific cell lines in order to modify the miRNA expression in selected cell lines. Another aim was to observe changes in the transcriptome prior and post transfection with miRNA mimics and inhibitors. Changes in the expression profiles between treated and untreated cell lines should be characterized by RNA sequencing. Differences in gene expression profiles were thought to provide insights into the molecular networks of the risk signature miRNAs and to unveil their functional role in the context of glioblastoma.

B Material and methods

B.1 Materials

B.1.1 Cell lines

Table 1 Cell lines used in this study

Cell line	Origin	Supplier
A172	Male, grade IV glioblastoma	American type culture collection (ATCC, Manassas, VA, USA)
LN18	Male, grade IV glioblastoma	ATCC
LN229	Female, grade IV glioblastoma	ATCC
T98G	Male, grade IV glioblastoma	ATCC
U87-MG	Male, origin unknown, possibly glioblastoma	ATCC
U138-MG	Male, grade IV glioblastoma	Cell line service (CLS GmbH, Eppelheim, Germany)
U251-MG	Male, grade IV glioblastoma	CLS

B.1.2 Solutions

Table 2 Buffers and solutions

Solution	Reagent	Concentration
20x SSC buffer	NaCl2 (Sigma-Aldrich) Trisodium citrate (Sigma-Aldrich) HCl (Merck)	3 M 300 mM ad 1 M ad to pH 7.0
5x ISO buffer	Tris-HCl pH 7.5 (Sigma-Aldrich) $MgCl_2$ (Sigma-Aldrich) dGTP (New England Biolabs) dCTP (New England Biolabs) dATP (New England Biolabs) dTTP (New England Biolabs) DTT (Sigmal-Aldrich) PEG-8000 (Sigmal-Aldrich) NAD (New England Biolabs) dH_2O	1 M 2 M 100 mM 100 mM 100 mM 100 mM 1 M 1.5 µg 100 mM ad to 6 ml
Agarose gel	Agose (Serva) TE buffer	0.5 to 1 g (1 or 2%) ad to 500 ml
Cresol red	Ficoll 400 (Fluka) dH_2O	10 g ad 100 ml
DAPI / Vectashield solution	4',6-diamidino-2-phenylindole (DAPI) (Sigma-Aldrich) Vectashield (Vector)	0.1% ad to 1000 µl
Denaturation solution	Formamide deionized (Applichem) SSC (Sigma-Aldrich) dH_2O HCl (Merck)	70% 2x ad to 100 ml ad 1 M to pH 7.0
Fixation solution for cell staining	Ethanol (Merck) Methylene blue (Sigma-Aldrich)	80% 0.3%
Fixation solution for metaphase prep.	Glacial acetic acid (Merck) Methanol (Merck)	25% 75%

Solution	Reagent	Concentration
Gibson assembly master mix	ISO Buffer	5x
	T5 exonuclease (New England Biolabs)	6.4 U
	Phusion polymerase (New England Biolabs)	40 U
	Taq polymerase (New England Biolabs)	6400 U
	dH_2O	ad to 1.2 ml
$MgCl_2$ / PBS	PBS	1x
	$MgCl_2$ (Sigma-Aldrich)	50 mM
	dH_2O	ad to 200 ml
Pepsin solution	Pepsin (Sigma-Aldrich)	0.001%
	HCl (Merck)	10 mM
	dH_2O	ad to 100 ml
Phosphate buffered saline (PBS)	PBS Dulbecco without Ca^{2+} and Mg^{2+} (Biochrom)	9.55 g / l
	dH_2O	ad to 10 l
Post fixation solution	Formaldehyde (Honeywell)	1%
	$MgCl_2$ / PBS	ad to 74 ml
SSC / Tween wash solution	SSC (Sigma-Aldrich)	4x
	Tween 20 (Sigma-Aldrich)	0.1%
STE buffer	NaCl (Sigma-Aldrich)	100 mM
	Tris-Cl pH 8.0 (Sigma-Aldrich)	10 mM
	EDTA (Sigma-Aldrich)	1 mM
Temozolomide (TMZ)	Temozolomide (Tocris)	10 mg
	Dimethlysulfoxide (Sigma-Aldrich)	ad 1.03 ml
Tris-EDTA (TE) buffer	Tris (Merck)	10 mM
	EDTA (Merck)	1 mM
	dH_2O	ad 1000 ml
	HCl (Merck)	ad 1 M to pH 7.5

B.1.3 Primers used in this study

Table 3 Sequence information of primers used in this study

Primer name	Sequence	Description
OS280	CAGGGTTATTGTCTCATGAGCGG	sequencing primer for MLM3636 fwd
Fwd let-7a	TTGTGGAAAGGACGAAACACTTTAGGGTCACACCCACCACTTTTAGAGCTAGAAATAGCAAGTT	gibson fwd primer for single guide cloning of let-7a in MLM3636
Rev let-7a	TGCTATTTCTAGCTCTAAAAGTGGTGGGTGTGACCCTAAAGTGTTTCGTCCTTTCCACAAGATA	gibson rev primer for single guide cloning of let-7a in MLM3636
Fwd let-7b	TTGTGGAAAGGACGAAACACGGTTGTATAGTTATCTTCCGTTTTAGAGCTAGAAATAGCAAGTT	gibson fwd primer for single guide cloning of let-7b in MLM3636
Rev let-7b	TGCTATTTCTAGCTCTAAAACGGAAGATAACTATACAACCGTGTTTCGTCCTTTCCACAAGATA	gibson rev primer for single guide cloning of let-7b in MLM3636
Fwd miR-125a	TTGTGGAAAGGACGAAACACTGGATGTCCTCACAGGTTAATTTTAGAGCTAGAAATAGCAAGTT	gibson fwd primer for single guide cloning of miR-125a in MLM3636
Rev miR-125a	TGCTATTTCTAGCTCTAAAATTAACCTGTGAGGACATCCAGTGTTTCGTCCTTTCCACAAGATA	gibson rev primer for single guide cloning of miR-125a in MLM3636
MLM3636-rev-seq	CAAGCTGGGCTGTGTGC	sequencing primer for MLM3636 rev
5’-arm-fwd-let7a	GGTACGGGCCCATCGATAAGCTTGCATGTGGCTATACAGCCGTCAG	gibson fwd primer for amplification of the 5' region of let-7a into pFG4
3’-arm-fwd-let7a	ATGCTATACGAACGGTACATCCGGATCCGTGATAGAAAAGTCTGCATCCAGGCG	gibson fwd primer for amplification of the 3' region of let-7a into pFG4
3’-arm-rev-let-7a	CACCGCGGTGGCGGCCGCTCTAGAGCACTGTGTGAATGAAGGACTACTTCAGG	gibson rev primer for amplification of the 3' region of let-7a into pFG4
5’-arm-fwd-let7b	GGTACGGGCCCATCGATAAGCTTGCAGGAGGTGCCTCTGGAAG	gibson fwd primer for amplification of the 5' region of let-7b into pFG4
3’-arm-fwd-let7b	ATGCTATACGAACGGTACATCCGGATCCTGAGGAGCCCAGTGACAC	gibson fwd primer for amplification of the 3' region of let-7b into pFG4
3’-arm-rev-let-7b	CACCGCGGTGGCGGCCGCTCTAGAGAGGACTGGCACAGATGGGTGTC	gibson rev primer for amplification of the 3' region of let-7b into pFG4
5’-arm-fwd-miR125	GGTACGGGCCCATCGATAAGCTTGCTGAGTCCTTGGATTCCAGG	gibson fwd primer for amplification of the 5' region of miR-125a into pFG4
3’-arm-fwd-miR125	ATGCTATACGAACGGTACATCCGGATCCCACAGGTGAGGTTCTTGGGAG	gibson fwd primer for amplification of the 3' region of miR-125a into pFG4
3’-arm-rev-miR125	CACCGCGGTGGCGGCCGCTCTAGAGATGCTTCCTGAGTCCCTCCCAAG	gibson rev primer for amplification of the 3' region of miR-125a into pFG4
7a-fwd-2	TAGGAACTGTAAGAAAACCAGCAG	Forward primer for T7 assay let-7a
7a-rev-2	CAAGTCTACTCCTCAGGGAAGGCA	Reverse primer for T7 assay let-7a

Primer name	Sequence	Description
7b-fwd-2	CTGAGCCGTACCCTCCACTGAGCA	Forward primer for T7 assay let-7b
7b-rev2	TTGGCAGTGCTCTGAGCTGCTGAC	Reverse primer for T7 assay let-7b
125a-fwd-1	CTGTCTGTCTGTCTGTCGGGTC	Forward primer for T7 assay miR-125a
125a-rev-1	CTGACTGTTTCTCTCTGTCTGTCCCTC	Reverse primer for T7 assay miR-125a
miRNA-rev	GAATCGAGCACCAGTTACG	Universal reverse primer for SYBR green qRT-PCR

B.2 Cell culture

B.2.1 Cultivation of cell lines

Material

- Cell culture flasks (Greiner) 175 cm^2
- Countess cell counter (Thermo Fisher)
- Counting chamber Countess (Thermo Fisher)
- Cryo preservation chamber (Nalgene)
- Cryotubes 1.0 ml (Nunc)
- Culture medium DMEM Glutamax (Thermo Fisher), supplemented with 10% fetal calf serum (FCS) (Sigma-Aldrich) and 1% Penicillin/Streptomycin (Thermo Fisher)
- Falcon tubes (Falcon) 50 ml
- Freeze medium (Culture medium supplemented with 10% DMSO (Sigma-Aldrich))
- Incubator 37°C, 7.5% CO_2 (Sigma)
- Microscope (Olympus)
- PBS
- Plastic pipettes (Greiner)
- Dissociation solution TrypLE Express (Thermo Fisher)

Procedure

All GBM cell lines were cultivated in a cell culture incubator at 37°C and 7.5% CO_2. The cells were passaged twice per week at a confluency of approx. 80%. All work was performed under sterile environment in a laminar flow bench.

Subculturing

After removal of the cell culture medium, the cell culture flask was washed with 10 ml PBS. The adherent cells were detached from culture vessel using 4 ml TrypLE

Express followed by incubation at 37°C for five minutes. Complete detachment was confirmed using a microscope. The reaction was stopped adding 6 ml culture medium and the suspension was transferred to a 50 ml falcon tube. The cells were centrifuged for five minutes at 300 g and the supernatant was discarded. The pellet was resuspended in cell culture medium and 10 µl was taken for cell counting. The cells were seeded in amounts of $5x10^5$ to $1x10^6$, depending on the cell line and subculturing duration, in 20 ml medium in a 175 cm^2 cell culture flask.

Cryo-preservation of cells

For long-term preservation, the cells are stored in cryotubes ($1x10^6$ cells per tube) in liquid nitrogen. After centrifugation for 5 min at 300 g, the supernatant was discarded and the cells were resuspended in freeze medium (culture medium supplemented with 10% DMSO). Before the vial was stored in liquid nitrogen, it was put in a cryo-preservation chamber and placed on -80°C for 24 hours.

B.2.2 GBM cell line panel

The human GBM cell lines A172, LN18, LN229, T98G, U87-MG, U138-MG and U251-MG (Table 1) were analyzed in this study. A172, LN18, LN229, U87-MG and T98G were obtained from the American type culture collection (ATCC, Manassas, Virginia, USA), U138-MG and U251-MG from a German cell lines repository (CLS, Eppelheim, Germany). As described in B.1.3, all cell lines were authenticated by STR typing.

B.2.3 STR Typing

Short tandem repeat (STR) analysis was utilized to characterize the origin of the cell lines used for this study. STRs contain two to thirteen base pair sequences that are repeated hundreds of times on a specific position on the DNA. The STRs were amplified using PCR and the size of the resulting products was characterized. The

resulting STR profiles were compared to validate profiles from the DSMZ database (www.dsmz.de).

Material

- 96-well PCR plates (Thermo Fisher)
- 96-well Barcode plates (Thermo Fisher)
- Applied biosystems genetic analyzer (Thermo Fisher)
- DSMZ database (Reinhart et al., 2000)
- GeneAmp PCR System 9700 (Applied Biosystems)
- Genemapper software (Thermo Fisher)
- Geneprint 10 system (Promega)

  5X Master Mix

  5X Primer Pair Mix

  Amplification grade water

  2800M Control DNA, 10 ng/µl

  Allelic Ladder Mix

  Internal Lane Standard 600
- Hi-Di formamide (Thermo Fisher)

Procedure

For cell line authentication, STR-typing was performed using the Geneprint 10 system. For setting up the PCR amplification of the short tandem repeats, 5 µl Master Mix and 5 µl Primer Pair Mix was added to 10 ng genomic DNA which was extracted as described in B.1.4. For the positive control, 2800M Control DNA was used. The samples were vortexed and transferred to 96-well PCR plates. Thermal cycling was carried out in a GeneAmp PCR System 9700 using the following conditions:

96°C for 1 min
94°C for 10 sec
59°C for 1 min

72°C for 30 sec

These steps were repeated for 30 cycles

60°C for 10 min

4°C ∞

Afterwards, the PCR products were diluted 1:10 and 1:50. A loading cocktail was prepared using 9.5 µl Hi-Di formamide and 0.5 µl Internal Lane Standard 600. The mix was vortexed and transferred to 96-well Barcode plates. 1 µl of the diluted DNAs were added to the loading cocktail. The samples were denatured at 95°C for 3 min and immediately chilled on ice. Evaluation of the STR-markers was carried out using an Applied Biosystems genetic analyzer and analysis of the data was performed using the Genemapper software. The size standard 'ILS600' and the Promega Geneprint 10 analysis panel were utilized in the software. The determined genotypes were compared to the DSMZ database (www.dsmz.de).

B.2.4 Spectral karyotyping

Material

- 15 ml centrifuge tubes (Falcon)
- Antidigoxigenin antibody (Roche)
- Avidin-Cy-5 antibody (Biomol)
- Avidin-Cy-5.5 antibody (Biomol)
- Colcemid (Roche)
- Coplin jar
- Fixogum
- Fluorescence microscope ZEISS Axioplan 2 (ZEISS)
- Heat block
- Metal box for incubation
- Microscope slides
- SKY-probe mixture SkyPaint DNA Kit (Applied Spectral Imaging)
- SpectreCube device and SkyView software (Applied Spectral Imaging)

- Water bath

Solutions (Table 2)

- DAPI / Vectashield solution
- ddH_2O
- Denaturation solution
- Dissociation solution TrypLE express (Thermo Fisher)
- Ethanol 70%, 90%, 100% (Merck)
- Fixation solution
- KCl 0.4%, 4%
- $MgCl_2$ / PBS
- PBS
- Pepsin solution
- Post fixation solution
- RNase 10 mg / ml (Fermentas)
- SSC 2x
- SSC/Tween wash solution

Procedure

For karyotyping, the cells were cultivated to 80% confluency as described in B.2.1. Chromosome spreads were prepared by addition of colcemid to the cell culture medium for 3 hours at 37°C. Afterwards, the medium was removed and the cells were washed with PBS and detached from the cell culture flask using TrypLE Express. The cell solution was transferred into 15 ml centrifuge tubes and the samples were centrifuged for 8 min, 1000 rpm at room temperature. The supernatant was discarded and 750 µl 0.4% KCl was added drop wise to the cell pellet. Afterwards, 4% KCl was added to a total volume of 10 ml. The samples were incubated for up to 45min at 37°C. Afterwards, 600 µl fixation solution was added to the mix. The tubes were centrifuged for 5min, 1000 rpm at room temperature and the supernatant was discarded. The pellet was resuspended in 10 ml fixation solution and incubated for 45min at 4°C. Afterwards, the cells were centrifuged for 5

min, 1000 rpm at room temperature and the pellet was washed with fixation solution. The wash procedure was repeated two times and the cells were resuspended in up to 2 ml fixation solution. The suspension was dropped onto microscope slides and was kept at room temperature.

For hybridization, the following steps were performed in coplin jars at room temperature unless specified. Initially, the samples were washed in 2x SSC for 3min and the slides were treated in a metal box with RNase for 4 min at 37°C. Afterwards, the slides were washed three times in 2x SSC for 2 min. The samples were treated using pepsin solution for 2min at 37°C in a water bath. Afterwards, the slides were washed in PBS for 5 min followed by an $MgCl_2$ / PBS wash for another 5 min. The samples were briefly washed with PBS and incubated in post fixation solution for 10 min. After another brief wash with PBS, the samples were incubated in PBS for 5 min and in 2x SSC for 2 min. The samples were treated in denaturation solution for 5 min at 72°C in a water bath and the reaction was stopped using 70% ethanol for 2 min at -20°C followed by incubation for 2 min in 90% ethanol at -4°C and 2 min in 100% ethanol at 4°C. The slides were allowed to dry on a heater for 5 min and the SKY-probe was pipetted on the samples. Hybridization was carried out for 16 hours at 37°C in a water bath. After hybridization, slides were washed using 0.5 × SSC 5 min at 75°C in a water bath followed by 4 × SSC/0.1% Tween 20 for 2 min at room temperature and H_2O 2 min at room temperature. The probes were detected using antidigoxigenin (1 : 250 dilution), avidin-Cy-5, and avidin-Cy-5.5 antibodies (both 1 : 100 dilution) according to the manufacturers protocols. Afterwards, metaphase spreads were counterstained using DAPI / Vectashield solution. Acquisition of stained metaphases was carried out using a fluorescence microscope (ZEISS Axioplan 2) equipped with SpectreCube device and SkyView software. Each individual chromosome was determined by a combination of up to five different fluorescent dyes (Table 4). Chromosomal aberrations could be identified by color junctions on the altered chromosomes.

Table 4: Combination of fluorescent dyes for SKY karyotyping

Chromosome	Fluorescent dyes
1	BCD
2	E
3	ACDE
4	CD
5	ABDE
6	BCDE
7	BC
8	D
9	ADE
10	CE
11	ACD
12	BE
13	AD
14	B
15	ABC
16	BD
17	C
18	ABD
19	AC
20	A
21	DE
22	DBCE
X	AE
Y	CDE

A spectrum orange, B Texas red, C Cy5, D spectrum green, E Cy5.5. Modified after Sanson et al., 2009

B.2.5 Microarray-based comparative genomic hybridization (aCGH)

Array CGH (aCGH) is a molecular cytogenetic method for determination of copy number variations compared to a reference sample. For this, an array is used which contains approx. 60.000 oligonucleotides that span the whole genome in approx. 13 kb intervals. In the procedure, tumor and control DNA are labeled with fluorescent dyes. Afterwards, the samples are added to the array and the DNA hybridizes to the oligonucleotides on the array. The hybridized arrays are analyzed in a microarray scanner and the recorded signals are evaluated using bioinformatics tools.

B.2.5.1 Random prime labeling

Material

- Enzo CGH Labeling Kit for Oligo Arrays
  Primers/Reaction buffer
  Cyanine 3-dUTP nucleotide mix
  Cyanine 5-dUTP nucleotide mix
  Klenow DNA-polymerase
  Stop buffer
- Promega Human reference DNA (female or male) pooled
- TE-buffer

Procedure

For random prime labeling 500 ng reference DNA was combined with 500 ng sample DNA. Therefore, the input DNAs were separately added to 20 µl Primer/Reaction buffer and 39 µl H_2O. Afterwards, the samples were denatured at 99°C for 10 minutes and chilled on ice for 2 minutes. To the tumor samples 10 µl Cy3-dUTP was added while 10 µl Cy5-dUTP was added to the reference samples. To each tube 1 µl Klenow-polymerase was added and the samples were incubated at 37°C for 4 hours. Afterwards, the reaction was stopped using 5 µl Stop-buffer. For purification of the DNA the samples were mixed with 430 µl TE-buffer and transferred to an Amicon Ultra-0.5-Filter. After centrifugation at 14000 g for 10 minutes, the flow-through was discarded and the filter was inverted in a new reaction tube and centrifuged again at 1000 g for 1 minute. Afterwards, the quality of the samples was evaluated using a Nanodrop ND-1000 device. For further processing of the samples, the specific activity (pmol fluorochrome per µg DNA) of the labeled DNA had to be at least 20 for Cy5-labeled DNA and 25 Cy3-labeled DNA.

B.2.5.2 Hybridization

Material

- Agilent 10x blocking agent
- Agilent 2x Hi-RPM buffer
- Agilent SurePrint G3 human CGH microarray, 4x180k
- Roche Human Cot-1 DNA

Procedure

For hybridization, the volume of all samples hat to be 19,5 µl. Therefore, the samples were dried in a vacuum rotator and the pellets were resuspended in 19,5 µl H_2O. Afterwards, the reference and sample DNAs were combined. A hybridization master mix was created for one slide (four samples) using 21,25 µl Cot-1 DNA, 46,75 µl Agilent 10x blocking reagent and 233,75 µl Agilent 2x Hi-RPM buffer. To each sample, 71 µl of the master mix was added. The samples were denatured at 95°C for 3 minutes and incubated at 37°C for 30 minutes. Afterwards, 100 µl of the sample was added to a chamber in a gasket slide. The array was placed on top of the gasket slide (with the Agilent label facing down) and the slides were sealed using a metal clamp. The array "sandwich" was placed in a rotating incubation oven at 65°C for 24 hours.

B.2.5.3 Wash and scan of the arrays

Material

- Agilent Oligo aCGH/ChIP-on-chip wash buffer 1
- Agilent Oligo aCGH/ChIP-on-chip wash buffer 2

Procedure

Washing of the hybridized slides was carried out using two buffers, wash buffer 1 which was kept at room temperature and wash buffer 2 which was preheated at 37°C. The array "sandwiches" were carefully opened while submerged in wash buffer 1 and the gasket slide was allowed to detach from the hybridized array. Afterwards, the array was transferred to another cuvette containing wash buffer 1 and the slide was incubated for 5 minutes. The array was transferred into the cuvette containing wash buffer 2 at 37°C and incubated for 1 minute. For scanning of the array, the slide was placed in an Agilent slide holder and covered using an ozone barrier. In the Agilent software, the profile "Agilent G3_CGH" was used for scanning of the slide. Afterwards, the resulting picture of the scanned slide was analyzed for uniform hybridization.

B.2.6 DNA-isolation from cell pellets

Material

- Ethanol 100% (Merck)
- PBS
- Qiagen Blood & Tissue Kit

  DNeasy Mini Spin Columns

  Collection tubes

  Lysis buffer AL

Wash buffer AW1

Wash buffer AW2

Elusion buffer AE

Proteinase K

Procedure

For DNA isolation, the cell lines were harvested and approx. $1x10^6$ cells were centrifuged at 300 g for 5 min. Afterwards, the supernatant was discarded and the pellet was resuspended in 200 µl PBS. After addition of 20 µl Proteinase K, 200 µl Buffer AL was pipetted to the samples. The mixture was vortexed thoroughly. After incubation at 56°C for 10 minutes, 200 µl ethanol was added and the samples were transferred to spin columns. Afterwards, the columns were centrifuged at 6000g for 1 minute and the flow-through and collection tube was discarded. 500 µl Buffer AW1 was added to the column. The samples were centrifuged at 6000 g for 1 minute and the flow-through was discarded. Afterwards, 500 µl Buffer AW2 was added and the columns were centrifuged at 20,000 g for 3 minutes. The columns were transferred to a microcentrifuge tube and 100 µl Buffer AE pipetted on the membrane. The DNA concentrations were measured as described in B.2.1.

B.2.7 RNA-isolation from cell pellets

Material

- Chloroform (Merck)
- Ethanol (Merck)
- Qiagen miRNeasy Mini Kit

  RNeasy Mini Spin Columns

  QIAzol Lysis Reagent

  Wash buffer RWT

  Wash buffer RPE

  RNase-Free water

Procedure

The cells were harvested as described in 1.3 and 700 µl QIAzol Lysis Reagent was pipetted onto the pellet. After 1 min of homogenization by vortexing, the mixture was incubated for 5 min at room temperature. 140 µl Chloroform was added to the samples and the contents were thoroughly mixed. The samples were incubated for 2 min at room temperature and centrifuged at 12000g for 15 min at 4°C. The upper aquatic phase (approx. 350 µl) was transferred to a new tube and 525 µl ethanol was added. The samples were pipetted into Spin columns and the tubes were centrifuged at 8000g for 30 sec. The flow through was discarded and 700 µl Buffer RWT was added onto the columns. The tubes were centrifuged at 8000 g for 30 sec and the flow through was discarded. The columns were washed twice with 500 µl Buffer RPE and were centrifuged at 8000 g for 30 sec and 2 min. Afterwards, the columns were centrifuged another time at 8000 g for 1 min to remove residual buffer from the columns. To elute the RNA, the columns were transferred into new collection tubes and 30 µl water was pipetted onto the membranes. The samples were incubated for 1 min at room temperature and centrifuged at 8000 g for 30 sec. The resulting RNA concentration was measured as described in B.2.1.

B.2.8 RNA-isolation in multi-well format

Material

- Ethanol 100% (Merck)
- PBS
- ZR-96 Quick-RNA Kit (Zymo)

  RNA Lysis Buffer

  RNA Prep Buffer

  RNA Wash Buffer

  DNase/RNase-Free Water

  DNase I

  DNA Digestion Buffer

  Silicon-A Plate

Collection Plate

Procedure

To analyze RNA from cells grown over a different period of time, culture dishes were prepared to harvest the cells after 24, 48 and 72 hours. At each time point, the culture medium was discarded, the cell layer was washed once with PBS and the cells were harvested. Afterwards, 100 µl lysis buffer was applied directly onto the cells. Cells were lysed and homogenized by pipetting and the lysates were transferred into a 96-well plate and stored in -80°C until further processing. For isolation of the RNA, the samples were mixed with 100% ethanol in equal amounts and transferred to a 96 well Silicon-A plate. The plates were centrifuged for 5min at 2500 g and the flow-through was discarded. Removal of residual DNA was carried out by DNase I treatment directly onto the columns. Therefore, the samples were washed with 400 µl RNA wash buffer once and the plates were centrifuged for 5min at 2500 g and the flow-through was discarded. For each sample, 5 µl DNase I was added to 35 µl DNA digestion buffer. The mix was added to the columns and incubated at room temperature for 15 min and the plates were centrifuged for 5min at 2500 g and the flow-through was discarded. Afterwards, 400 µl RNA prep buffer was pipetted to the samples and the plates were centrifuged another time for 5min at 2500 g. 500 µl RNA wash buffer was applied to the columns and the plates were centrifuged for 5 min at 2500 g. This step was repeated once. For removal of residual ethanol, the plates were centrifuged another time for 5min at 2500 g. The Silicon-A plate was placed on top of an elution plate and 25 µl DNase/RNase free water was added to the columns. The samples were centrifuged for 5min at 2500 g and the resulting RNA concentrations were measured as described in B.2.1.

B.2.9 Generation of cell lines with modulated signature miRNA expressions

Lipofection-based transfection systems were used in this study for generation of transgenic cell lines. Lipofection utilizes positively charged liposomes that form complexes with negatively charged DNA. These complexes inherit phospholipid bilayers, which can easily merge with the cell membrane and deliver the DNA to the cytoplasm of the cells. For these experiments the cell lines A172 and U138-MG were used.

B.2.9.1 Determination of transfection efficiency and optimal concentration using siRNA

Material

- 24-well cell culture plates (Greiner)
- Fluorescence-activated cell sorter (FACS) BD LSR II (BD Biosciences)
- Block-iT Alexa Fluor Red Fluorescent Control (Thermo Fisher), 20 µM stock
- Culture medium DMEM Glutamax (Thermo Fisher), supplemented with 10% FCS (Sigma-Aldrich) and 1% Penicillin/Streptomycin (Thermo Fisher)
- DMEM Glutamax (Thermo Fisher) without additives
- Lipofectamine RNAiMAX transfection Reagent (Thermo Fisher)
- miRVana miRNA Inhibitor Negative Control #2 (Thermo Fisher), 20 µM stock
- mirVana miRNA Mimic Negative Control #1 (Thermo Fisher), 20 µM stock
- PBS
- Dissociation solution TrypLE Express (Thermo Fisher)

Procedure

The cells were seeded in 24-well plates 24 hours prior transfection. The stock solutions were diluted to a final concentration of 5 µM. For transfection, two microcentrifuge tubes were prepared as described below and the respective volumes were scaled according to the number of transfected wells. 25 µl additive-

free DMEM Glutamax was mixed with 1 µl of the respective siRNAs in the first tube, resulting in a final concentration of 10 nM (alternatively 0.5 µl for a concentration of 5 nM). In the second tube, 25 µl additive-free DMEM was mixed with 1.5 µl RNAiMAX reagent. The siRNA mixture of tube 1 was pipetted into the tube containing the RNAiMAX reagent. After 5 min incubation at room temperature, 50 µl of the transfection mixture was added to the wells. Four hours after transfection, the medium was replaced with fresh culture medium. The transfection efficiency was determined 24-hours after transfection using FACS. Therefore, the culture medium was removed from the wells and the cells were washed with PBS once. For detachment of the cells, 100 µl TrypLE Express was added to the wells and the plates were incubated for 5 min at 37°C. Afterwards, 100 µl culture medium was pipetted to the wells and the suspension was transferred into microcentrifuge tubes. The tubes were centrifuged at 300 g for 5 min and the supernatant was discarded. The pellet was washed twice with PBS and the cells were resuspended in 100 µl PBS and transferred into FACS tubes. Analysis of the transfected cells was carried out using a BD LSR II device.

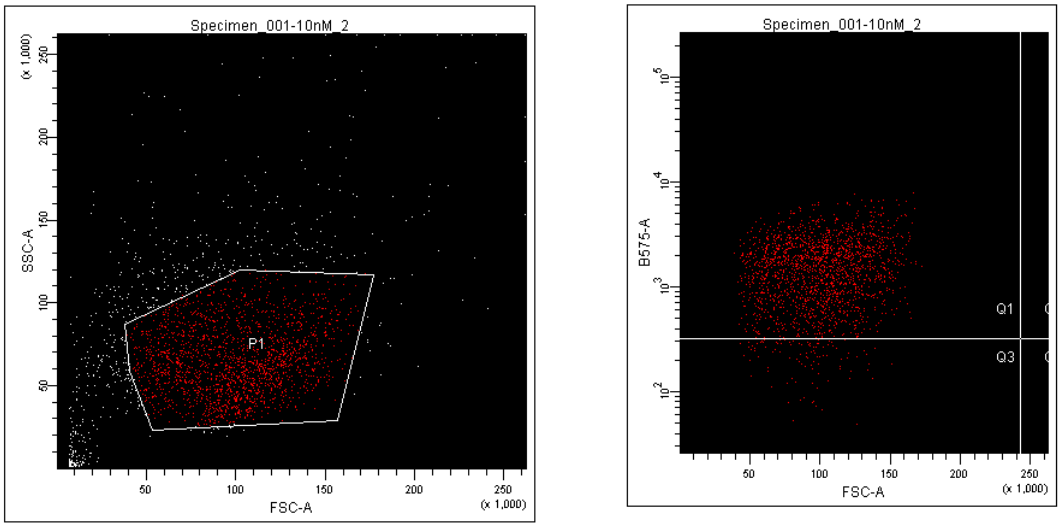

Experiment Name: A172-Testtransfektion-Alexa_24-well_10_5_1_0...
Specimen Name: Specimen_001
Tube Name: 10nM_2
Record Date: Apr 18, 2018 2:01:50 PM
$OP: Randy

Population	#Events	%Parent	FSC-A Mean	B575-A Mean
P1	1,758	74.7	99,028	1,694
Q1	1,653	94.0	99,650	1,787
Q2	0	0.0	####	####
Q3	105	6.0	89,250	219
Q4	0	0.0	####	####

Figure 3: FACS analysis of A172 cells transfected with Block-iT Alexa

The top left panel shows the total distribution of the cell suspension, where the P1 (parental) area represents the supposed population of living cells. The cells were distinguished by their size (forward scatter: FSC) and their granularity (side scatter: SSC). The top right panel is displaying the amount of fluorescent cells out of the P1 area. To visualize Block-iT Alexa, which is a red fluorescent siRNA, a 575 nM laser was used. The bottom panel shows the distribution of living cells P1, fluorescent cells Q1 and non-fluorescent cells Q3.

B.2.9.2 Transfection of miRNA mimics and inhibitors

For modulation of the endogenous miRNA expression, miRNA mimics and inhibitors were used. These molecules either functionally up-regulate the miRNA expression or down-regulate the miRNA activity. Mimics are chemically modified double stranded RNAs that are mimicking endogenous miRNA function and can bind to the target gene for posttranscriptional repression of the respective gene. Inhibitors are

chemically modified, single stranded RNAs that are complementary to the target miRNA. These inhibitors confer the ability to reduce the endogenous miRNA level, thus increasing the target gene expression.

Material

- 24-well cell culture plates (Greiner)
- DMEM Glutamax (Thermo Fisher) without additives
- Lipofectamine RNAiMAX transfection reagent (Thermo Fisher)
- mirVana miRNA Inhibitor (Thermo Fisher), 20 µM stock
- miRVana miRNA Inhibitor Negative Control #2 (Thermo Fisher), 20 µM stock
- mirVana miRNA Mimic (Thermo Fisher), 20 µM stock
- mirVana miRNA Mimic Negative Control #1 (Thermo Fisher), 20 µM stock

Procedure

To monitor the siRNA presence in the cells over time and to determine the optimal siRNA concentration, the cells were seeded and transfected according to B.1.5.1. After 24, 48 and 78 hours the cells were lysed and RNA was extracted as described in B.1.4.

B.2.9.3 Transfection of plasmids

Material

- 6-well cell culture plates (Greiner)
- FACS device BD LSR II (BD Biosciences)
- Culture medium DMEM Glutamax (Thermo Fisher), supplemented with 10% FCS (Sigma-Aldrich) and 1% Penicillin/Streptomycin (Thermo Fisher)
- DMEM Glutamax (Thermo Fisher) without additives
- eSpCas9 1.1 GFP Plasmid, 1 µg/µl stock

- Lipofectamine transfection 3000 (Thermo Fisher)
- P3000 transfection additive (Thermo Fisher)
- PBS
- Dissociation solution TrypLE Express (Thermo Fisher)

Procedure

The cells were seeded in 6-well plates in amounts between 150,000 and 250,000 cells 24 hours prior transfection. The amount of cells varied depending on the cell line to achieve a confluency of 70-90% on the day of transfection. For the transfection mix, two microcentrifuge tubes were prepared for each condition. In the first tube, 125 µl additive-free DMEM was placed and 3, 5 or 7 µg plasmid DNA and 5 µl P3000 reagent were added. In the second tube, 125 µl additive free-DMEM was combined with 3.75, 5.6 or 7.5 µl Lipofectamine 3000. Afterwards, 125 µl of the DNA containing mix was added to the corresponding Lipofectamine tube. The samples were incubated for 15 min at room temperature and 250 µl of the transfection mix was added onto the cells. The plates were incubated for four hours. Afterwards, the cell culture medium was discarded and fresh medium was added to the cells. Fluorescence-activated cell sorting was carried out 24 hours after transfection. Therefore, the culture medium was discarded and the cells were washed with PBS once. For detachment of the cells, 500 µl TrypLE Express was added to the wells and the plates were incubated at 37°C for 5 min. The reaction was terminated with 500 µl DMEM, the cells were transferred to a centrifugation tube and the samples were centrifuged at 300 g for 5 min. The supernatant was discarded and the cells were washed twice with PBS. Afterwards, the pellet was resuspended in 300 µl PBS and the suspension was transferred into FACS tubes. Analysis of the transfected cells was carried out using a fluorescence-activated cell sorter (BD LSR II).

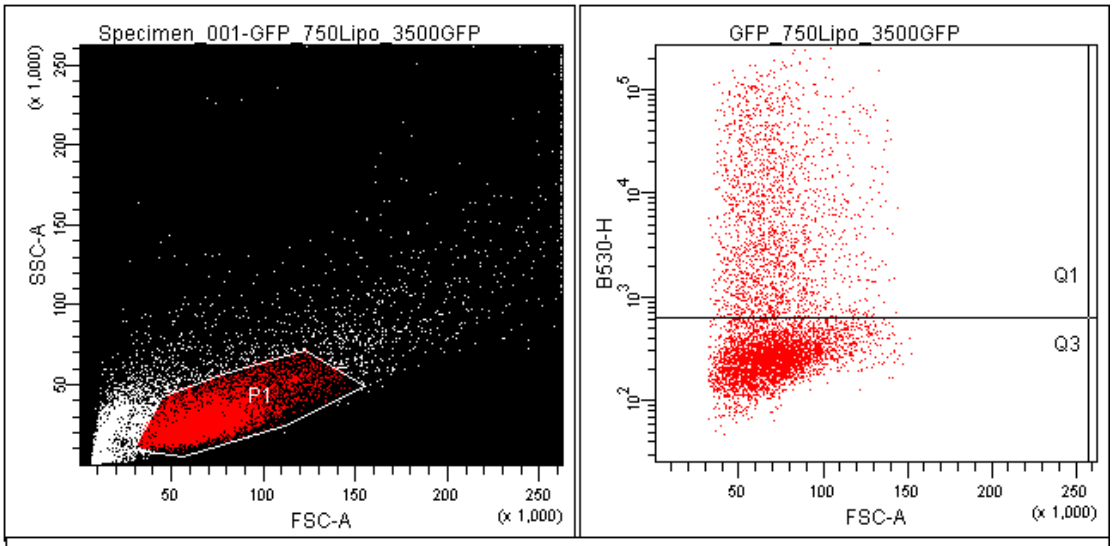

Experiment Name: SpCas9-GFP_Testtransfection_U87_150k
Specimen Name: Specimen_001
Tube Name: GFP_750Lipo_3500GFP
Record Date: Aug 3, 2017 3:27:05 PM

Population	Parent Name	#Events	%Parent	B530-H Median	B530-H Mean	B575-H Median	R660-H Median
P1	####	5,835	58.4	322	5,956	397	33
Q1	P1	1,832	31.4	4,661	18,366	1,214	34
Q3	P1	4,003	68.6	254	276	323	32

Figure 4: FACS analysis of U87 cells transfected with eSpCas9 GFP

The top left panel shows the total distribution of the cell suspension, where the parental (P1) area represents the supposed population of living cells. The cells were distinguished by their size (forward scatter: FSC) and their granularity (side scatter: SSC). The top right panel is displaying the amount of GFP expressing cells out of the P1 area. To visualize GFP a 530 nM laser was used. The bottom panel shows the distribution of living cells P1, GFP expressing cells Q1 and non-expressing cells Q3.

B.2.10 Single cell cloning

For the generation of cell clones, the transgenic cells were subjected to single cell cloning. This task is generally performed by FACS-based approaches or seeding the cells in increasing dilutions until a theoretical amount of one cell per well is reached. In this study, the cells were seeded in low density on large cell culture plates. After sufficient growth, distinct cell colonies were individually removed from the plate using sterile filter paper. Expansion of the cells was done gradually from 24-well

plates to 6-well plates. This technique has the advantage of multiple numbers of growing cells on a single petri dish thus avoiding cell cloning from a single cell origin.

Material

- 24-well cell culture plates (Greiner)
- 6-well cell culture plates (Greiner)
- Cell culture dishes 10 cm and 15 cm diameter (Greiner)
- Culture medium DMEM Glutamax (Thermo Fisher), supplemented with 10% FCS (Sigma-Aldrich) and 1% Penicillin/Streptomycin (Thermo Fisher)
- PBS
- Sterile filter paper (Sigma-Aldrich) cut in circles of approx. 4-5 mm diameter
- Dissociation solution TrypLE Express (Thermo Fisher)

Procedure

For the generation of single clones, the cells were seeded on cell culture dishes in low density of about 125-750 cells per plate. The cells were grown for 14 days. Afterwards, the colonies were observed under a microscope and evenly distributed colonies were designated for further treatment. The culture medium was discarded and the cells were washed with PBS once. The sterile filter paper was immerged in TrypLE Express and the papers were placed directly onto the marked colonies. Afterwards, the plates were incubated at 37°C for 5 min. The papers were removed from the plate and transferred into 24-well containing culture medium. The floating filter papers were removed from the 24-well plate after 24 hours and the cells were observed daily. After the cells were grown to a confluency of approx. 80% the cells were detached from the plates as described above. Afterwards, the clones were transferred into 6-well plates and observed for cell growth and morphology daily. After colonies of at least 1000 cells were established, the single clones were transferred into culture flasks or frozen in liquid nitrogen as described in B.2.1.

B.2.11 Colony formation assay

Cell survival after irradiation or chemotherapeutic treatment was measured based on the clonogenic survival of cells. For this experiment, the cells were seeded on culture dish with increasing cell numbers depending on the irradiation dose or the concentration of the chemotherapeutic agent. Afterwards, the cells were grown for 14 days and the colonies were stained and counted. A major component of this experiment is the plating efficiency (PE). This value displays the amount of colonies grown without treatment and is highly variable between cell lines. Survival of the cells after treatment was normalized to the PE.

Material

- 6-well or 24-well cell culture dishes (Greiner)
- Culture medium DMEM Glutamax (Thermo Fisher), supplemented with 10% FCS (Sigma-Aldrich) and 1% Penicillin/Streptomycin (Thermo Fisher)
- Dimethyl sulfoxide (DMSO) (Sigma-Aldrich)
- Fixation solution 80% ethanol (Merck), 0.3% methylene blue (Sigma-Aldrich)
- RS225 irradiation chamber (X-Strahl)
- Temozolomide (TMZ) (Tocris) dissolved in DMSO with a stock concentration of 50 µM

Procedure

For the determination of the clonogenic survival upon irradiation or temozolomide treatment, the cells were seeded in 6-well or 24-well plates. The number of cells per well varied between 50-500,000 cells depending of the size of the plate and the respective treatment. Generally, approximately 50 colonies per well were suitable for evaluation of the clonogenic growth. After seeding of the cells, attachment of cells was allowed for 4 h, medium was changed, and cells were irradiated at 0, 1, 2, 4, 6, or 8 Gy, respectively. Three independent experiments were performed per cell line.

Clonogenic survival upon TMZ treatment was determined accordingly. Four hours after seeding, medium was exchanged, and TMZ was added to a final concentration of 0, 5, 10, 50, 100, 200, or 500 µM respectively. 24 hours later, TMZ-containing medium was removed and fresh, TMZ-free medium was added. After 14 days cells were fixed with 80% ethanol solution containing 0.3% methylene blue followed by extensive washing in deionized water and air-drying. Colonies of at least 50 cells were counted using a binocular or a light microscope. The experiment was conducted in triplicates and several persons determined the cell number. The surviving fractions (SFs) for each condition were calculated by normalizing on the determined plating efficiency.

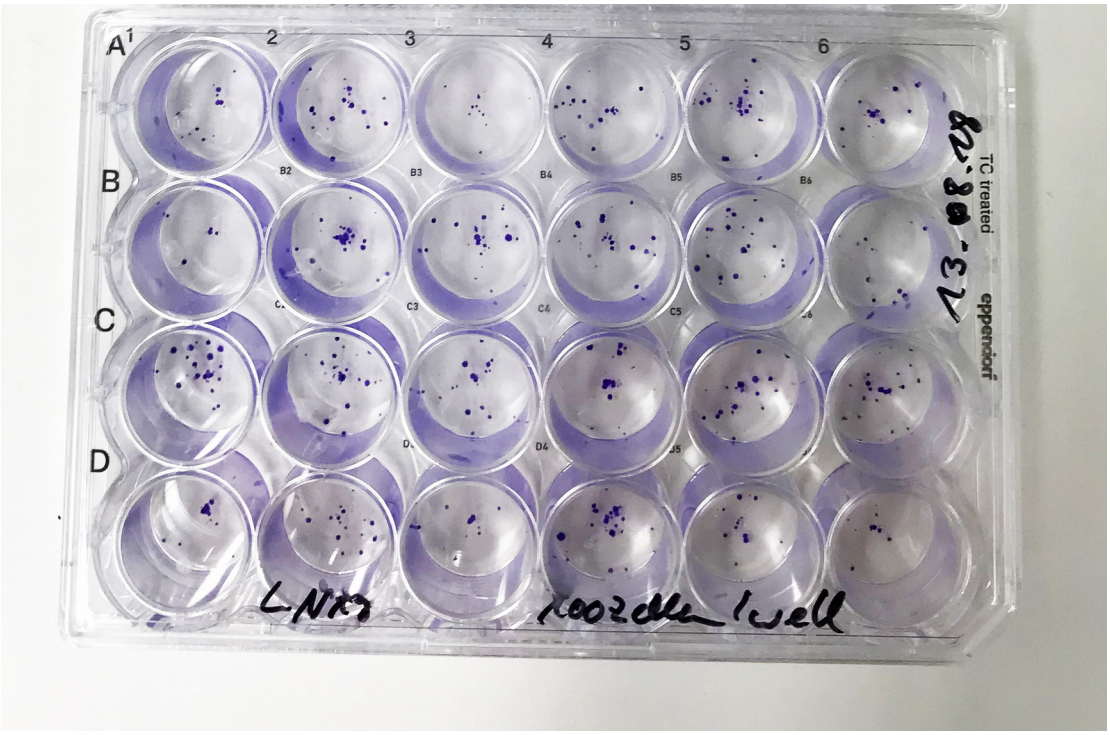

Figure 5: Stained colony formation assay using LN18 cells

Pictures show the stained plates from the top of the plate. The grown colonies appear as blue dots on the surface of the respective wells. 100 cells were seeded per well.

B.2.12 Assessment of the MGMT promoter methylation status

Material

- Promega M16 Blood DNA purification kit

Procedure

Assessment of the MGMT promoter methylation status was performed in collaboration with Dr. Viktoria Ruf from the Center of Neuropathology and Prion Research of the LMU University Hospital Munich. The sample DNA was isolated from cell suspensions on a Maxwell® 16 MDx instrument using the M16 Blood DNA purification kit according to manufacturer's instructions. DNA concentration was assessed using a NanoDrop1 ND-1000 Spectrophotometer.

The MGMT promoter methylation status was assessed by MSP PCR and sequencing. After sodium bisulfide treatment of the DNA, MSP PCR was performed using primers specific for methylated or unmethylated DNA and PCR products were visualized using the FlashGel™ System. For bisulfide sequencing, a 316 bp fragment with 25 CpG sites of the MGMT promoter region was amplified after bisulfide treatment. Sequencing of purified PCR products was subsequently performed on an ABI3130 sequencer. The MGMT promoter sequence was considered 'methylated' if ≥ 13 of the 25 CpG sites showed methylation specific peaks, i.e. at least 50% signal intensity of the corresponding thymine peak.

B.3 qPCR

A quantification of the expressed miRNAs was carried out by qPCR analysis using the Qiagen miScript II System. It is based on a polymerase chain reaction in combination with a fluorescent dye, which incorporates with double-stranded DNA and acts as a reporter for quantification of the produced amount of DNA. Additionally, a background fluorescent dye is added that is used for normalization (ROX). The miScript II System utilizes the SYBR green technology that interacts unspecifically with double stranded DNA. At the same time, ROX is used for normalization purposes. To generate constructs suitable for PCR analysis, the miRNAs are first polyadenylated. Subsequently, an oligo-dT primer with a universal tag is ligated to the 3'-end of the miRNAs (Figure 6). Afterwards, the RNA undergoes a reverse transcription reaction to generate cDNA. In the following PCR reaction, the mature miRNA sequence acts as the binding site for the miRNA specific forward primer, whereas the universal tag acts as the binding site for the unspecific reverse primer. As an indicator for the produced DNA, threshold cycle (C_T) values were analyzed. The C_T value correlates to the PCR cycle where the reporter fluorescence is significantly higher than the background signal. For a relative quantification, the C_T values of the target genes were normalized to the C_T values of endogenously expressed RNA. In this study, small nucleolar RNAs (snoRNAs) were used for normalization. After the PCR cycles were completed, a melting curve analysis was added to the PCR protocol. A single melt curve peak indicates that a pure PCR product was produced whereas multiple peaks indicate secondary PCR products. To ensure reproducibility of the qPCR experiment, a single PCR product is required. To optimize the PCR and to avoid secondary products, the efficiency of the used primers was analyzed and the optimal cycling conditions were determined.

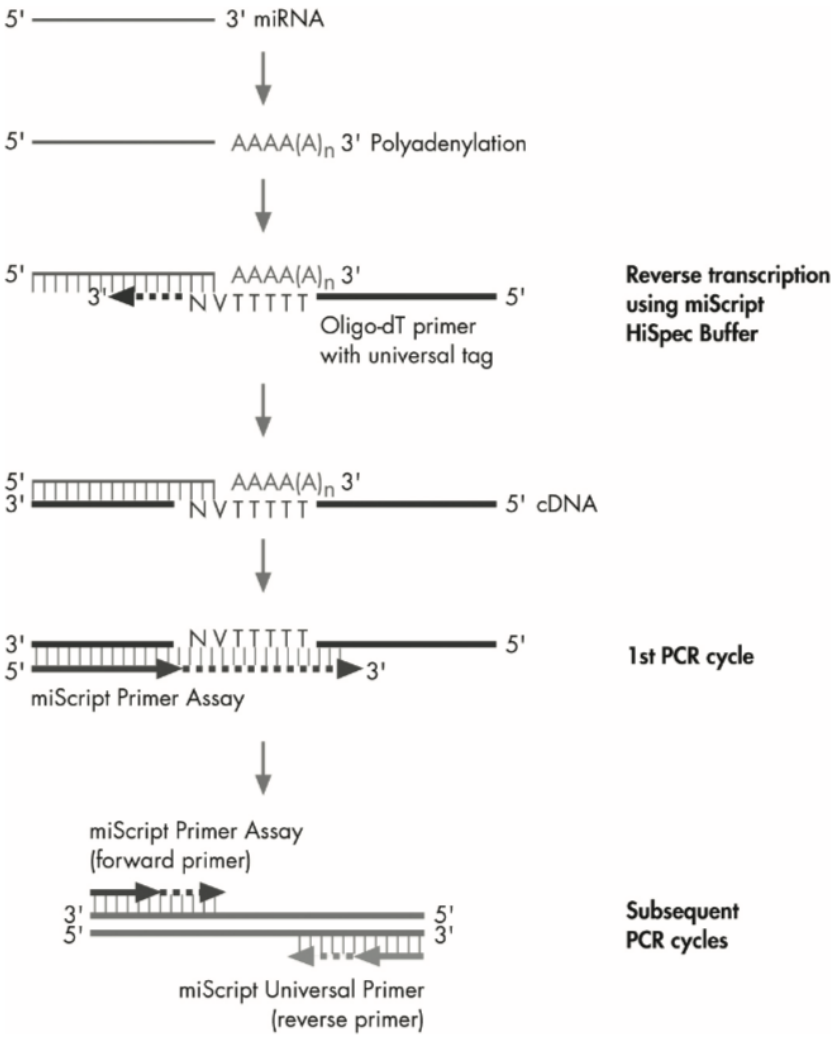

Figure 6: Selective conversion of mature miRNAs into cDNA

In the reverse transcription reaction, mature miRNAs are polyadenylated (A) and an oligo-dT primer with universal tag is ligated to poly-A tail (B). The oligo-dT primer is used for creating double stranded cDNA out of the single stranded miRNA sequence (C). In the qPCR reaction, the forward primer binds to the miRNA sequence for synthesis of the first PCR product (D). In subsequent PCR cycles, the forward miScript primer and the reverse universal primer are utilized for synthesis of DNA molecules (E).

B.3.1 qRT-PCR

Material

- Nanodrop Spectrophotometer ND1000 (Nanodrop Technologies)
- 10x miScript PCR Control RNU6 (Qiagen)
- 10x miScript PCR Control SNORD-61 (Qiagen)
- 10x miScript PCR Control SNORD-68 (Qiagen)
- 10x miScript PCR Control SNORD-95 (Qiagen)
- 10x miScript primer assay hsa-let-7a-5p (Qiagen)
- 10x miScript primer assay hsa-let-7b-5p (Qiagen)
- 10x miScript primer assay hsa-miR-125a-5p (Qiagen)
- 10x miScript primer assay hsa-miR-615-5p (Qiagen)
- 96-well PCR plates (ThermoFisher)
- GeneAmp PCR System 9700 (Applied Biosystems)
- MicroAmp Optical 384-Well Reaction Plate (Applied Biosystems)
- MicroAmp Optical Adhesive Film (Applied Biosystems)
- miScript SYBR Green PCR Kit (Qiagen)

  10x miScript universal reverse primer

  2x QuantiTect SYBR Green PCR Master Mix

  RNase-free water
- Qiagen miScript II reverse transcription Kit (Qiagen)

  miScript Reverse Transkriptase Mix

  10x miScript Nucleics Mix

  5x miScript HiSpec reverse transcription buffer

  RNase-Free Water
- Viia 7 Real-Time PCR System (Applied Biosystems)

Procedure

Quantification of purified DNA or RNA is carried out using a Nanodrop device at a wavelength of 260 nm. The instrument is calibrated using 1 µl H_2O and measurement of the nucleic acids is performed using 1 µl of the sample. Purity of DNA or RNA is measured using the ratio of the absorption at 260/280 nm and 260/230 nm. Pure DNA shows a 260/280 ratio of >1.8 and pure RNA shows a ratio of >2.0. The resulted concentrations are received in ng / µl.

For the reverse transcription reaction, the HiSpec buffer was utilized to specifically transcribe mature miRNAs. The sample preparation was performed on ice under a sterile laminar flow bench that was designated for working with RNA. In a 96-well PCR plate, 10 ng RNA in 2.4 µl RNase-Free water was added to 0.8 µl 5x HiSpec buffer mixed with 0.4 µl Nucleics Mix and 0.4 µl Reverse Transcriptase Mix. The samples were incubated on a GeneAmp PCR System at 60°C for 60 min and at 95°C for 5 min. Afterwards, the reaction was cooled to 4°C and diluted with 16 µl RNase-free water to a total volume of 20 µl. The resulting cDNA was stored at -20°C.

For each reaction, 5 µl QuantiTect PCR Master Mix was mixed with 1 µl of the respective miScript Primer assay, 1 µl of the universal reverse primer and 2 µl RNase-free water. The master mix was dispersed into designated wells of a 384-well plate. Afterwards, 1 µl of the diluted cDNA was added to each well. The plates were sealed with MicroAmp Optical film and the samples were vortexed and centrifuged. PCR was performed on a Viia 7 device. For setting up the experiment, the Viia 7 software was utilized. The following cycling conditions were applied:

95°C for 15 min
94°C for 15 sec
55°C for 30 sec
70°C for 30 sec
These steps were repeated for 40 cycles

B.3.2 Determination of optimal PCR conditions

Analysis of the primer efficiency

An optimal performance of the involved primes is crucial for generating reproducible data. Determination of the efficiency of the respective primer pairs was done by a standard curve experiment. Therefore, prepared cDNA as described in B.2.2 was diluted in 1:5 ratios in RNase-free water. For each primer pair, five data points in triplicates were generated. The PCR was conducted as described in B.2.3. In the Viia 7 software, the option "Standard curve experiment" was selected. Slope of the resulting curves was retrieved from the results. All primer pairs had to have an efficiency of >95%. The efficiency was calculated as:

$$E = 10^{-1/m} - 1$$

E: Efficiency of the primer

m: Slope of the standard curve. The slope is calculated from the vertical and horizontal difference of two points of a line.

Determination of the optimal primer concentration

For primer pairs that did not show >95% efficiency, a primer matrix was created. For this purpose, the 5 µM stock primers were diluted to 2.5 µM, 1 µM and 500 nM and all possible combinations of forward and reverse primer concentrations were applied in the PCR reactions. The PCR was conducted as described in B.3.1. The resulting C_T values were plotted against the ΔRn values. The ΔRn value represents the normalized reporter signal minus the background signal and reflects the magnitude of the specific signal generated from a given set of PCR conditions. The primer sets showing a combination of highest ΔRn value and lowest C_T, were subjected to standard curve analysis as described above.

B.4 Analysis of global gene expression

To characterize the global gene expressions of the GBM cell lines, gene expression microarray analysis and RNA sequencing was utilized in this study. Microarrays are a hybridization-based approach that typically consists of fluorescent-labeled cRNA binding to oligos spotted on a glass slide. Microarrays are a well-developed approach with a fast and standardized workflow for generation of expression data. The drawback of microarrays is relying on known sequences and the difficulty of analyzing FFPE derived RNA. RNA sequencing has risen in popularity in the recent years, with the advantage of characterizing different species of transcripts from mRNA to non-coding RNA and small RNAs and not relying on previous known sequences (Wang et al., 2009). Also, RNA sequencing is suitable for analyzing FFPE derived RNA. The principle of microarray analysis usually involves conversion of total sample RNA into cDNA. Afterwards, fluorescent-labeled cRNA is transcribed from the cDNA. The cRNA is then hybridized with the microarray slides overnight. Here, the cRNA binds to the corresponding probes on the array. After washing of the slides, the microarrays are analyzed in a slide scanner that creates high-resolution images of the arrays. For evaluation of the microarray experiment, the fluorescent intensity of the sports are correlated to the corresponding probes. Higher fluorescent intensities reflect higher gene expression and vice versa.

B.4.1 Qubit measurement

RNA concentrations were determined using a Qubit device. The Qubit technology utilizes fluorescent dyes that bind specific to RNA, DNA or Protein. In this study the RNA broad range (BR) Kit was used for RNA concentrations more than 20 ng/µl or the RNA high sensitivity (HS) Kit for concentrations below 20 ng/µl.

Material

- Qubit 4 Fluorometer (Thermo Fisher)
- Qubit RNA BR or HS Assay Kit (Thermo Fisher)

  Qubit RNA Buffer

  Qubit RNA Reagent

  Qubit RNA Standard #1

  Qubit RNA Standard #2

Procedure

Before the measurement was started, all reagents were brought to room temperature. For the two standards and all samples a working solution was prepared combining 199 µl RNA Buffer and 1 µl RNA Reagent. From each sample, 1 µl was used in addition to 199 µl working solution. Additionally, 10 µl of the respective standard was combined with 190 µl working solution. The tubes were mixed and incubated at room temperature for 2 min. Afterwards, the sample concentration was assessed using a Qubit 4 device according to the manufacturer's manual using the respective RNA broad range or high sensitivity program.

B.4.2 Bioanalyzer measurement

For the determination of RNA integrity, a bioanalyzer measurement was conducted. The Bioanalyzer uses a capillary electrophoresis (CE) principle for size separation of the nucleic acids. Typically, 12 nucleic acid samples can be analyzed on a single chip within 30 minutes. The chips are fabricated from glass and comprise an interconnected network of fluid reservoirs and microchannels, which must be filled with a gel-dye mixture. Each chip contains 16 wells: 3 for loading the gel-dye mixture, 1 for a molecular size ladder, and 12 for experimental samples. The movement of nucleic acids through the microchannels is controlled by a series of electrodes, each of which is independently connected to a power supply. The gel-dye mixture consists of a polymer and an intercalating dye. Each experiment also

contains a molecular marker for determination of fragment sizes of the nucleic acids (Panaro et al., 2000). The quality of the analyzed RNA is displayed using the RNA integrity number (RIN). The RIN value is based on an algorithm that uses features from the bioanalyzer experiment. Most importantly, the ratio of the area under the 18S and 28S peaks (Figure 7) is calculated to the total area under the curve (Schroeder et al., 2006).

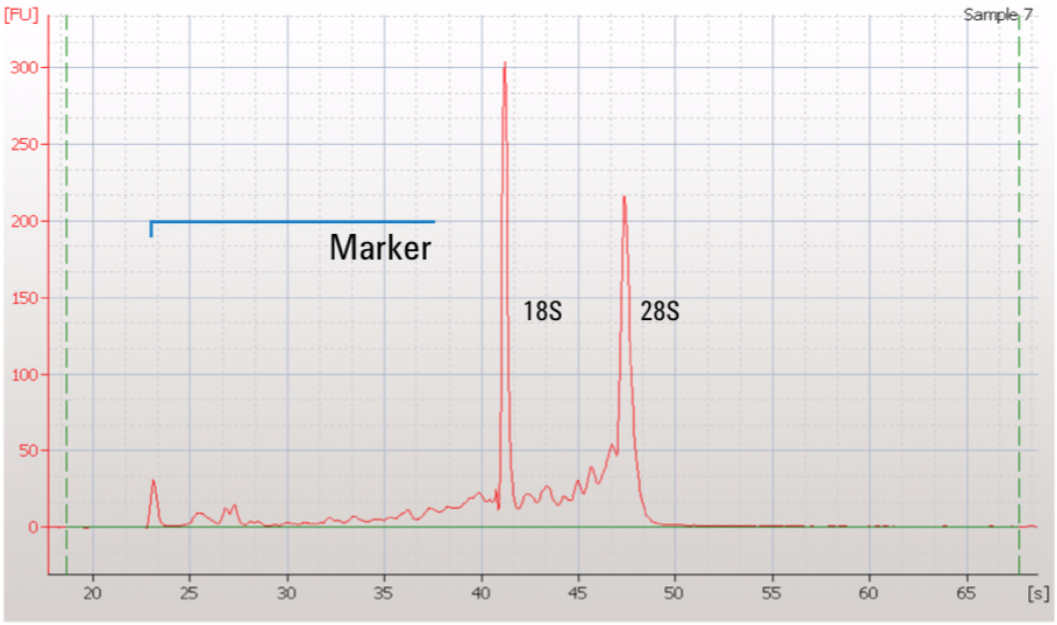

Figure 7: RNA profile of a bioanalyzer measurement using eukaryotic total RNA

The capillary electrophoresis profile of a successful bioanalyzer run is shown. Clearly visible are the 18S and 28S peaks whereas the marker peak resembles the smaller peak at the start of the curve. (Agilent)

Material

- Agilent Bioanalyzer 2100 (Agilent)
- Agilent RNA 6000 Nano Kit (Agilent)

  Agilent RNA 6000 Gel Matrix

  Agilent RNA 6000 Ladder

  Agilent RNA 6000 Nano Marker

  Electrode Cleaners

RNA Nano Chips

RNA Nano Dye Concentrate

Spin filters

- Chip priming station
- RNaseZAP (Ambion)

Procedure

To avoid degradation of the analyzed RNA, the electrodes of the bioanalyzer device were decontaminated before each experiment. The wells of the electrode cleaner chip were filled with 350 µl RNaseZAP and the chip was placed in the bioanalyzer device for 1 min. Afterwards, the chip was replaced with another electrode cleaner chip containing 350 µl RNase-free water. The chip was placed in the device for 10 sec and afterwards the electrodes were dried for another 10 sec.

Furthermore, the supplied RNA ladder was prepared. Therefore, it was heat denaturated for 2 min at 70°C. Afterwards, it was cooled on ice and aliquots were prepared. The aliquots were stored on -80°C until usage. For sample preparation, a gel matrix was prepared. Therefore, 550 µl RNA 6000 Nano gel matrix was placed into the top of a spin filter. Afterwards, the tubes were centrifuged for 10 minutes at 1500 g. For creation of the gel-dye mix, 1 µl RNA 6000 Nano dye concentrate was added to 65 µl of the previously prepared gel. The mix was vortexed thoroughly and the tubes were centrifuged for 10 min at 13000 g. Afterwards, 9 µl of the gel-dye mix was pipetted to the bottom of the well marked ‘G’ on the chip. The chip was placed in a priming station and the plunger of the syringe was pushed down until the clip held it. After 30 sec, the clip was released and the plunger was allowed to return to its initial position. Afterwards, 5 µl RNA marker was added to all sample wells. In the well marked with a ladder, 1 µl of the prepared ladder was added whereas in each sample well, 1 µl of the corresponding RNA was added. The chip was vortexed and immediately analyzed using the Bioanalyzer 2100 device according to the manufacturers protocol. For data evaluation the RNA Nano program was used.

B.4.3 Gene expression microarray

Microarrays are a technology that allows the simultaneous measurement of thousands of nucleic acids in parallel. Typically, microarrays consist of DNA sequences (probes) that are covalently attached to a surface, such as a glass slide. Each probe represents a sequence of interest. Usually, RNA samples are labeled using fluorescent dyes and are hybridized to the corresponding probes during sample preparation. The probes are clustered in spots on the array and the amount of spots reflect the resolution of the array (Bumgarner, 2013). In this study, microarrays were used to analyze global mRNA expression of GBM cell lines using Agilent human 8x60k arrays which allow simultaneous processing of eight samples, each of which containing approx. 60.000 probes per array. For this, total RNA was extracted from the cells and cDNA was prepared. Afterwards, labeled cRNA was synthesized from the cDNA. The cRNA was purified and hybridized to the arrays. The slides were washed and scanned using an Agilent microarray scanner. Finally, the data was exported using the Agilent feature extraction software. An overview of the sample preparation workflow is displayed in Figure 8.

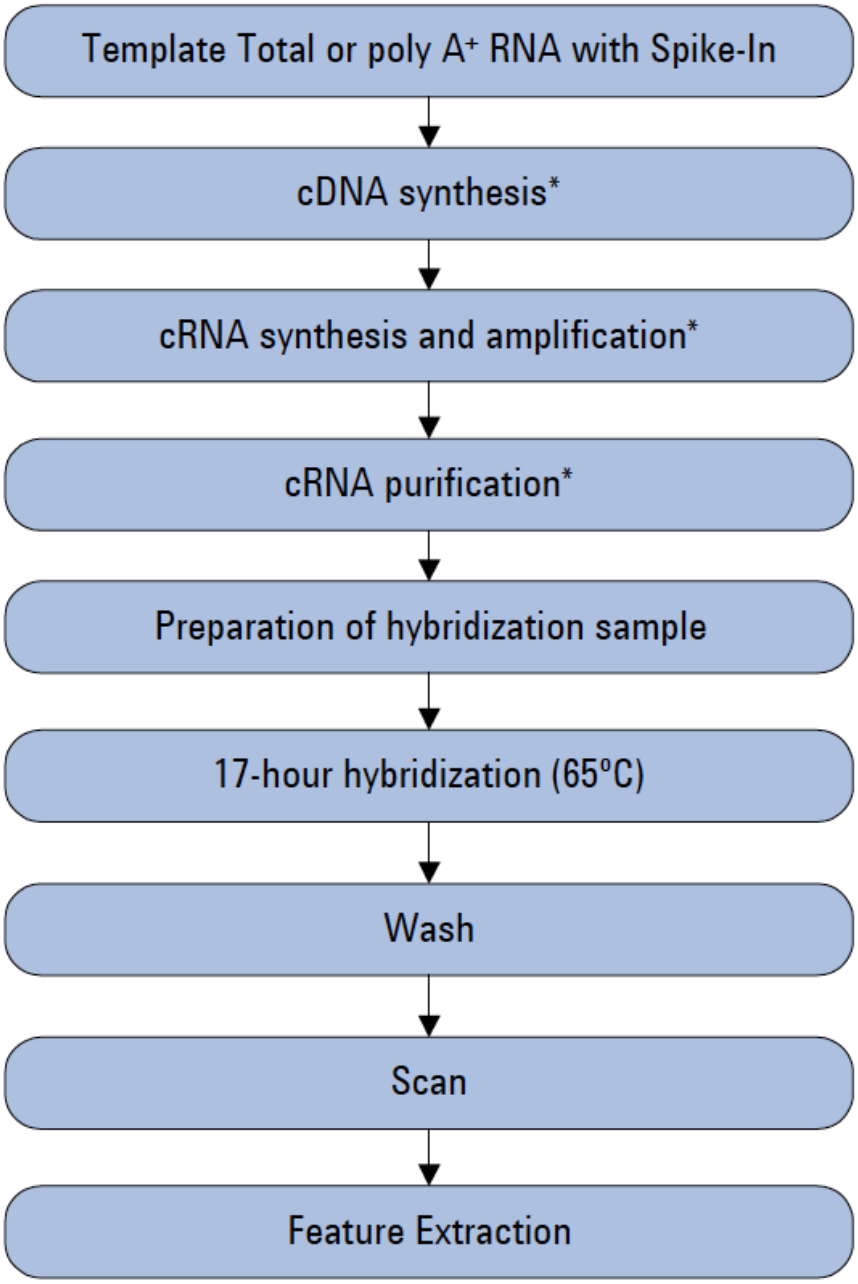

Figure 8: Workflow of an Agilent microarray analysis

In a microarray workflow, the input RNA is first converted to cDNA prior fluorescence labeling, purification and hybridization overnight at 65°C. Afterwards, the slides are washed and scanned using a microarray scanner. Finally, the data are exported using the Agilent feature extraction software. The intensity of each spot reflects expression of a gene of interest. Higher fluorescent intensities represent higher gene expression and vice versa.

Material

- Agilent Microarray Scanner (Agilent)
- DNase/RNase-free water
- Feature Extraction Software (Agilent)
- G3 Human Gene Expression 8 x 60k v3 Microarray Kit (Agilent)
- Gene Expression Hybridization Kit (Agilent)
- Gene Expression Wash Buffer (Agilent)
- GeneAmp PCR System 9700 (Applied Biosystems)
- Hybridization Chamber, stainless (Agilent)
- Hybridization gasket slides (Agilent)
- Hybridization Oven equipped with rotator (Agilent)
- Low Input Quick Amp Labeling Kit, One-Color (Agilent)
- Ozone-Barrier Slide Cover (Agilent)
- RNA Spike-In Kit, One-Color (Agilent)
- RNeasy Mini Kit (Qiagen)

Procedure

Preparation of the Spike-in mix

The spike-in mix was vortexed, incubated at 37°C for 5 min and the tube was spun down. Four dilutions of the spike mix were prepared in RNase-free water. The first dilution (1:20) was created using 2 µl spike mix and 38 µl dilution buffer. The tube was vortexed and the contents were spun down before preparation of the next dilution. The second dilution (1:25) was prepared using 2 µl first dilution and 48 µl dilution buffer. The third dilution was prepared using 2 µl second dilution and 38 µl dilution buffer whereas the fourth dilution (1:2) was prepared using 20 µl of the third dilution in addition to 20 µl dilution buffer.

Preparation of the labeling reaction

For labeling of the RNA, 50 ng samples in 1.5 µl nuclease-free water was used. 2 µl of the spike mix was added to the samples. A T7 primer mix was prepared using 0.8 µl T7 primer and 1 µl nuclease-free water. The solution was added to the samples and the tubes were incubated at 65°C for 10 min. Afterwards, the reactions were put on ice for 5 min. To generate cDNA, 2 µl first strand buffer was added to 1 µl of 0.1 M DTT and 0.5 nM dNTP mix and 1.2 µl Affinity Script RNase Block Mix. The first strand buffer was heated for 3 min at 80°C and cooled to room temperature prior use. The samples were incubated at 40°C for 2 hours and at 70°C for 15 min. Afterwards, the tubes were placed on ice and the contents were centrifuged briefly. Next, cRNA was prepared using a T7 polymerase. Therefore, a master mix was produced containing 0.75 µl nuclease-free water, 3.2 µl transcription buffer, 0.6 µl 0.1 M DTT, 1 µl NTP mix, 0.21 µl T7 RNA polymerase blend and 0.24 µl Cyanine 3-CTP. To each sample, 6 µl master mix was added and the tubes were incubated at 40°C for 2 hours.

Purification of the labeled RNA

For purification of the RNA, the samples were processed using the Qiagen RNeasy Kit. 84 µl nuclease-free water was added to the tubes and the samples were mixed with 350 µl buffer RLT. The solutions were mixed with 250 µl 100% ethanol and transferred onto RNeasy Spin Columns. After centrifugation for 30 seconds at 4°C, 13000 rpm, the flow through and collection tube was discarded and 500 µl buffer RPE was added to the column. The samples were centrifuged again as described above and the flow through was discarded. Another 500 µl buffer RPE was added onto the columns and the tubes were centrifuged for 60 seconds at 4°C, 13000 rpm. The flow through and collection tube was discarded. To elute the purified RNA, 30 µl nuclease-free water was added directly on the columns. The samples were incubated for 60 seconds and centrifuged for 30 seconds at 4°C, 13000 rpm.

Quantification of the cRNA

Quantification of the purified RNA was carried out using a Nanodrop device. The measurement was performed as described in B.2.1. In the Nanodrop software, the

options Microarray Measurement and sample type 'RNA-40' was chosen. The following values were recorded: Cyanine 3 dye concentration (pmol/µl), RNA absorbance ratio (260 nm/280 nm) and cRNA concentration (ng/µl). The yield and the specific activity of the labeled RNA was determined as:

$$\mu gofcRNA = \frac{(ConcentrationofcRNA)\, x\, 30\ \mu l\, (elutionvolume)}{1000}$$

$$PmolCy3\ per\mu gcRNA = \frac{ConcentrationofCy3}{ConcentrationofcRNA}\, x\, 1000$$

For further sample preparation, the yield must be of at least 0.825 µg and an activity of equal or greater than 6.

Hybridization

For hybridization, 600 ng of the labeled cRNA was mixed with 5 µl 10x Gene Expression Blocking Agent and 1 µl 25x Fragmentation Buffer. The samples were brought to a total volume of 25 µl using nuclease-free water. Afterwards, the tubes were incubated for 30 min at 60°C and immediately cooled on ice. 25 µl Hi-RPM buffer was carefully added to the mix by avoiding bubble formation. For loading of the slides, a clean gasket slide was placed in a hybridization chamber with the label facing up. Afterwards, 40 µl of the hybridization mix was carefully dispensed onto the chambers of the gasket slide. It was ensured that the pipette tip did not touch the surface of the slide or the walls. Any unused wells were filled with 40 µl 1x Hi-RPM Hybridization Buffer. The microarray slide was gripped on one side and slowly placed on the gasket slide. The hybridization cover was placed on top of the slide sandwich and the chamber was closed using the hybridization chamber clamp. The chamber was manually rotated to ensure all bubbles were moving freely. Stuck bubbles could be moved by gently tapping the chamber on a surface. The chamber was placed in a rotor of a hybridization oven and the samples were incubated at 65°C, 10 rpm for 17 hours.

Washing procedure

For washing of the microarrays, dedicated coplin jars for the different solutions and experiments were used. The hybridization chamber was disassembled and the array-gasket sandwich was submerged in Gene Expression Wash Buffer 1. While submerged, the slides were separated and the gasket slide was allowed to drop to the bottom of the dish. The array was transferred to a slide rack and submerged in Gene Expression Wash Buffer 1. The slides were incubated for 1 min and the slide rack was transferred to a third dish containing Gene Expression Wash Buffer 2 at 37°C. After 1 minute, the slide rack was slowly removed from the dish ensuring no droplets remained on the slide.

Figure 9: Slide in slide holder for SureScan microarray scanner

(Agilent)

The hybridized slide was carefully placed in a slide holder (Figure 9) with the "Agilent"-labeled side facing up. Afterwards, an ozone-barrier slide was carefully put on top of the array. The slide holder was closed and the arrays were immediately scanned.

Microarray scan and data collection

For scanning of the microarrays, the Agilent Scan Control software was used. In the software, the settings for one-color scans were chosen (Scan region: 61 x 21.6 mm, 5 µm scan resolution, 5 µm scanning mode: single pass, eXtended Dynamix range: (selected), Dye channel: green, Green PMT: XDR Hi 100% XDR Lo 10%). Afterwards,

the images were opened and the spots were manually evaluated for even distribution of the signals around the edges and for obvious outliers.

Microarray data extraction

Extraction of the data into a text file was carried out using the Agilent Feature Extraction software (version 11.0.1.1). The scanned images were loaded into the program and for data generation the protocol GE1_1100_Jul11 was chosen. Furthermore, the array specific grid template for 8 x 60k arrays was utilized. After the data was extracted, the quality of each spot was evaluated (Figure 10).

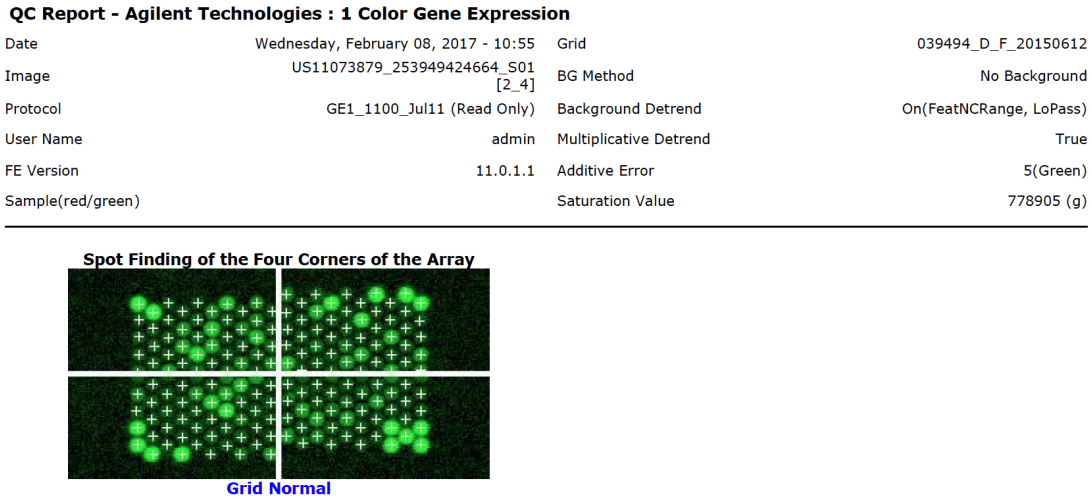

Figure 10: Example of a quality control report for one spot of the 8x60k microarray, generated by the feature extraction software

Quality report of the gene expression data generated from the A172 cell line. The utilized options of the gene extraction software are displayed in the top panel. Obvious outliers can be identified in the grid setup displayed below. For correct data extraction, the grid had to be perfectly aligned to the four corners of the spot.

B.4.4 3'-RNA sequencing

3'-RNA sequencing is a novel approach to generate gene expression values. In a first step libraries of sample RNAs are created that can be sequenced on common platforms such as the Illumina devices. This method uses total RNA as input whereas the polyadenylation tail of the mRNA is utilized to initiate library generation by oligo-dT priming. After synthesis of the first strand, the RNA template is degenerated and second strand synthesis is initiated by random priming. Consecutively, a DNA polymerase allows amplification the cDNA. Afterwards, the cDNA is purified using magnetic beads. Finally, the cDNA library is generated by amplification of the purified cDNAs. For this step, adapters required for sequencing are introduced on the forward and reverse primers.

Material

- Lexogen QUANTSEQ 3'mRNA-Seq Library Prep Kit
  First Strand cDNA Synthesis Mix 1
  First Strand cDNA Synthesis Mix 2
  Enzyme Mix 1
  RNA Removal Solution
  Second Strand Synthesis Mix 1
  Second Strand Synthesis Mix 2
  Enzyme Mix 2
  PCR Mix
  Enzyme Mix 3
  I7 Index Plate
  Purification Beads
  Purification Solution
  Elution Buffer

Procedure

Library preparation and sequencing was performed in collaboration with Steffen Heuer, Peter Weber and Theresa Heider from the Research Unit of Radiation Cytogenetics of the Helmholtz Center Munich. Sample preparation was carried out using the Lexogen Quant Seq protocol according to the manufacturer's instructions. Briefly, 40 ng total RNA was mixed with 5 µl first strand synthesis mix 1 and the samples were denatured for 3 minutes at 85°C. Afterwards, the RNA was cooled down to 42°C.

For first strand cDNA synthesis a mastermix was created using 9,5 µl first strand cDNA synthesis mix 2 and 0,5 µl enzyme mix. The mastermix was pre-warmed at 42°C and 10 µl was added to the samples. The reaction was carried out for 15 minutes at 42°C. Afterwards, the template RNA was removed by addition of 5 µl RNA removal solution and the samples were incubated for 10 minutes at 95°C and cooled down to 25°C.

For synthesis of the second strand, 10 µl second strand synthesis mix 1 was added to the cDNA and the samples were incubated for 1 minute at 98°C and cooled down to 25°C slowly at 0,5°C/second. Afterwards, the samples were incubated for 30 minutes at 25°C. A mastermix was created using 4 µl second strand synthesis mix 2 and 1 µl enzyme mix 2 and 5 µl was added to each sample. The tubes were incubated for 15 minutes at 25°C.

Purification of the cDNA was carried out using magnetic beads. To each reaction, 16 µl resuspended purification beads was added and incubated for 5 minutes at room temperature. The samples were placed on a magnet and the beads were allowed to settle on the bottom of the tubes. The supernatant was removed and 40 µl elution buffer was added to the samples. The tubes were removed from the magnet and resuspended properly. Afterwards, 56 µl purification solution was added and the samples were incubated for 5 minutes at room temperature. The tubes were placed on the magnet again and the supernatant was removed. The beads were washed twice using 120 µl 80% ethanol and the beads were allowed to dry at room temperature. To each tube 20 µl elution buffer was added and the beads were resuspended and incubated for 2 minutes at room temperature. Afterwards, the

tubes were placed on the magnet again and 17 µl purified sample was transferred into fresh PCR plates.

Finally, the cDNAs were amplified by adding adapter sequences required for sequencing. A mastermix was prepared using 7 µl PCR mix and 1 µl enzyme mix 3 and 8 µl was added to each sample. Twenty PCR cycles were performed in according to the protocol. The finished libraries were purified using magnetic beads as described above. The libraries were sequenced using an Illumina HiSeq device at the core facility of the Helmholtz Center Munich.

B.5 CRISPR-Cas9

For knockout of the mature miRNAs a CRISPR-Cas9 system was established. The knockout strategy was intended to introduce a double strand break in the mature miRNA sequence and in parallel, to introduce an expression cassette carrying an antibiotic resistance gene or a fluorescent protein via homologous recombination. Therefore, three plasmids had to be transfected in the cells, one carrying the Cas9 endonuclease, one plasmid for expression of the guide RNA and a linearized plasmid that contains the selection cassette. For this approach, a Cas9 vector (VP12) was utilized that included a Cas9 expression cassette that was co-transfected with a plasmid for guide RNA expression (MLM3636). The guide RNAs were designed to target the genomic location of the mature miRNAs. Additionally, for each miRNA, a vector was constructed that carried 1000 bp overlapping DNA sequences homologous to the immediate upstream and downstream region of the miRNAs attached to an antibiotic resistance cassette and a fluorescent protein. All described constructs had to be transfected into to the cells for a knockout of one miRNA.

B.5.1 Guide RNA design

For generation of the CRISPR guide RNAs, a tool for design and off-target prediction was utilized (crispr.mit.edu). For this purpose, the miRNA genomic locations and sequences were retrieved from the NCBI nucleotide browser (www.ncbi.nlm.nih.gov/nuccore). The positions of the miRNA precursor sequence including the 1000 bp upstream and downstream regions were downloaded in a text file. The miRNA precursor sequences were uploaded in the crispr.mit tool. The software assigns scores for possible guide RNAs that reflect the reverse probability of off-target binding. Only guide RNAs with the highest scores (>80) were subjected to cloning into the vectors.

B.5.2 Plasmid overview

Three vectors were needed for the CRISPR approach of this study, one plasmid expressing the Cas9 nuclease (VP12 Figure 11), one plasmid expressing the guide RNA (MLM3636 Figure 12) and another plasmid (pFG4-GFP Figure 13) for expression of the selection cassette. The VP12 plasmid was received from Dr. Rupert Öllinger (TU München). The plasmid was originally purchased from Addgene (Addgene plasmid #72247, Kleinstiver et al., 2016) that allows the constitutive expression of Cas9 using a CMV promoter. MLM3636 was also purchased from Addgene (Addgene plasmid #43860, unpublished) that carried a cloning site for the introduction of the target-specific guide sequence. The guide RNA was expressed under control of the RNA promoter U6. For expression of the selection cassette, the plasmid pFG4-GFP was used. With support of Randy Caldwell the plasmid was established at HMGU in the research unit Radiation Cytogenetics. The vector carried two cloning sites for introduction of the miRNA specific target arms. The construct included two loxP recombination sites for optional modification of the integrated plasmid. Two genes

for selection were part of the vector, GFP and a puromycin resistance gene that were fused via an internal ribosome entry site (IRES) sequence.

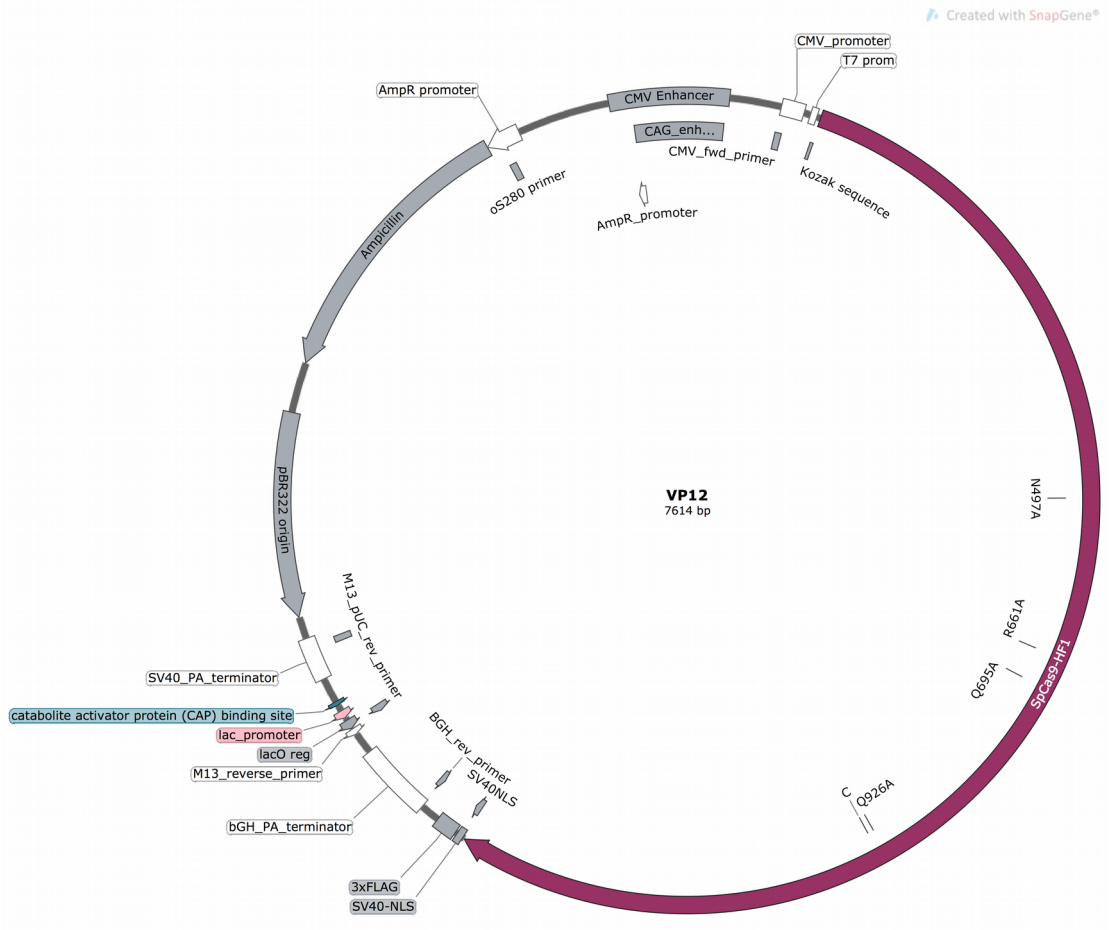

Figure 11: Overview of the Cas9 expression vector VP12

The features of the vector are displayed simplified. The vector carried the Cas9 expression cassette under control of a constitutive CMV promoter for expression in mammalian cells. For bacterial transformation and selection, an ampicillin resistance gene was present in the vector.

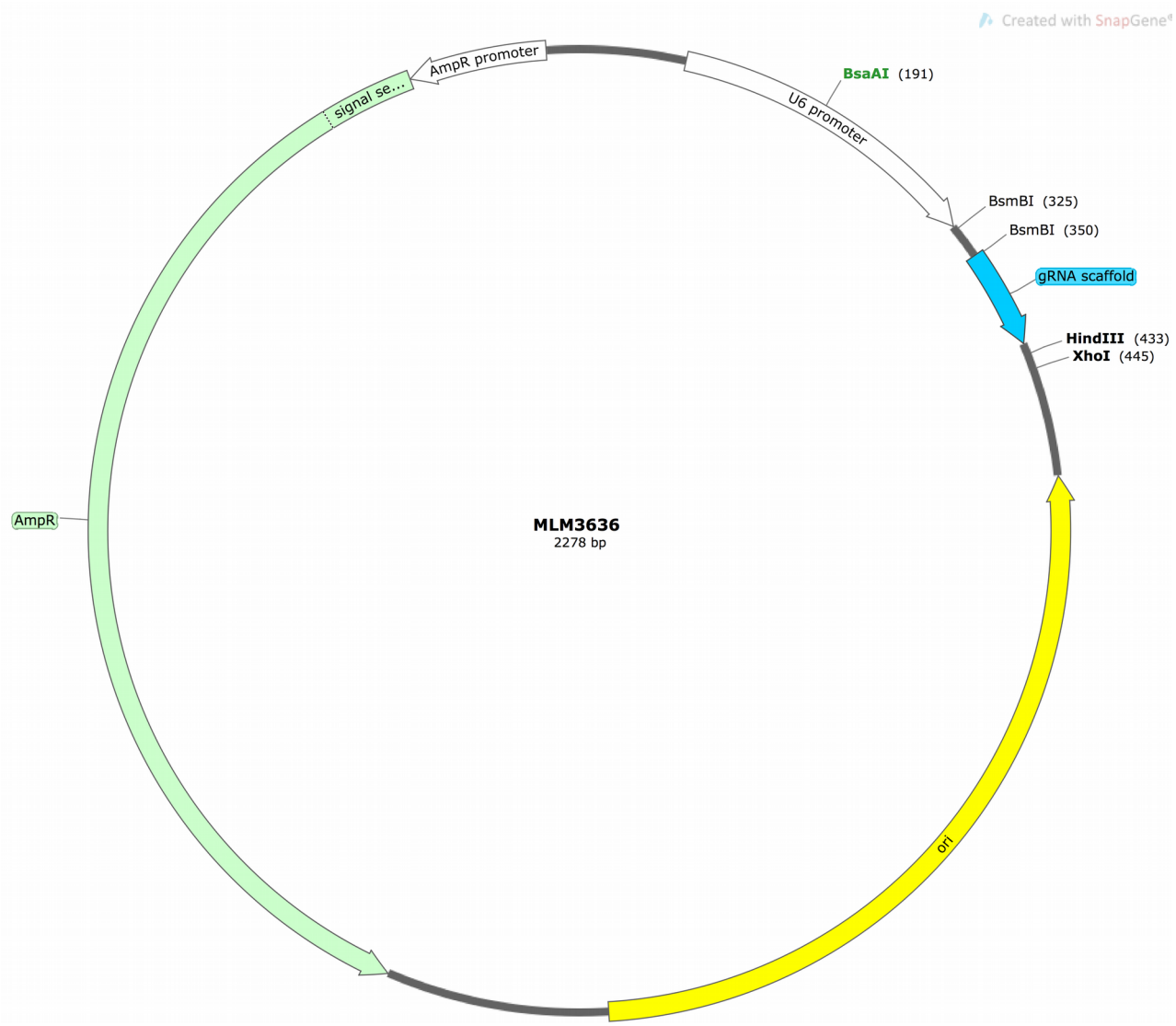

Figure 12: Overview of the guide RNA expression vector MLM3636

The features of the vector are displayed in a simplified scheme. The vector carried a cloning site for introduction of the target specific guide sequence. The guide RNA was expressed under control of the RNA promoter U6. Furthermore, for bacterial transformation and selection, an ampicillin resistance gene was present in the vector.

Figure 13: Overview of the selection cassette expression vector pFG4-GFP

The features of the vector are displayed in asimplified scheme. The vector carried two cloning sites for introduction of the miRNA specific target arms. The construct included two loxP recombination sites for optional modification of the integrated plasmid. Two genes for selection were part of the vector, GFP and puromycin resistance gene fused via an IRES sequence. Furthermore, for bacterial transformation and selection, an ampicillin resistance gene was present on the vector.

B.5.3 Plasmid linearization and purification

Material

- BsmBI (NEB)
- GeneJET PCR purification Kit (Thermo Fisher)

  DNA Binding buffer

  Wash buffer (100% ethanol added prior use)

  Elution buffer

  GeneJET Purification Columns
- Centrifuge Biofuge pico (Heraeus)
- RNase/DNase-free water
- Alkaline Phosphatase, Calf Intestinal (CIP) (NEB)
- BamHI-HF (NEB)
- NEBuffer 3.1

Procedure

For linearization of the plasmids, MLM3636 was digested using the restriction enzyme BsmBI at 55°C, pFG4-GFP was digested using BamHI-HF at 37°C. For the reaction, 20 µl of the plasmid was added to 5 µl NEBuffer 3.1, 23 µl RNase/DNase-free water and 2 µl of the respective enzymes. The reaction was incubated over night at the respective temperatures. To avoid self ligation of the plasmids, 1 µl CIP was added to each reaction and the vectors were incubated at 37°C for one hour. Afterwards, 50 µl binding buffer was added to each reaction and the mixture was transferred onto a GeneJET purification column. The samples were centrifuged at 12000 g for 1 min and the flow through was discarded. Afterwards, 700 µl wash buffer was added to the columns and the samples were centrifuged at 12000 g for 1 min. The flow through was discarded and the columns were centrifuged again to dry the membranes. To elute the DNA, 35 µl elution buffer was added directly on the membranes and the samples were incubated for 1 min. Afterwards, the columns were centrifuged at 12000 g for 1 min and the DNA concentration was measured using a Nanodrop device as described in B.3.1.

B.5.4 Gibson cloning

Gibson cloning is an alternative technique that allows vector/insert cloning without the need of specific restriction enzymes. It can also be used for sequential cloning of multiple fragments in one step. The protocol requires overlapping DNA fragments and utilizes a 5' exonuclease, a DNA ligase and a DNA polymerase for combining the fragments (Gibson et al., 2009).

Material

- 100 mM dATP (NEB)
- 100 mM dCTP (NEB)
- 100 mM dGTP (NEB)
- 100 mM dTTP (NEB)
- 100 mM NAD (NEB)
- 1M DTT (Sigma-Aldrich)
- 1M Tris-HCl pH 7.5 (Sigma-Aldrich)
- 2M $MgCl_2$ (Sigma-Aldrich)
- PEG-8000 (Sigma-Aldrich)
- Phusion DNA polymerase (NEB)
- T5 exonuclease (NEB)
- Taq DNA ligase (NEB)

Procedure

On a first step, a 5x ISO buffer was created:

3 ml	1M Tris-HCl pH 7.5
150 µl	2M $MgCl_2$
60 µl	of each 100 mM dNTPs (dGTP, dCTP, dATP, dTTP)
300 µl	1M DTT
1.5 µg	PEG-8000

300 µl	100 mM NAD
up to 6 ml	dH_2O

The 5x ISO buffer was divided in 320 µl aliquots and stored at -20°C.

In a second step, the Gibson assembly master mix was produced:

320 µl	5x ISO Buffer
0.64 µl	10U/µl T5 exonuclease
20 µl	2U/µl Phusion polymerase
160 µl	40U/µl Taq polymerase
699 µl	dH_2O

The Gibson master mix was stored at -20°C in 15 µl aliquots. For each reaction one aliquot is used.

B.5.4.1 PCR-amplification of the homologous arms

Material

- 10 mM dNTP Mix (Fermentas)
- 10x Crezol Red
- 5x Q5 reaction buffer (NEB)
- 100 µM Primer (B.4.11) (Sigma-Aldrich)
- Agarose gel (1-2%)
- Centrifuge Biofuge pico (Heraeus)
- DMSO (NEB)
- GeneAmp PCR System 9700 (Applied Biosystems)
- GeneJET PCR purification Kit (Thermo Fisher)
  DNA Binding buffer
  Wash buffer (100% ethanol added prior use)
  Elution buffer

GeneJET Purification Columns

- Q5 high fidelity DNA polymerase (NEB)
- TE buffer
- U87-MG genomic DNA

Procedure

The amplification of the homologous arms was carried out using purified U87-MG genomic DNA. The primers used are displayed in B.4.11 and one primer pair was designed for each 5'- and 3'-arm for the respective miRNAs.

The PCR setup was as following:

10 µl	Q5 reaction buffer
5 µl	Crezol Red
1 µl	10 mM dNTPs
1 µl	DMSO
1 µl	25 µM forward primer
1 µl	25 µM reverse primer
0.5 µl	Q5 high fidelity DNA polymerase
29.5 µl	H_2O

The following PCR program was used:

98°C for 30 sec

98°C for 10 sec

60°C for 20 sec

72°C for 60 sec

These steps were repeated for 35 cycles

72°C for 120 sec

4°C hold

The resulting PCR products were analyzed on an 1% agarose gel (90V, 45min). The DNA fragments with the correct size (approx. 1000 bp) were removed from the gel

and the samples were purified using the GeneJET PCR purification Kit as described in B.5.3.

B.5.4.2 Ligation and transformation

Material

- 100 µM Primer (B.4.11) (Sigma-Aldrich)
- *E. coli*-DH5α (NEB)
- Gibson master mix
- Guide RNA Primers
- LB agar plates containing ampicillin
- Linearized vectors
- PCR products of the homologous arms
- SOC outgrowth medium (NEB)
- STE buffer
- Viia 7 (ThermoFisher)

Procedure

For cloning of the guide RNA, two primer for each miRNA (details of the used primers displayed in B.4.11) were annealed in a thermocycler. Therefore, 2 µl of each forward and reverse primer was added to 2 µl STE buffer and 14 µl H_2O. The mixture was incubated in a Viia 7 machine at 95°C for 5 min and afterwards the temperature was decreased by exactly 1°C per 30 sec down to 25°C. The primer duplexes were diluted 1:500 (to approx. 0.02 pmol) using H_2O. For Gibson cloning, the linearized vectors and the inserts were mixed in equimolar amounts using the following formula:

$$pmols = (weight\ ng)\ x\ 1{,}000/(basepairs\ x\ 650\ daltons)$$

For each ligation, a 15 µl Gibson master mix aliquot was thawed and 5 µl of the equimolar vector/insert mixture was added. The samples were incubated at 50°C for

60 min. For transformation of the ligation mix in *E. coli*-DH5α, the bacteria were thawed on ice for 30 min. Afterwards, 2 µl of the ligation mix was added to 25 µl of the *E. coli* suspension. The bacteria were heat-shocked at 42°C for exactly 45 sec and the tubes were placed on ice for 2 min. 500 µl SOC outgrowth medium was added to the samples and the bacteria were incubated at 37°C for one hour. Afterwards, the suspension was plated on pre-warmed LB agar plates containing ampicillin. The plates were incubated at 37°C over night. Single colonies were picked and transferred into 96-well plates containing 100 µl LB medium with ampicillin. The bacteria were incubated over night and the clones were analyzed as described in B.5.9.

B.5.5 Small scale plasmid preparation

Material

- Centrifuge Biofuge pico (Heraeus)
- GeneJET Plasmid Miniprep Kit (Thermo Fisher)
  Resuspension solution with RNase
  Lysis Solution
  Neutralization Solution
  Wash Solution with 100% ethanol
  Elution Buffer
  GeneJET Spin Columns
  Collection Tubes 2 ml

Procedure

For plasmid preparation, 50 µl of the picked clones were transferred into centrifugation tubes containing 2 ml LB medium with ampicillin. After incubation at 37°C over night, the cultures were transferred into 2 ml Eppendorf tubes and centrifuged at 8000 rpm for 2 min. 250 µl resuspension solution was added to the pellet and the tubes were mixed until the bacteria were resuspended. 250 µl lysis buffer was added to the suspension and the reaction was stopped using 350 µl

neutralization buffer. The tubes were centrifuged at 12000 g for 5 min and the supernatant was transferred onto a GeneJET spin column. The samples were centrifuged at 12000 g for 1 min and the column was washed twice using 500 µl wash buffer. For each wash step, the samples were centrifuged at 12000 g for 1 min and the flow through was discarded. The column was centrifuged once more to remove residual ethanol. Afterwards, 50 µl elution buffer was pipetted onto the membrane and the samples were incubated for 2 min. To elute the DNA, the columns were centrifuged for 2 min and the concentration of the DNA was measured using a nanodrop device as described in B.3.1.

B.5.6 Large scale plasmid preparation

Material

- Centrifugation cups
- Centrifuge Multifuge 3 S-R (Heraeus)
- Centrifuge pico (Heraeus)
- Chloroform (Merck)
- Ethanol 70% (Merck)
- Falcon Tubes 50 ml (BD Falcon)
- Isopropanol (Merck)
- LyseBlue reagent (Qiagen)
- Qiagen Plasmid Purification Maxi Kit (Qiagen)

  Resuspension buffer P1

  Lysis buffer P2 (LyseBlue reagent added)

  Neutralization buffer P3

  Column equilibration buffer QBT

  Wash buffer QC

  Elution buffer QF
- TE buffer

Procedure

For generation of larger amounts of plasmids, 400 ml LB medium containing ampicillin was inoculated with bacteria grown from one colony. The cultures grew overnight and the suspension was transferred into a centrifugation vessel and centrifuged at 4000 rpm for 30 min. The supernatant was discarded and the pellet was resuspended in 10 ml buffer P1 and transferred into 50 ml falcon tubes. Afterwards, 10 ml buffer P2 was added and the samples were incubated for 5 min. The reaction was stopped by adding 10 ml buffer P3 and the samples were incubated on ice for 20 min. Afterwards, 750 µl cooled chloroform was added to the samples and the tubes were centrifuged at 4000 rpm 4°C for 30 min. Meanwhile, the purification columns were equilibrated using 10 ml buffer QBT and 10.5 ml isopropanol was placed in a 50 ml elution tube. After centrifugation, the supernatant was carefully transferred onto the purification columns, avoiding carry over of cell debris. The columns were washed twice with wash buffer QC and the plasmids were eluted into the prepared elusion tube using 15 ml elution buffer QF. The tubes were mixed thoroughly and centrifuged at 4000 rpm 4°C for 30 min. The supernatant was carefully discarded and the pellet was washed with 1 ml 70% ethanol and centrifuged again at 4000 rpm 4°C for 5 min. The supernatant was discarded and the pellet was air dried for 30 min. Afterwards, 300 µl TE buffer was added and the samples were resuspended over night at 4°C. The DNA concentration was measured as described in B.2.1 and the plasmids were diluted to a final concentration of 1 µg / µl.

B.5.7 Screening of positive clones

B.5.7.1 Restriction analysis

Material

- Agarose gel 1%
- Restriction enzyme BamHI-HF (NEB)
- Purified plasmids
- NEBuffer 3.1
- RNase/DNase-free water
- TE buffer

Procedure

The correct assembly of the pFG4-GFP plasmid with homologous arms was analyzed by restriction enzyme digest. Therefore, 5 µl of the purified plasmid as described in B.4.7 was mixed with 2 µl NEBuffer 3.1, 0.2 µl BSA, 1 µl BamHI-HF and 11.8 µl H_2O. The samples were incubated for 2 hours at 37°C and the DNA fragments were analyzed on a 1% agarose gel (90V, 45min).

B.5.7.2 Sanger Sequencing

Material

- 96-well PCR plates (Applied Biosystems)
- BigDye Terminator Sequencing Kit (Applied Biosystems)
- DEPC H_2O
- DMSO (Sigma-Aldrich)
- DNA sequencer ABI 3730 (Applied Biosystems)
- EDTA 125 mM
- Ethanol 100% and 70% (Merck)
- GeneAmp PCR System 9700 (Applied Biosystems)

- Primer 100 µl (Sigma-Aldrich) see B.4.12
  OS280 forward
  MLM3636-rev-seq reverse
- SnapGene software

Procedure

For confirmation of the correct assembly of the produced plasmids, Sanger sequencing was performed. Therefore, 200 ng plasmid DNA was mixed with 0.4 µl primer, 0.5 µl DMSO, 4.1 µl DEPC H_2O, 1 µl BDT Sequencing buffer and 2 µl Ready Reaction Mix BigDye. The PCR mix was dispersed in 96-wells and the plates were incubated in a thermo cycler using the following protocol:

95°C for 4 min
95°C for 15 sec
50°C for 10 sec
60°C for 4 min
These steps were repeated for 40 cycles
4°C hold

Afterwards, 2.5 µl 125 mM EDTA was added to each well. The plates were centrifuged at 4000 g for 2 min and 30 µl 100% ethanol was added to the wells. The samples were incubated for 15 min at room temperature and the plates were centrifuged at 4000 g for 30 min at 4°C. The liquid was removed from the wells by gently tapping on a paper towel and another 50 µl 70% ethanol was added to the wells. Afterwards, the ethanol was removed again by gently tapping on a paper towel. The plates were centrifuged briefly to collect the contents on the bottom of the wells and the PCR products were resuspended in 40 µl H_2O. Sequencing was carried out using an ABI 3730 DNA sequencer at the GAC (Genome Analysis Center) of the Helmholtz Center Munich. The resulting sequence information was analyzed using the SnapGene software.

B.5.8 T7 endonuclease assay

T7 endonuclease assay was used for identification of successful knockout events in transfected cell pools. The assay utilizes an enzyme that specifically cuts DNA mismatches. Briefly, PCR was performed that amplified a region of interest where base pair modification was expected. The PCR products were denatured and reannealed which created heteroduplexes of wild type and knockout PCR products. These heteroduplexes contained bulges that were cut by the T7 endonuclease, creating two short fragments. Afterwards, the samples were analyzed using an agarose gel. In the case of a successful knockout, one large band and two smaller bands were visible on the gel (Figure 14).

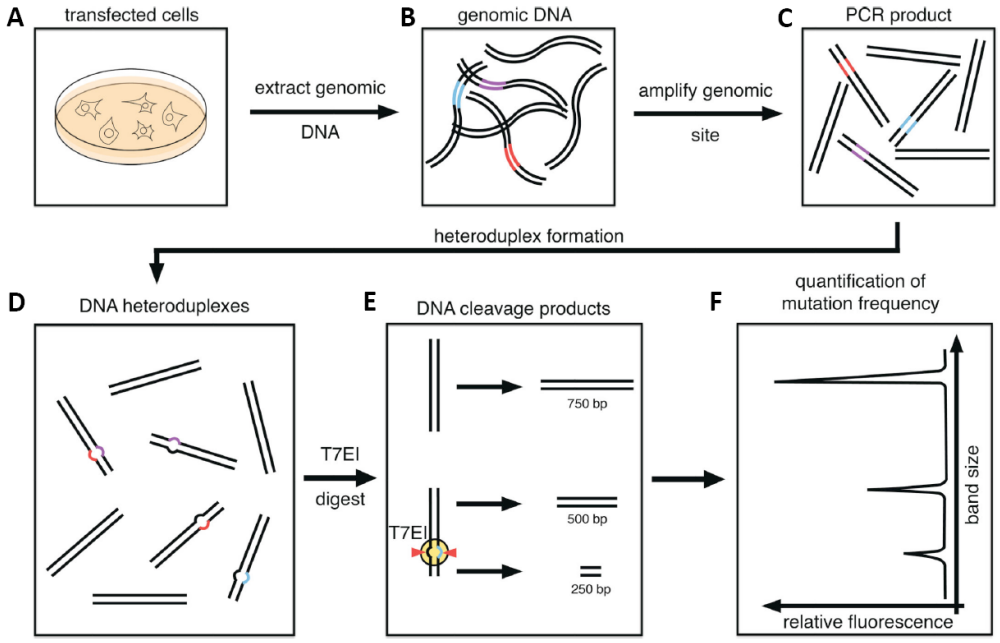

Figure 14: Schematic overview of the T7 endonuclease assay

The protocol required transfected cells with introduced genomic modifications (A). Genomic DNA was extracted from the cells (B) and a PCR was performed spanning the site of the desired modifications (C). The PCR products contained heterogeneously wild type and knockout sequences. The fragments were heated and realigned forming DNA heteroduplexes (D). T7 endonuclease specifically cleaves DNA mismatches that resulted in fragmentation of the knockout PCR products (E). The size differences were visualized on an agarose gel (F) (modified from Wyvekens et al., 2015).

Material

- 10 mM dNTP Mix (Fermentas)
- 10x Crezol Red
- 5x Q5 reaction buffer (NEB)
- 100 µM Primer (Sigma-Aldrich)

  7a-fwd-2 (Table 3)

  7a-rev-2 (Table 3)

  7b-fwd-2 (Table 3)

  7b-rev-2 (Table 3)

  125a-fwd-1 (Table 3)

  125a-rev-1 (Table 3)
- Agarose gel 2%
- Centrifuge Biofuge pico (Heraeus)
- DMSO (NEB)
- GeneAmp PCR System 9700 (Applied Biosystems)
- NEBuffer 2 (NEB)
- Q5 high fidelity DNA polymerase (NEB)
- T7 endonuclease I (NEB)
- TE buffer
- Viia 7 PCR device (Thermo Fisher)

Procedure

Cells were co-transfected using one of the cloned MLM3636 plasmids for let-7a-1, let-7b and miR-125a targeting and the VP12 plasmid. Transfection of the cells was performed as described in B.1.7.3. After 48 hours, the cells were harvested and genomic DNA was isolated as described in B.2.4. For each target site, one PCR reaction was performed in addition to a negative transfection control and a negative PCR control:

10 µl	genomic DNA template
10 µl	Q5 reaction buffer

5 µl	Crezol Red
1 µl	10 mM dNTPs
1 µl	DMSO
1 µl	25 µM forward primer
1 µl	25 µM reverse primer
0.5 µl	Q5 high fidelity DNA polymerase
20.5 µl	H_2O

The following PCR program was used:

98°C for 30 sec

98°C for 10 sec

72°C for 20 sec ramp down 1°C per cycle to 62°C

72°C for 60 sec

These steps were repeated for 10 cycles

98°C for 10 sec

62°C for 20 sec

72°C for 60 sec

These steps were repeated for 20 cycles

72°C for 120 sec

4°C hold

The PCR reactions were purified using the GeneJET purification protocol as described in B.5.3 and the DNA concentrations were measured using a nanodrop device as described in B.2.1. For the generation of DNA heteroduplexes, 200 ng purified PCR product was mixed with 2 µl NEBuffer 2 and the DNA was denatured and hybridized in a Viia 7 device using the following protocol:

95°C for 5 min denature

95°C ramp down at 2°C/sec for 5 sec

85°C ramp down at 0.1°C/sec for 10 min

The samples were put on ice and 1 µl T7 endonuclease was added to the tubes. Cleavage of the DNA was performed at 37°C for 15 min using a GeneAmp PCR device. Afterwards, the samples were immediately put on ice and the reaction was stopped adding 2 µl 0.25M EDTA to each sample. The samples were loaded on a 2% agarose gel (90V, 45min) and the resulting fragments were analyzed.

B.5.11 Survival of cells after puromycin treatment

A selection of clones that carry a double strand break in the genomic miRNA locations and have integrated the selection cassette was performed by antibiotic treatment. In this assay, the antibiotic concentration necessary for killing all non-transfected cells over the period of one week was analyzed.

Material

- 6-well cell culture dishes (Greiner)
- Culture medium DMEM Glutamax (Thermo Fisher), supplemented with 10% FCS (Sigma-Aldrich) and 1% Penicillin/Streptomycin (Thermo Fisher)
- Microscope (Olympus)
- Puromycin stock 1 mg/ml (Invitrogen)

Procedure

The effect of puromycin on the cells was analyzed by a growth-curve. Therefore, the cells were seeded in 6-well plates with different concentrations of puromycin. The final concentrations used were: 0 µg/ml (control), 0.25 µg/ml, 0.5 µg/ml, 0.75 µg/ml, 1 µg/ml, 2 µg/ml and 5 µg/ml. The cells were observed over a period of one week and the medium was replaced with fresh medium after 3 days and 5 days. On each day the cells were observed using a microscope and the fraction of the surviving cells was analyzed.

C Results

In this thesis a prognostic 4-miRNA signature was characterized and the cellular function of these miRNAs was analyzed. The strategy of the study was to utilize seven established in vitro GBM models and to modulate the miRNA expression for studying mRNA co-expressions enabling an identification of potential targets of the miRNAs. As a first step, a seven GBM cell line panel was characterized at different molecular levels and functional phenotypes to find the most optimal model system for the following experiments. Emphasis was put on cytogenetic and transcriptomic features of the cell lines as well as various phenotypic properties like the response to ionizing radiation and TMZ. Afterwards, a transient overexpression and knock down system for the miRNAs was established and the modulated cell lines were analyzed by global 3'-mRNA sequencing. Additionally, a stable CRISPR/Cas9 knockout system was established.

C.1 Cell line characterization

For the characterization of the 4-miRNA signature, a GBM cell line panel was analyzed to find the most optimal cell lines for a functional analysis of the miRNAs of the signature by using appropriate in vitro assays. For intended modification of miRNA expressions, various features of the cell lines were of special interest like the complexity of the karyotypes, the different responses towards in vitro ionizing radiation and TMZ treatment, global gene expression profiles and the related classification into GBM-specific subtypes. Seven of the most prominent cell lines in GBM research were selected for this thesis and were subsequently characterized: A172, LN18, LN229, T98G, U87, U138 and U251. After identification of the optimal in vitro model system, the expression of the 4-miRNAs was modified by transient siRNA transfection and later by stable CRISPR/Cas9 knockout. In advance of implementation of genetic and functional experiments an unambiguously authentication of the selected cell lines was mandatory.

C.1.1 STR-typing for authentication of the GBM cell lines

The cell lines were obtained from ATCC (A172, LN18, LN229, T98G, U87-MG) and CLS (U138-MG and U251-MG) in the frame of a collaboration project with Prof. Kirsten Lauber from the Department of Radiation Oncology of the LMU University Hospital Munich. STR-typing for analyzing the genomic repeats of nine STR markers was performed to verify to origin of the cell lines. We found that all analyzed STR-markers (Table 5) matched the corresponding database from the biorepository center "Deutsche Sammlung von Mikroorganismen und Zellkulturen GmbH" (www.dsmz.de) entries. Notably, the U251-MG cell line shows STR-markers identical to SNB-19, U373 and TK1 cell lines which presents an unambiguous identification (Torsvik et al., 2014).

Table 5: Overview of the STR-typing of seven glioblastoma cell lines

Cell line	Marker	AMEL	CSF1PO	D13S317	D16S539	D5S818	D7S820	TH01	TPOX	vWA
A172	Allele 1	X	9	11	12	11	11	6	8	20
	Allele 2	Y	12	11	12	12	11	9.3	11	20
LN18	Allele 1	X	12	12	11	11	8	9	8	17
	Allele 2	Y	12	13	13	13	10	9	8	18
LN229	Allele 1	X	12	10	12	11	8	9.3	8	16
	Allele 2	X	12	11	12	12	11	9.3	8	19
T98G	Allele 1	X	10	13	13	10	9	7	8	17
	Allele 2	Y	12	13	13	12	10	9.3	8	20
U87-MG	Allele 1	X	10	8	12	11	8	9.3	8	15
	Allele 2	X	11	11	12	12	9	9.3	8	17
U138-MG	Allele 1	X	12	9	12	11	9	6	8	18
	Allele 2	Y	12	11	13	11	9	6	8	18
U251-MG*	Allele 1	X	11	10	12	11	10	9.3	8	16
	Allele 2	Y	12	11	12	12	12	9.3	8	18

Analyzed alleles according to CODIS (Combined DNA index system) whereas numbers shown represent the individual repeats of the allele. X and Y depicts whether the respective gonosome is present. Turquoise marker represents matching features as reported in the DSMZ database (www.dsmz.de). *Other cell lines that show an identical STR-profile including SNB-19, U373-MG and TK-1.

C.1.2 GBM cell lines harbor complex karyotypes and structural aberrations

Spectral karyotyping analysis of the individual karyotypes was performed in collaboration with Isabella Zagorski from the Research Unit Radiation Cytogenetics at the Helmholtz Center Munich. The ploidy of the cell lines as well as numerical and structural chromosome aberrations were analyzed. Despite all cell lines were anticipated to originate from the same tumor type, the karyotypes were highly variable among the cell lines. Exemplary karyotypes of each cell line are shown in Figure 15. Clonal aberrations are depicted in Table 6. The ploidy ranged from near-diploid (U87-MG) to near-hexaploid (T98G). Additionally, subclones were present in A172, LN18, LN229, U87-MG and T98G cell lines while no subclones were identified in U138-MG and U251-MG cell lines.

The A172 cell line showed a near-tetraploid karyotype with two subclones present in the cell line. Two subclones were also present in the hypotriploid LN18 cell line. LN229 and T98G showed the highest ploidy with a hypotetraploid and hypohexaploid karyotype, respectively. Additionally, subclones could be detected in both cell lines. In contrary, the cell line U87-MG showed a near-diploid karyotype. Nevertheless, two subclones with different aberrations could be identified in this cell line as well. Notably, the cell lines U138-MG and U251-MG showed a hypotriploid karyotype with consistent chromosomal aberrations. Typical chromosomal changes in GBM are gains in chromosome 7 (Bigner et al., 1988) and loss of heterozygosity in chromosome 10 (Ohgaki and Kleihues, 2007). Amplifications of chromosome 7 were found in all cell lines except in U87-MG. In contrary to the loss of heterozygosity, which was only found in the U87-MG cell line.

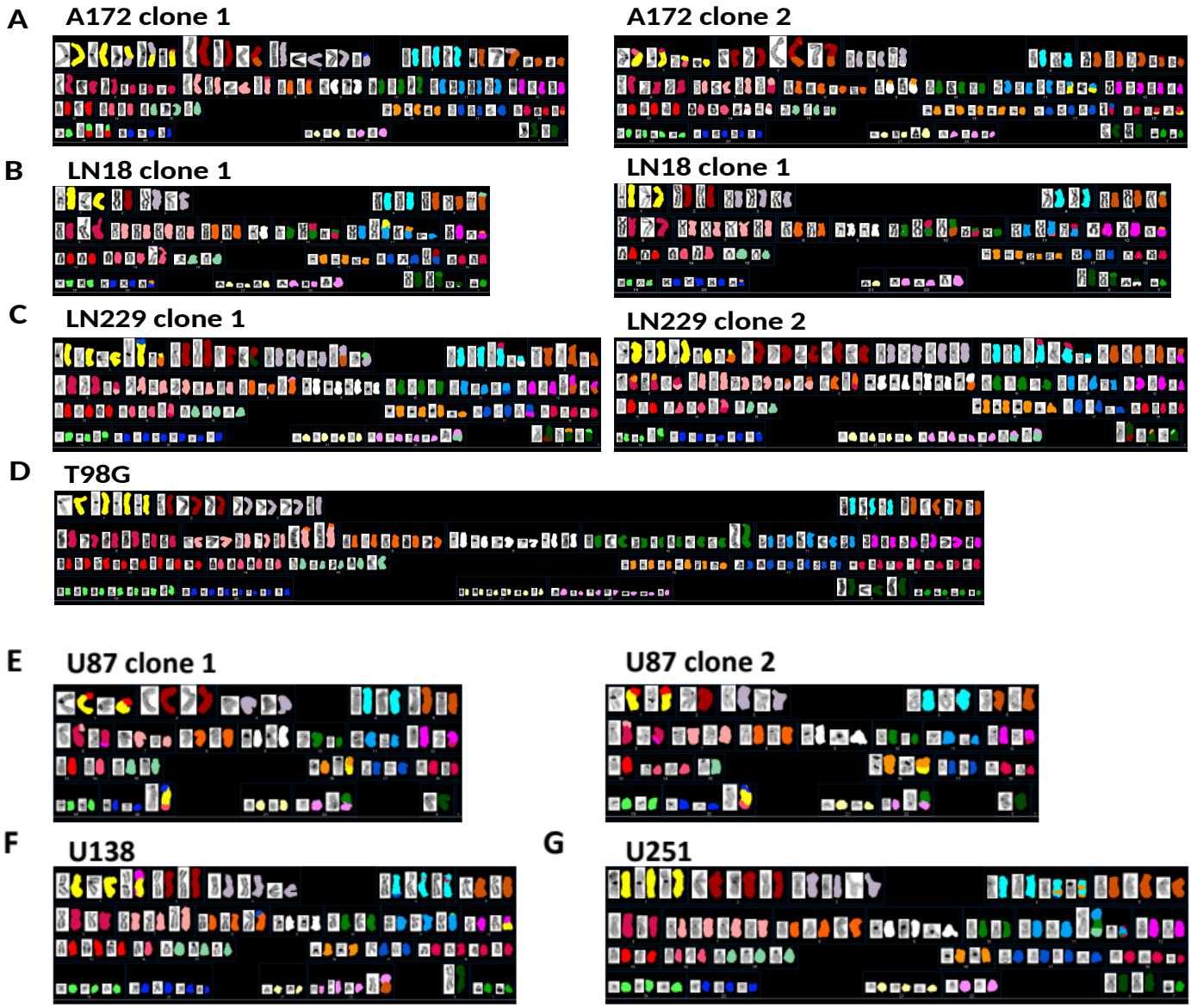

Figure 15: SKY karyotyping of GBM cell lines

Representative karyograms of each cell line after SKY analyses. Each chromosome was displayed in an individual false color along with DAPI-banded chromosomes. Color junctions indicate chromosomal aberrations. The respective karyotypes are described below.

A. A172 karyotypes

71,X,+X,Y,Y,+der(1)t(1;3)(q12;?),+der(1)(1;3)(p12;?),+der(3)t(1;6)(p12;?),+der(2)t(2;5)(q31;?),+3,+der(3)t(3;20)(p12.2;?),
+4,der(5)t(3;5)(?;p11),del(5)(q15)x2,+6,del(6)(q13)x2,+del(6)(q11),+7,+der(7)t(6;7)(?;p13),der(8)t(6;8)(?;p11),
+10,+11,+11,+12,+15,+16,+17,+der(18)t(8;18)(?;q21.1),der(19)t(14;19)(?;q13),+der(19)t(14;19)(?;q13),+20

83,X,+X,Y,+Y,der(1)t(1;14)(p13;?),der(1)t(1;18)(p22;?),+der(1)del(1)(p11)t(1;14)(q21;?),+del(1)(p22;q11),+der(2)t(2;5)
(q31;?)x2,+der(3)(3;9)(q25;?),+5,+der(5)del(5)(q15)t(2;5)(?;p13)x2,+6,+7,+der(7)t(6;7)(q22;?),del(8)(q23),+del(8)(q11),+del(8)
(q13),der(9)t(9;16)(p11;?)x2,+10,+11,+der(11)t(1;11)(?;p11)x2,+12,+12,+13,+der(14)t(9;14)
(?;q13)x2,+15,+16,+16,+16,+17,+der(17)t(17;18)(q11;?),der(18)t(1;18)(?;q21),+der(18)t(1;18)(?;q21),+19,+19,+20,+20,add(21)
(q21),+22

B. LN18 karyotypes

58,XY,+t(x;10)(q?,q11),+t(x;9)(p?;p?);+t(5;15)(p13;q?),+7,+7,t(6;10)(q11;q?),+t(6;10)(p11;p?),t(1;11)(q?;q?),+t(11;16)(q?;p11),
+del(11)(q11),t(12;16)(q?;p11),+14,+i(1;6)(p10),t(2;17)(p11;q?),t(16;20)(p11;q?),+21,+add(22)(q?)

61,XY,+t(x;10)(q?;q11),+t(x;9)(p?;p?),+3,+t(5;15)(p13;q?),+7,+7,t(6;10)(q11;q?),+t(5;10)(q11;q?),+t(6;10)(p11;p?),+t(10)
(p10),t(11;14)(q?;?),+t(11,18)(q?;q11),+t(12;16)(q?;p11),+20,+t(16;20)(p11;q?)+add22(q?)

C. LN229 karyotypes

76,XXX,der(X)t(X;2)(q23;?),der(X)t(X;16)(p11;?),+der(X)t(X;19)(p21;?),+1,+der(1)t(1;17)(p32;?),+der(1)t(1;8)(?;q11),
+2,+der(2)t(X;2)(?;q22),+3,+der(3)t(3;5)(q12;?),+der(3)t(3;19)(p12;?),+der(4)t(4;6)(p14;?),+der(4)t(4;9)(q11;?),+der(5)t(5;8)
(q14;?),+der(6)t(6;7)(?;?),+7,+7,+7,i(8)(p10),+der(8)(t8;22)(p22;?),+9,+9,+10,+der(11)t(11;17)(q14;?),+der(12)t(5;12)(?;q15),
+der(12)t(5;12)(?;q12),+13,+der(14)t(14;18)(q24;?),+15,+16,+del(16)(p11),+der(17)t(12;17)(?;q21),+18,+der(19)t(X;19)(?;q12),
+20,+20,+20,+20,+21,+21,+22,+22,+der(22)t(15;22)(?;p12)

D. T98G karyotype

131,XY,+X,+X,+Y,+Y,+Y,+mar trc(7;7;7)(q?;p?;p?)x2,+t(7;8)(q?;p?)x2,+mar dic(10;10)(q?;q?)x1,+i15(q10)

E. U87-MG karyotypes

44,X,X,t(1)(1:13)(p22;p?)x2,der(6)t(6;7)(p21;p?),der(6)t(6;12)(q23;?),del(7)(q10),del(10)(q21),der(12)t(6;12)(?;q22),-13,-
14,der(16)t(1;16)(?;q13),del(20)(p11),+der(20)t(1;14;20)(?;?;q12),t(22)(10;22)(?;p12)

43,X,-X,t(1)(1;13)(p22;p?)x2,-2,der(6)t(6;7)(p21;p?),der(6)t(6;12)(q23;?),del(10)(q21),del(11)(q11),der(12)t(6;12)(?;q22),-13,-
15,dic(16)(16;16),der(16)t(1;16)(?;q13),del(20)(p11),+der(20)t(1;14;20)(q12;?;?),der(22)t(10;22)(?;p12)

F. U138-MG karyotype

61-62,XYY,+Y,+der(1)t(1;12)(p31;?),+3,der(4)t(4;17)(q32;?),ins(4)(4;14;4)(p15;?;p13)x2,+7,+der(8)t(8;17)(p21;?),
+der(11)t(11;19)(p13;?),der(12)t(1;12)(?;q14),+13,-14,+15,+18,+der(18)t(6;18)(?;q12),+del(19)(p12),
+20,+20,+22,+der(22)t(5;22)(?;q11)

G. U251-MG karyotype

66,XXY,+1,+2,+3,+insdic(4;16;4;20)(q12;p11::q?;q?;q?),ins(4)(4;16;4;16)(p?;q?;q?;q?),+5,+7,+7,+iso(8)(q10),
+9,+der(11)t(10;11;15)(q10;q?;q?),+der(11)t(6;10;11)(q?;q?;q?),+15,+17,+17,+del(18)(q12),+19,+20,+21

Table 6: Overview of cytogenetic characteristics of A172, LN18, LN229, T98G, U87-MG, U138-MG and U251-MG cells

Cell line	Predominant clonal karyotype	Subclones
A172	83,X,+X,Y,+Y,der(1)t(1;14)(p13;?),der(1)t(1;18)(p22;?),+der(1)del(1)(p11)t(1;14)(q21;?),+del(1)(p22;q11),+der(2)t(2;5)(q31;?)x2,+der(3)(3;9)(q25;?), +5,+der(5)del(5)(q15)t(2;5)(?;p13)x2,+6,+7,+der(7)t(6;7)(q22;?),del(8)(q23),+del(8)(q11),+del(8)(q13),der(9)t(9;16)(p11;?)x2,+10,+11,+der(11)t(1;11) (?;p11)x2,+12,+12,+13,+der(14)t(9;14)(?;q13)x2,+15,+16,+16,+16,+17,+der(17)t(17;18)(q11;?),der(18)t(1;18)(?;q21),+der(18)t(1;18)(?;q21), +19,+19,+20,+20,add(21)(q21),+22	Yes*
LN18	61,XY,+t(x;10)(q?;q11),+t(x;9)(p?;p?),+3,+t(5;15)(p13;q?),+7,+7,t(6;10)(q11;q?),+t(5;10)(q11;q?),+t(6;10)(p11;p?),+t(10)(p10),t(11;14)(q?;?),+t(11,18) (q?;q11),+t(12;16)(q?;p11),+20,+t(16;20)(p11;q?)+add22(q?)	Yes*
LN229	86,XXX,der(X)t(x;2)(q23;?),der(X)t(X;16)(p11;?),+der(X)t(X;19)(p21;?),+1,del(1)(p10),+der(1)t(1;18)(?;q11),+2,+2,+2,+3,+3,+der(4)t(4;6) (p14;?)x2,+der(4)t(4;9)(q11;?),+5,+der(5)t(5;12)(p11;?),+der(6)t(6;16)(p13;?)x2,+der(6)t(6;7)(?;?),+7,+7,+der(7)t(5;7)(?;p11)x2,+der(8)t(6;8)(?;q22), +9,+9,+der(9)t(8;9)(?;q10),+10,+der(11)(q14),+del(12)(q13),+der(14)t(14;18)(q24;?),+16,+16,+del(17)(q12),+18,+der(19)t(X;19)(?;q12), +20,+20,+20,+21,+21,+22,+22,+der(22)t(15;22)(?;p12)x2	Yes*
T98G	131,XY,+X,+X,+Y,+Y,+Y,+mar trc(7;7;7)(q?;p?;p?)x2,+t(7;8)(q?;p?)x2,+mar dic(10;10)(q?;q?)x1,+i15(q10)	Yes*
U87-MG	44,X,-X,t(1)(1:13)(p22;p?)x2,der(6)t(6;7)(p21;p?),der(6)t(6;12)(q23;?),del(7)(q10),del(10)(q21),der(12)t(6;12)(?;q22),-13,-14,der(16)t(1;16)(?;q13),del(20) (p11),+der(20)t(1;14;20)(?;?;q12),t(22)(10;22)(?;p12)	Yes*
U138-MG	61-62,XYY,+Y,+der(1)t(1;12)(p31;?),+3,der(4)t(4;17)(q32;?),ins(4)(4;14;4)(p15;?;p13)x2,+7,+der(8)t(8;17)(p21;?),+der(11)t(11;19)(p13;?),der(12)t(1;12) (?;q14),+13,-14,+15,+18,+der(18)t(6;18)(?;q12),+del(19)(p12),+20,+20,+22,+der(22)t(5;22)(?;q11)	No
U251-MG	66,XXY,+1,+2,+3,+insdic(4;16;4;20)(q12;p11::q?;q?;q?),ins(4)(4;16;4;16)(p?;q?;q?;q?),+5,+7,+7,+iso(8)(q10),+9,+der(11)t(10;11;15)(q10;q?;q?), +der(11)t(6;10;11)(q?;q?;q?),+15,+17,+17,+del(18)(q12),+19,+20,+21	No

The second column describes the predominant clonal karyotype including all chromosomal aberrations. The last column shows whether subclones are present in the cell lines. The individual karyotypes of the subclones are listed in the supplement (*).

C.1.3 GBM cell lines response to irradiation and TMZ treatment

To characterize the response towards ionizing radiation and TMZ treatment of the cells' clonogenic survival was investigated for each cell line. Therefore, the cells were irradiated with 0, 1, 2, 4, 6, 8 or 10 Gy and the cells were allowed to grow for 14 days. For TMZ treatment, the cells were incubated in the presence of 0, 25, 50, 100, 200 or 500 µM TMZ for 24 hours. Likewise, the cells were grown for 14 days.

The resulting response of the cell lines to irradiation is shown in Figure 16. With regard to clonogenic survival in a dose range from from 1 to 10 Gy, T98G and U87-MG cell line exhibited the highest survival while the LN229 cell line showed the poorest survival. Pairwise statistical testing using ANOVA of two linear quadratic cell survival curves (Torsvik et al., 2014), revealed no significant difference for clonogenic survival between A172, LN18 and U251 cells (Table 7). Also, the survival curves of LN18 and U138-MG showed no significant difference.

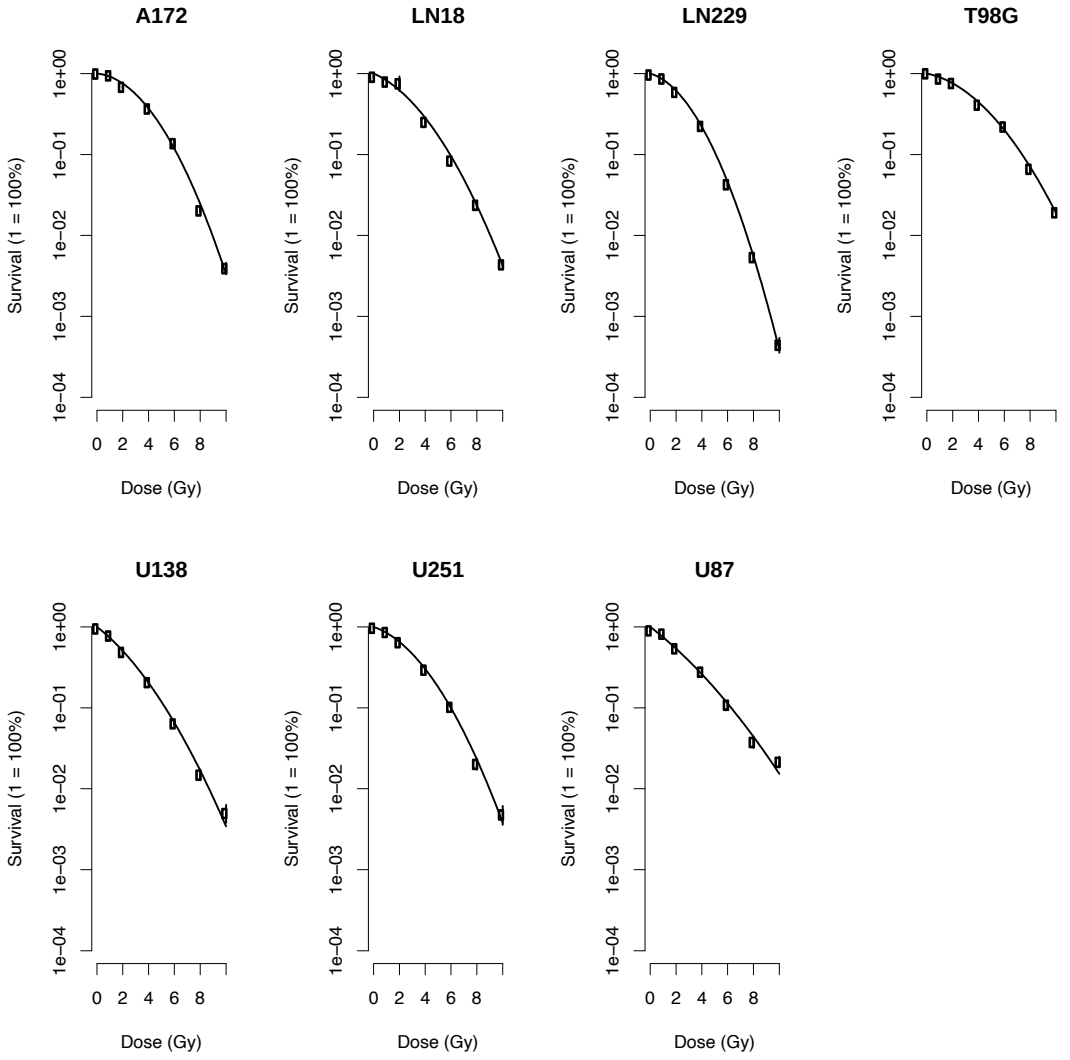

Figure 16: Clonogenic survival after X-ray irradiation

Survival curves of GBM cell lines irradiated with 1, 2, 4, 6, 8 and 10 Gy. The cells were treated four hours after seeding and the cells were grown for 14 days before staining of the colonies.

This observation allowed the formation of three groups for radioresistance; T98G and U87-MG which showed the highest resistance, A172, LN18, U138-MG and U251-MG which showed intermediate resistance and LN229 which was most sensitive. The survival of the GBM cell lines to TMZ treatment is displayed in Figure 17. The cell lines LN18, T98G, U138-MG and U251-MG show a significantly higher survival after TMZ treatment than the cell lines A172, LN229 and U87-MG. As described in A.1.1, MGMT expression and promoter methylation plays an important role in the outcome

of TMZ treatment. Therefore, the expression of the MGMT gene was analyzed by qRT-PCR in collaboration with Prof. Kirsten Lauber. Additionally, the promoter methylation status of the MGMT gene was analyzed by pyrosequencing in collaboration with Dr. Victoria Ruf of the Institute of Neuropathology at the University Hospital of the LMU Munich.

Table 7: Statistical testing using the R package CFassay (Braselmann et al., 2015) of the survival curves of the cell lines after irradiation

Cell line 1	Cell line 2	p-value
A172	LN18	0.115706763
A172	**LN229**	**1.82528E-13**
A172	**T98G**	**2.52879E-14**
A172	**U138**	**0.000325362**
A172	U251	0.207081714
A172	**U87**	**2.68299E-08**
LN18	**LN229**	**5.55177E-12**
LN18	**T98G**	**7.67182E-10**
LN18	U138	0.080210882
LN18	U251	0.835961966
LN18	**U87**	**1.40524E-05**
LN229	**T98G**	**1.8834E-24**
LN229	**U138**	**1.01189E-11**
LN229	**U251**	**1.28925E-12**
LN229	**U87**	**1.16124E-17**
T98G	**U138**	**1.98373E-12**
T98G	**U251**	**4.23232E-10**
T98G	**U87**	**0.000790985**
U138	**U251**	**0.001746446**
U138	**U87**	**9.28599E-07**
U251	**U87**	**9.5784E-06**

The columns show the compared cell lines and the corresponding p-value. Bold labeled rows depicted a statistical significant difference.

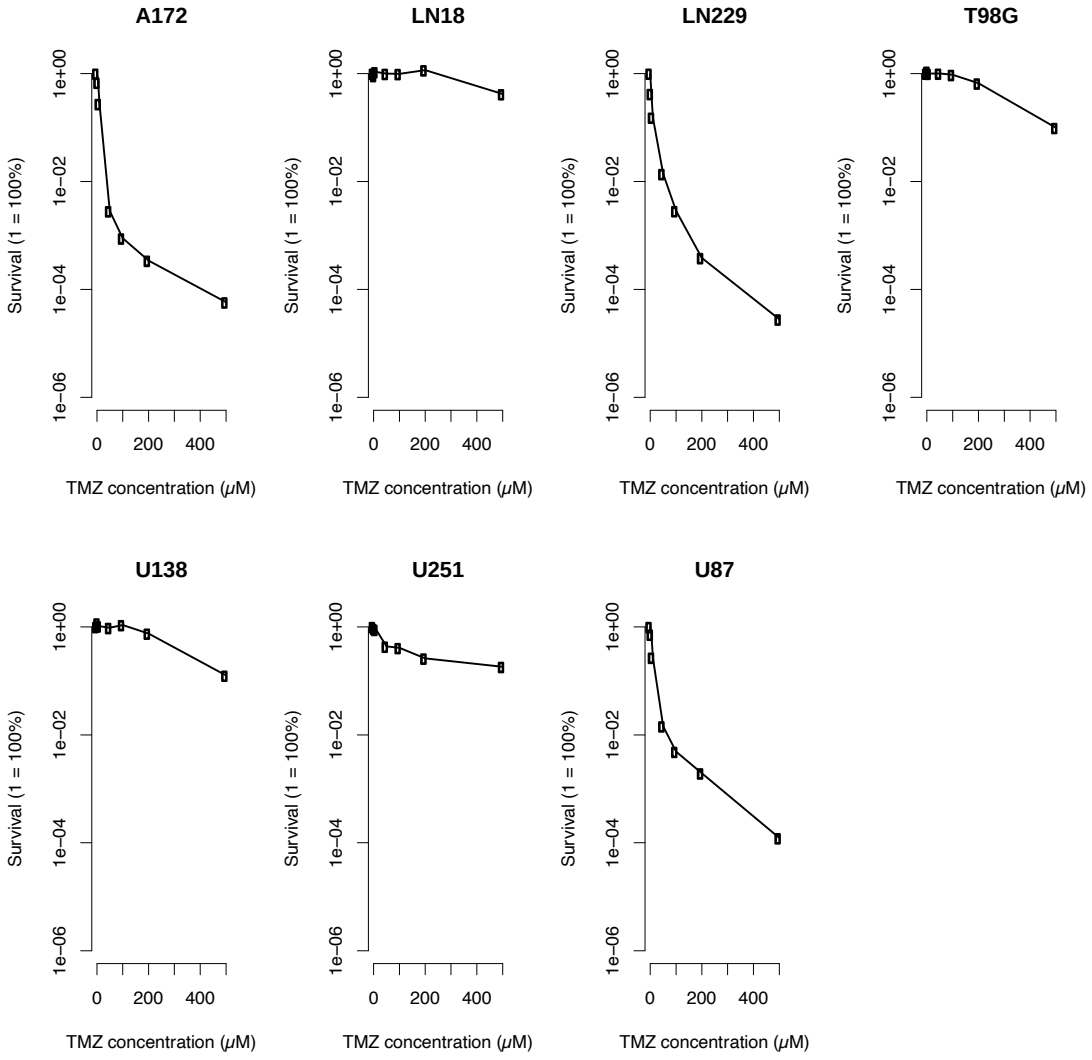

Figure 17: Clonogenic survival after TMZ treatment

Survival curves of GBM cells lines after treatment with different concentrations (5, 10, 50, 100, 200 and 500µM) of TMZ. The TMZ treatment began four hours after seeding and the TMZ containing medium was replaced with culture medium after another 24 hours. The cells were stained after 14 days.

I found MGMT expression in the cell lines LN18, T98G, U138 and U251 (Table 8). The cell lines A172, LN229 and U87 showed no expression of MGMT. Additionally, the promoter was methylated in A172, LN229, T98G, U87 and U251 cells while the promoter of LN18 and U138 cells was not methylated. Notably, the cell lines T98G and U251 showed MGMT expression even in the presence of a methylated

promoter. Therefore, the observed response to TMZ treatment was more dependent on the expression of the MGMT gene than on promoter methylation.

Table 8: Overview of the MGMT-promoter methylation, expression of MGMT and TMZ resistance of the cell lines

Cell line	MGMT-promoter-methylation	Expression of MGMT by qRT-PCR	Colony formation assay upon TMZ treatment
A172	Methylated	-	More sensitive
LN18	Not methylated	0.62	More resistant
LN229	Methylated	-	More sensitive
T98G	Methylated	0.43	More resistant
U87-MG	Methylated	-	More sensitive
U138-MG	Not methylated	0.61	More resistant
U251-MG	Methylated	0.17	More resistant

MGMT-promoter methylation data was obtained by pyrosequencing. The Ct values were created by qRT-PCR and referenced to 18S rRNA, δ-amino-laevulinate-synthase, and β2-microglobulin. The MGMT expression of normal human astrocytes was used as calibrator sample. The response towards TMZ was assessed by colony formation assay. The cell lines were classified as more resistant if the survival at 10 µM TMZ treatment was greater than 80% and vice versa.

C.1.4 Expression of the 4-miRNA signature allows assignment of cell lines to published risk groups

For the characterization of the 4-miRNA expression in the GBM cell lines, qRT-PCR was performed. In this study, a SYBR green qRT-PCR system was utilized to measure the miRNA expression. In a first step, a robust endogenous control for the GBM cell lines was established. Here, the expression of small nucleolar RNAs RNU6, SNORD61, SNORD68 and SNORD96 was analyzed (Figure 18) to find a control that is highly and uniformly expressed among the cell line panel. Out of the analyzed controls, SNORD68 shows the highest expression (median Ct = 21.24) and the most uniform distribution of Ct values (Figure 18). The other controls had a higher variance and a lower median expression. The median Ct was 22.45 for RNU6, 23.12 for SNORD61 and 21.54 for SNORD95. Afterwards, the primer efficiency of the miRNA-specific forward primers and the endogenous control in combination with the reverse primer was analyzed. For optimal thermocycling conditions, the efficiency of each primer pair had to be greater than 95%. For this, a standard curve experiment was conducted. Here, previously generated cDNA was diluted in 1:5 ratios to generate five data points. Afterwards, qRT-PCR was performed for each primer pair and dilution. The resulting Ct values were plotted against the dilution ratio (Figure 19) and the efficiency was calculated using the slope of the curves as described in B.3.2. The efficiency of the measured primer pairs was greater than 95% except for the miR-615-5p primer. Therefore, further optimization experiments had to be conducted as described below.

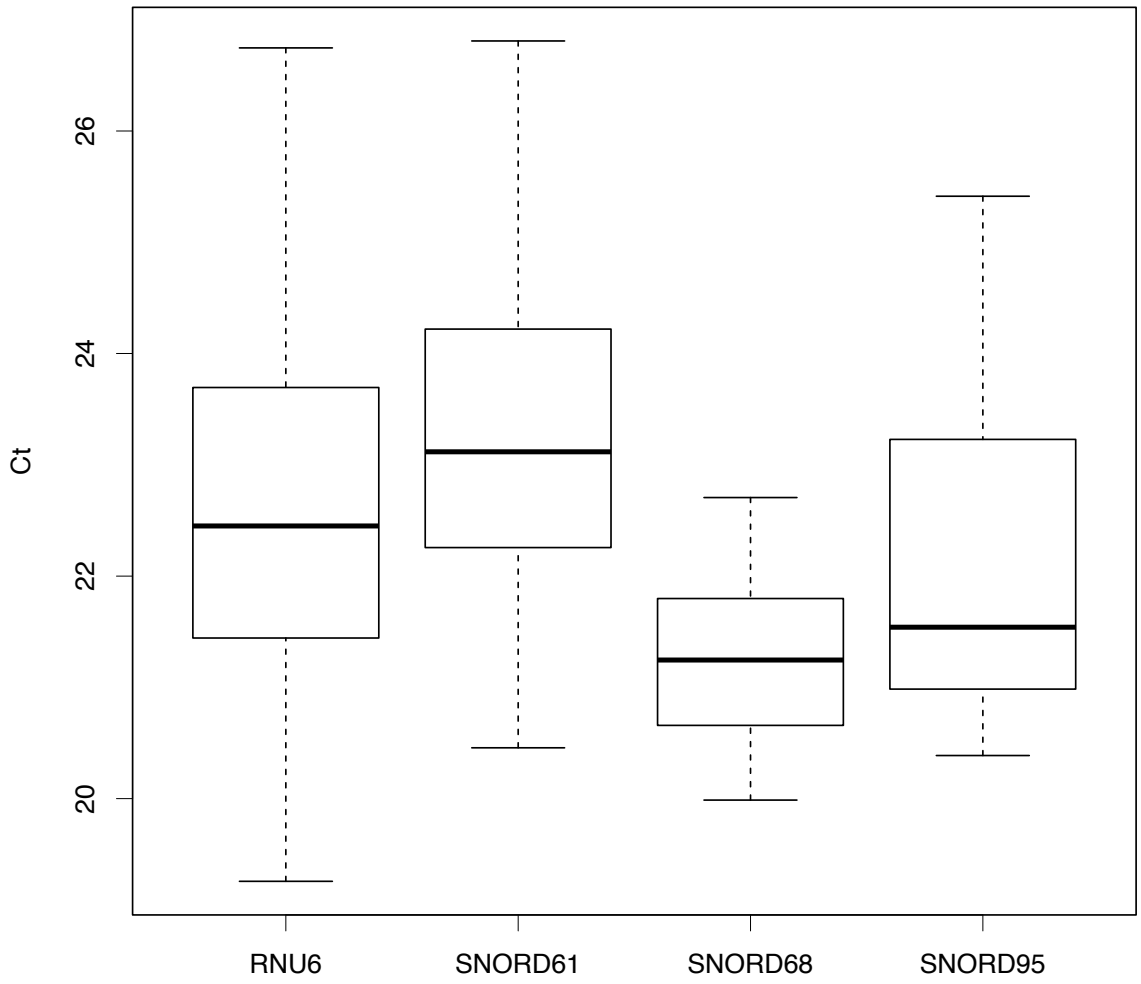

Figure 18: Identification of a robust endogenous control for qRT-PCR

Boxplots displaying the Ct values from the analyzed endogenous controls RNU6, SNORD61, SNORD68 and SNORD95. The boxes represent 50% of the variance in the data set whereas the bold line indicates the median of the data points. The dashed lines represent the lowest and highest 25% of the data points which is an indicator for the overall distribution of the data. The Ct values were created from SYBR green qRT-PCR using the cell lines A172, LN18, LN229, T98G, U87, U138 and U251 in triplicates.

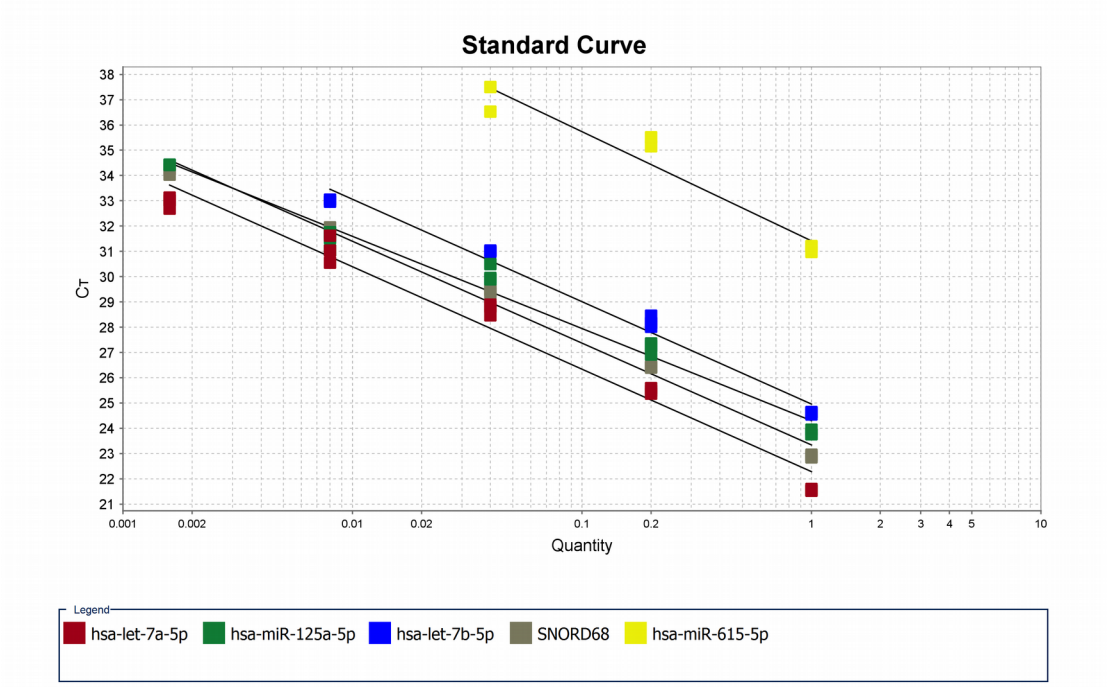

Figure 19: Determination of the qRT-PCR primer efficiency

The standard curves were created using 1:5 dilutions of cDNA. The colors represent the individual primer pairs using the miRNA-specific forward primer and the universal reverse primer. The resulting Ct values were plotted against the dilution factor. The experiment was conducted in triplicates and five different dilutions were produced.

To optimize the efficiency of the miR-615-5p primer within the qRT-PCR reaction, a primer matrix experiment was performed. For this experiment, the forward and the reverse primers were analyzed in different concentrations of 1000, 500, 250, 100 and 50 nM and qRT-PCR was performed for each combination. The optimal combination of primer concentrations would yield the highest amount of PCR product (delta Rn) and the lowest Ct value. The delta Rn values and the corresponding Ct values were analyzed and thereby the combination of 1000 nM forward and reverse primer showed the optimal concentration (Figure 20). Afterwards, another standard curve experiment was conducted as described above to analyze the primer efficiency using the optimized primer concentration (Figure 21).

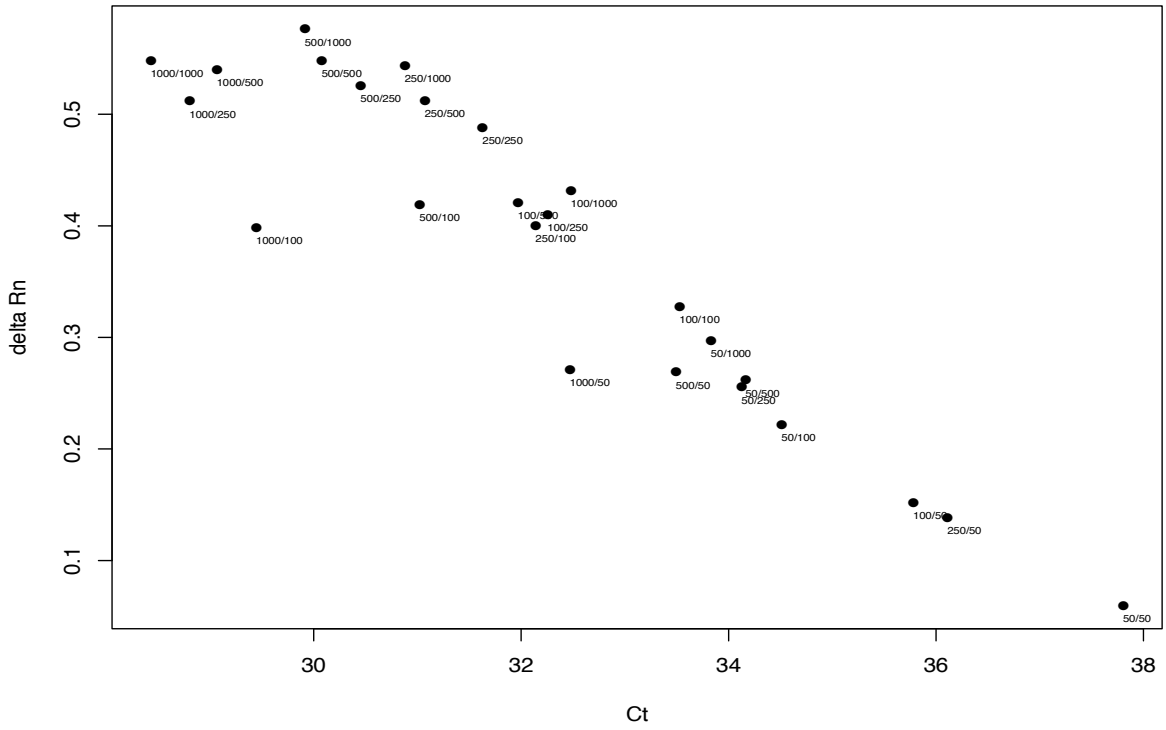

Figure 20: Optimal primer concentrations are analyzed using different combinations of primer concentrations

The results of the primer matrix experiments were created using the miR-615-5p forward primer and the universal reverse primer. The numbers reflect the combination of forward and reverse primer concentration in nM. The relative amount of generated PCR product (delta Rn) was plotted against the respective Ct values. Optimal primer combinations show a high delta Rn value and a low Ct number (1000/1000, 1000/500, 1000/250).

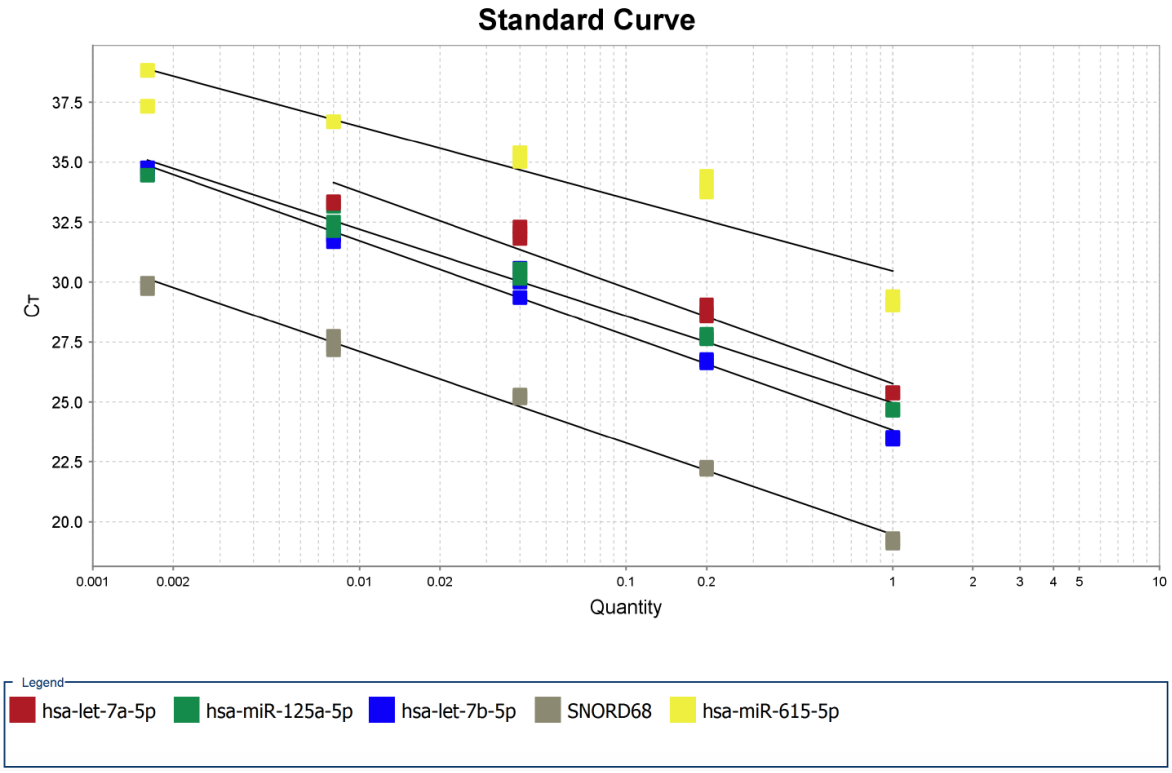

Figure 21: Determination of the qRT-PCR primer efficiency after optimization of the primer concentration

The standard curves were created using 1:5 dilutions of cDNA. The colors represent the individual primer pairs using the miRNA specific forward primer and the universal reverse primer in concentrations of 1000 nM. The resulting Ct values were plotted against the dilution factor. The experiment was conducted in triplicates and five different dilutions were produced.

After the PCR conditions were optimized, the expression of the miRNAs let-7a-5p, let-7b-5p, miR-125a-5p and miR-615-5p were analyzed in the cell lines. The expression of let-7a-5p was highest in U87-MG cells while the rest of the cell lines showed comparable expression (Figure 22). This is in contrast to the expression of let-7b-5p and miR-125a-5p, which was lower in LN229, U138-MG, LN18 and A172 cells than in T98G, U251-MG and U87-MG cells. The expression of miR-615-5p was highest in U251-MG, U87-MG and A172 and lower in T98G, LN229, U138-MG and LN18 cells. For alignment of cell lines to patient risk groups that were identified by the 4-miRNA signature by Niyazi et al. (2016) risk factors were calculated based on patient-derived risk scores.

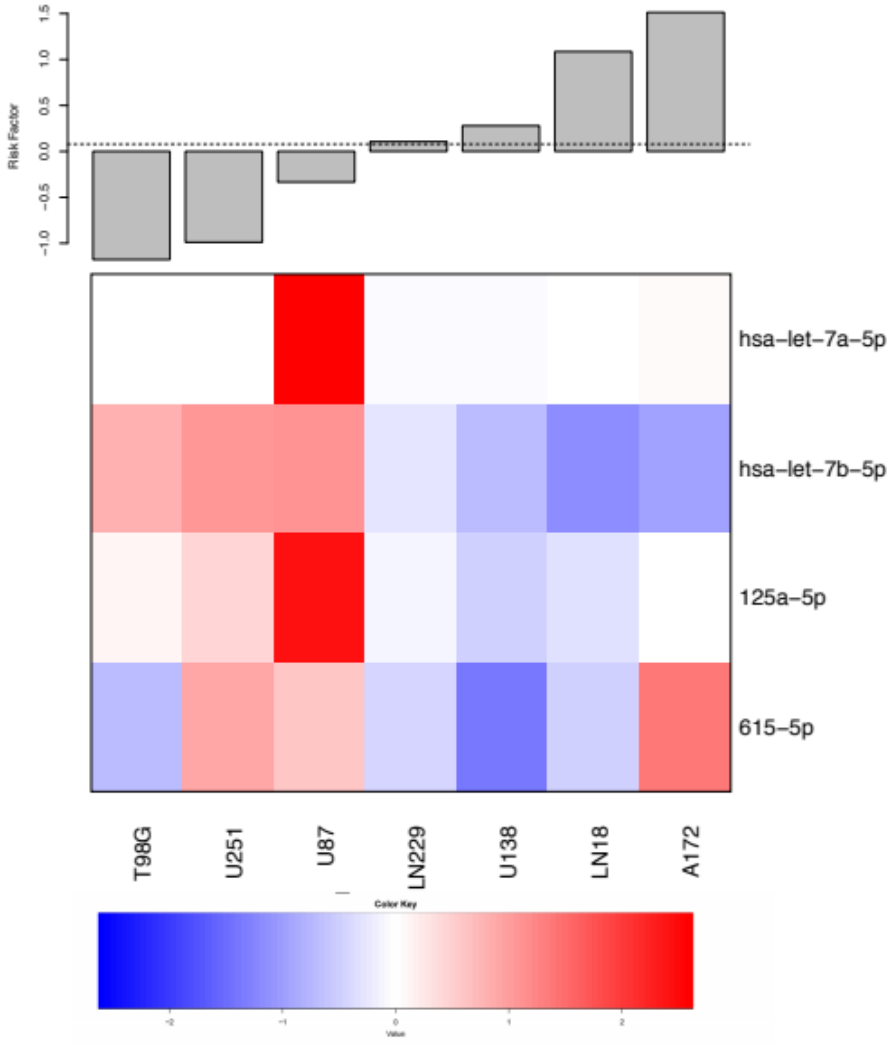

Figure 22: Heatmap of the 4-miRNA expression in the GBM cell lines and formation of an associated risk factor

The miRNA expression of the cell lines was analyzed by qRT-PCR (bottom panel). The colors represent higher expression (red) and lower expression (blue) The relative expression of the miRNAs compared to the endogenous control (SNORD68) is displayed. Risk factors were calculated by linear combination based on the patient derived risk scores (top panel). The dashed line reflects the threshold that allowed classification of cell lines in low-risk (risk factor was smaller than the threshold) and high-risk (risk factor was larger than the threshold) groups.

Briefly, the survival of GBM patients was correlated to the expression of the 4-miRNAs. Depending on the influence of the individual miRNA to the survival of the patients, a risk score could be determined. The relative expression of the 4-miRNAs was determined in comparison to the endogenous control SNORD68. Risk factors were calculated by building the scalar products using the Niyazi et al. (2016) cox proportional hazard model coefficients and signature miRNA expression values. The following coefficients from model were used:

miRNA	Coefficient
Let-7a-5p	0.5059587
Let-7b-5p	-0.9669152
miR-125a-5p	-0.2821517
miR-615-5p	0.3254795

For classification into high- and low-risk group, the threshold (0.07811832) from the patient derived model was applied (Niyazi et al., 2016). If the risk factor of the cell line was higher than the threshold, it was classified as high risk. Likewise, if the risk score was lower than the threshold, the cell line was considered as low-risk. The risk factors of the individual cell lines is shown in Table 9. Longer survival was associated with expression of let-7b-5p and miR-125a-5p while shorter survival was linked to the expression of let-7a-5p and miR-615-5p. Among the GBM cell lines, A172 had the highest risk score followed by LN18, U138-MG, LN229, U87-MG, U251-MG and T98G with the lowest risk score.

Table 9: Determined risk factors of the GBM cell lines and the corresponding risk group

Cell line	Risk factor	Risk group
T98G	-1.783621	Low risk
U251	-0.9891519	Low risk
U87	-0.3347058	Low risk
LN229	0.109434	High risk
U138	0.2791465	High risk
LN18	1.0854292	High risk
A172	1.5121806	High risk

The risk scores were determined using coefficients from a prognostic model described by Niyazi et al. (2016) in combination with the signature miRNA expressions. For classification into a specific risk group the threshold 0.07811832 from the patient cohort was used. Cell lines with higher risk factors were considered high-risk while cell lines with lower risk factors were considered low-risk.

Using the described approach above, the expression and the related risk factors were calculated for a retrospective GBM patient cohort from the university hospital of the LMU München. From 37 patients, 17 patients were classified high risk while 20 patients were classified low risk (Figure 23). Overall survival of the patients (Figure 24) was significantly longer for patients belonging to the low risk group than for patients belonging to the high risk group.

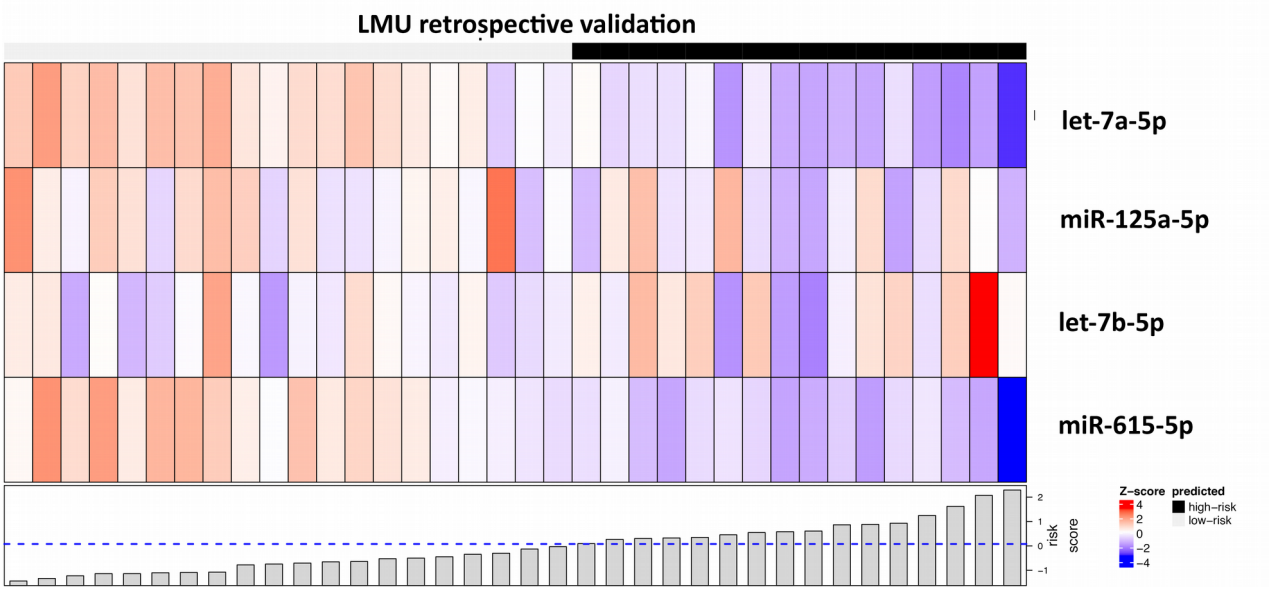

Figure 23: Validation of the 4-miRNA signature by qRT-PCR in a retrospective LMU cohort

A heatmap of the miRNA expression of a retrospective cohort analyzed by qRT-PCR is shown. The colors represent higher expression (red) and lower expression (blue) Risk factors from the patient derived risk scores multiplied by the miRNA expression are displayed in the bottom panel. The dashed line reflects the threshold that allowed classification of patients in low-risk (risk factor was smaller than the threshold) and high-risk (risk factor was larger than the threshold) groups.

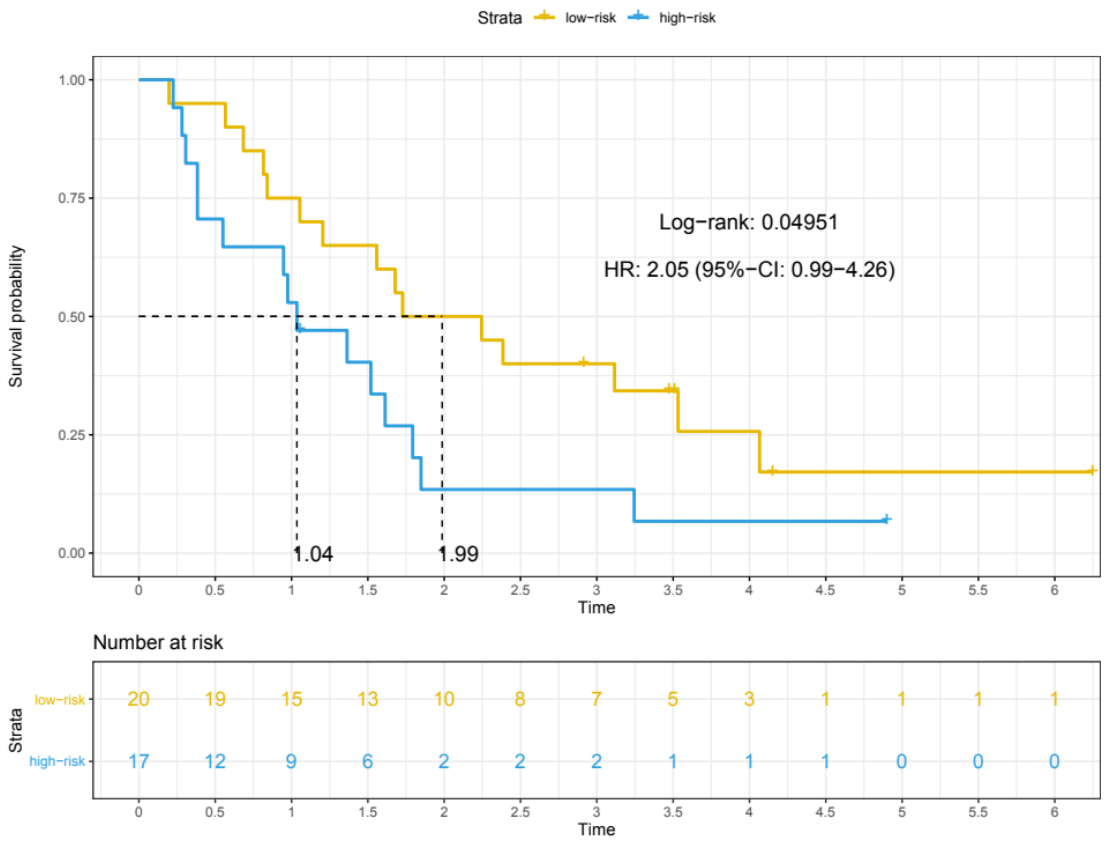

Figure 24: Overall survival of the LMU cohort stratified by the 4-miRNA signature risk groups

Kaplan-Meier analysis according to the risk groups generated by the 4-miRNA signature. Low risk patients (yellow) show a significant longer survival than high risk patients (blue). The number of patients at each time point (years) is depicted at the bottom of the figure.

C.1.5 Gene expression analysis unveils deregulated pathways among the cell line panel

Differences in global gene expression between radiation sensitive and resistant and TMZ sensitive and resistant cells were analyzed. For this purpose, microarray analysis was performed to characterize mRNA expression using a 8 x 60k micro array, which allowed the analysis of eight samples on a single slide with 60,000 probes spotted on each array. For this experiment, total RNA was isolated from the cell lines and the

quality of the purified RNA was analyzed using a Bioanalyzer device. The derived RNA integrity number (RIN), which describes the quality of RNA, showed sufficient (> 7) scores for all analyzed RNAs (Figure 25) that were considered for microarray analysis.

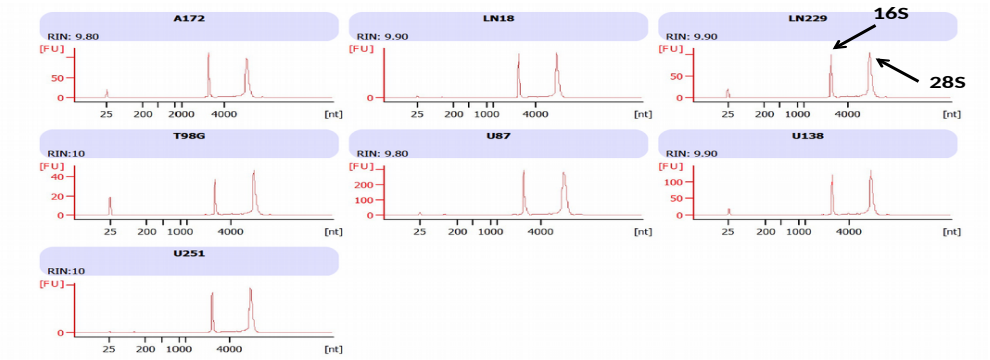

Figure 25: Quality assurance of extracted total RNA via capillary electrophoresis

RIN (RNA integrity number) score represents a measurement for the quality of analyzed RNA. Unfragmented RNA shows distinct 16S and 28S. The electropherograms of the analyzed RNAs show clearly visible 16S and 28S peaks (arrows) and high (>9) RIN scores thus being suitable for global gene analysis.

Afterwards, the RNA was labeled and the slides were hybridized as described in B.4.3. The slides were scanned and the intensities of the spots were exported using the manufacturers software. An example of a scanned microarray is shown in Figure 26.

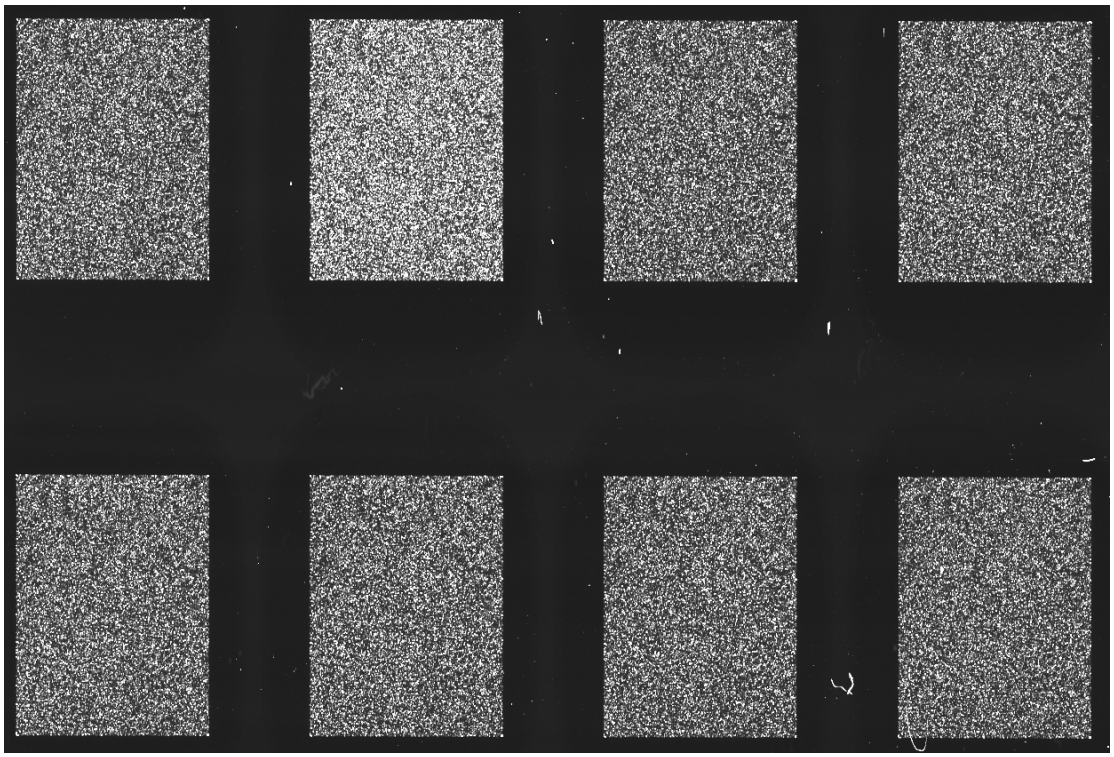

Figure 26: Scanned 8 x 60k human gene expression micro array

The image shows a scanned 8 x 60k microarray. The format represents eight arrays on a single glass slide, each harboring 60,000 probes for different transcripts. The probes were annotated to the NBCI human genome build 38 (GRCh38, December 2013). The fluorescence intensities correspond to the mRNA gene expression reflected by brightness of the spots.

The micro array data has been deposited at the NCBI Gene Expression Omnibus repository (Edgar et al., 2002) and is accessible through GEO Series accession numbers GSE119468 (https://www.ncbi.nlm.nih.gov/geo/query/acc.cgi?acc=GSE119468), GSE119486 (https://www.ncbi.nlm.nih.gov/geo/query/acc.cgi?acc=GSE119586) and GSE119492 (https://www.ncbi.nlm.nih.gov/geo/query/acc.cgi?acc=GSE119592). Data processing and visualization was performed with support of Dr. Kristian Unger of the Research Unit Radiation Cytogenetics at the Helmholtz Center Munich. Briefly, the data was filtered and processed using the R software and the Bioconductor packages limma and Agi4x44PreProcess. Differential gene expression was analyzed between TMZ resistant and sensitive cell lines and radiation resistant and sensitive cell lines. The obtained fold changes were analyzed using

gene set enrichment analysis (GSEA) to determine deregulated pathways in the Reactome database.

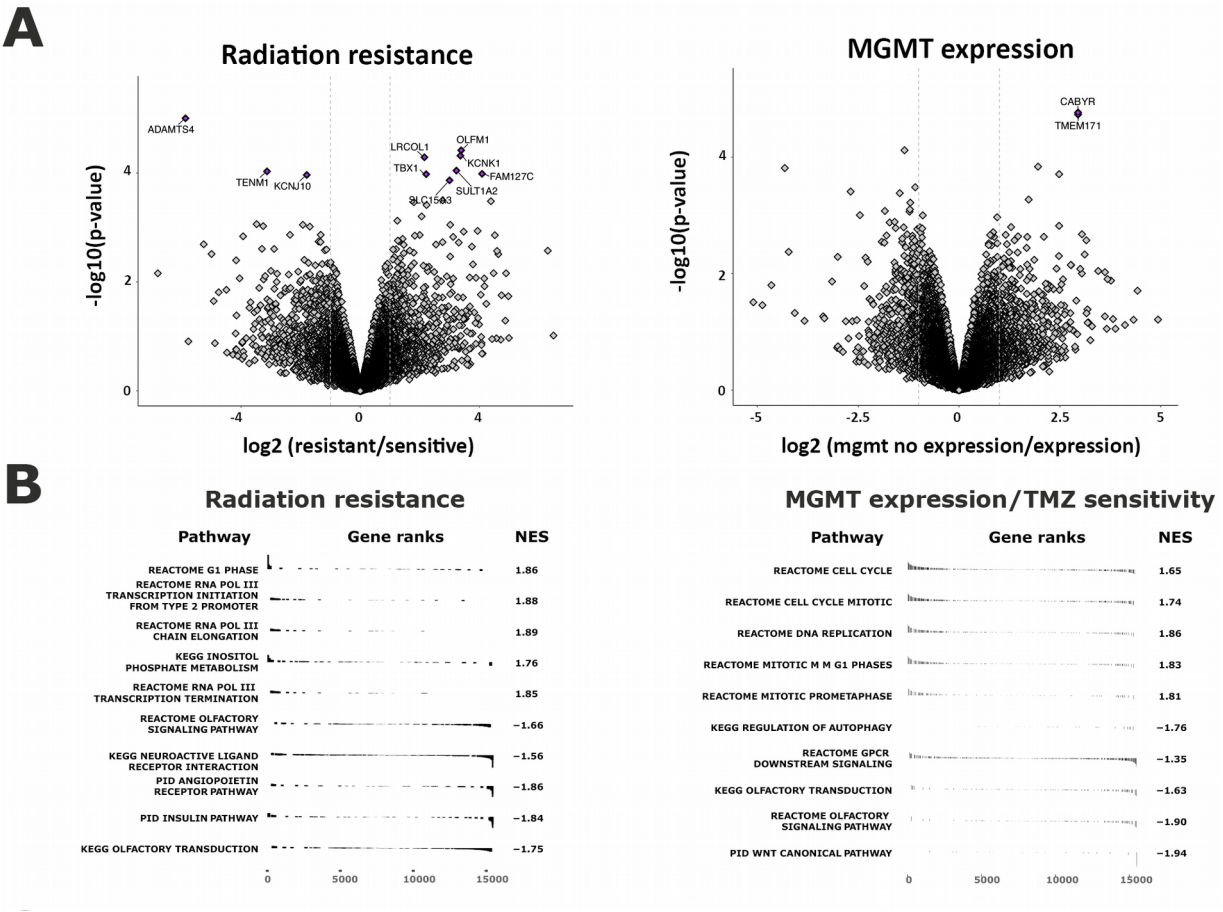

Figure 27: Gene expression microarray analysis

A. Volcano plots depicting gene expression fold-changes (log2 scale, x-axis) and p-values (-log10-transformed, y-axis) of all genes in the data set. Left: Comparison of radiation resistant and sensitive cell lines. Right: cell lines expressing the MGMT gene (TMZ resistant) and not expressing the MGMT gene (TMZ sensitive). Gene symbols are shown for significantly differentially expressed genes (FDR < 0.1).

B. Top ten statistically significant pathways (ranked according to FDR value) after gene set enrichment analysis (GSEA). NES: normalized enrichment score. Positive scores indicate up-regulated pathways while negative scores reflect down-regulated pathways in the dataset. Left: comparison of radiation resistant and sensitive cell lines. Right: cell lines expressing the MGMT gene (TMZ resistant) and not expressing the MGMT gene (TMZ sensitive).

Volcano plots showing the genes with the highest differential expression are depicted in Figure 26, top panel (A). Among the cell lines showing different sensitivity to radiation the ADAMTS4 gene was significantly down-regulated. Other significantly down-regulated genes were TENM1 and KCNJ10. Furthermore, genes that were strongly up-regulated in radiation resistant cell lines were identified including LRCOL1, OLFM1, KCNK1, TBX1, SULT1A2 and FAM127C. For cell lines with different sensitivity to TMZ treatment, the genes CABYR and TMEM171 were considerably deregulated. GSEA revealed up-regulated pathways in cell lines showing difference in radiation sensitivity (Figure 26, mid panel, left) that were mainly involved in G1 phase, RNA polymerase III transcription initiation and RNA polymerase III chain elongation. Among the down-regulated pathways, angiopoietin receptor, insulin and olfactory transduction were identified. Furthermore, deregulated pathways between cells showing differences in MGMT expression were unveiled (Figure 27, mid panel, right). Notably, up-regulated pathways were primarily involved in cell cycle and DNA replication. In contrary, the down-regulated pathways were involved in autophagy, GPCR downstream signaling, olfactory transduction and signaling and WNT signaling pathway.

C.1.5 Karyotypic and molecular features of the cell lines allow classification into GBM specific subtypes

Studies from the TCGA consortium revealed a classification in GBM based on different molecular features. The subtypes are classified in classical, mesenchymal and proneural mainly based on the expression of EGFR (classical), NF1 (mesenchymal) and PDGFRA (proneural). Patients belonging to the classical and mesenchymal subtypes showed a reduction in overall survival while this observation was absent in the proneural subtype. In the present study, the cell lines were classified according to the patient derived subtypes using gene expression data and cytogenetic array CGH data. For this purpose, deregulation of major driver genes as well as chromosomal deletions and amplifications were scored based on their

occurrence in the cell lines. For amplifications and deletions in specific genes, the genomic location of the genes was retrieved from the NCBI genome browser (https://www.ncbi.nlm.nih.gov/genome). In the regions table derived from the aCGH experiments, the correlating regions were analyzed whether an amplification (+1), a deletion (-1 or -2), or no change (0) was present in the gene. As depicted in Table 10, features present in the cell lines were scored as '1' while absent features were scored as '0'. The sum of all features of a subtype was used to build a consensus score for every cell line and subtype. As shown in Table 10, the majority of the cell lines (A172, LN18, T98G, U87 and U138) were assigned to the mesenchymal subtype. The remaining cell lines LN229 and U251 were classified as classical subtype. The proneural subtype could not be identified in the cell line panel.

Table 10: Overview of GBM subtype specific chromosomal amplifications and deletions and subtype specific expression of relevant driver genes.

Subtype	Feature	A172	LN18	LN229	T98G	U87	U138	U251
Classical	Chr. 7 amplification and Chr. 10 loss	0	1	1	1	1	1	1
	EGFR amplification	1	1	1	0	0	0	1
	Focal 9p21.3 deletion	1	1	1	1	1	1	1
	NES expression	1	0	1	0	0	0	1
	NOTCH3 expression	1	0	0	0	1	0	0
	SMO expression	1	0	1	1	0	0	1
Score classical		0.83	0.5	0.83	0.5	0.5	0.33	0.83
Mesenchymal	Hemizygous deletion at 17q11.2 (NF1)	1	0	0	0	0	0	0
	CHI3L1 expression	1	1	1	1	1	1	1
	TRADD, RELB, TNFRSF1A expression	1	1	1	1	1	1	1
Score mesenchymal		1	0.67	0.67	0.67	0.67	0.67	0.67
Proneural	Focal 4q12 amplification (PDGFRA)	0	0	0	0	0	0	1
	NKX2-2, OLIG2 expression	0	0	0	0	0	0	0
	SOX genes expression	1	0	1	0	0	0	1
Score proneural		0.333	0	0.333	0	0	0	0.67
Consensus		M	M	C	M	M	M	C

For each subtype based on cytogenetic alterations and aberrant gene expression, a score was built. The highest score determined the cytogenetic molecular subtype.

C.2 Modulation of miRNA expression by siRNA transfection reveals potential targets of the 4-miRNA signature

After characterization of the cell line panel, the expression of the four miRNAs let-7a-5p, let-7b-5p, miR-125a-5p and miR-615-5p was modulated by small RNA transfection. The cells were transfected using specific miRNA mimics for overexpression and miRNA inhibitors for knockdown of the respective miRNAs. In a first step, the transfection efficiency of the cell lines A172, LN18, U87, U138 and U251 was analyzed. The cell lines LN229 and T98G were excluded from the experiment because of their karyotypic complexity. The transfection efficiency was assessed by FACS using fluorescent-labeled siRNA with concentrations of 10, 5, 1 and 0.5 nM (Figure 28).

The highest transfection efficiency was observed for the cell lines A172, U87 and U251 using 10 nM siRNA. The efficiency for these cell lines remained high at 5 nM siRNA but declined at lower concentrations. The cell lines LN18 and U138 showed considerably lower efficiency at all siRNA concentrations.

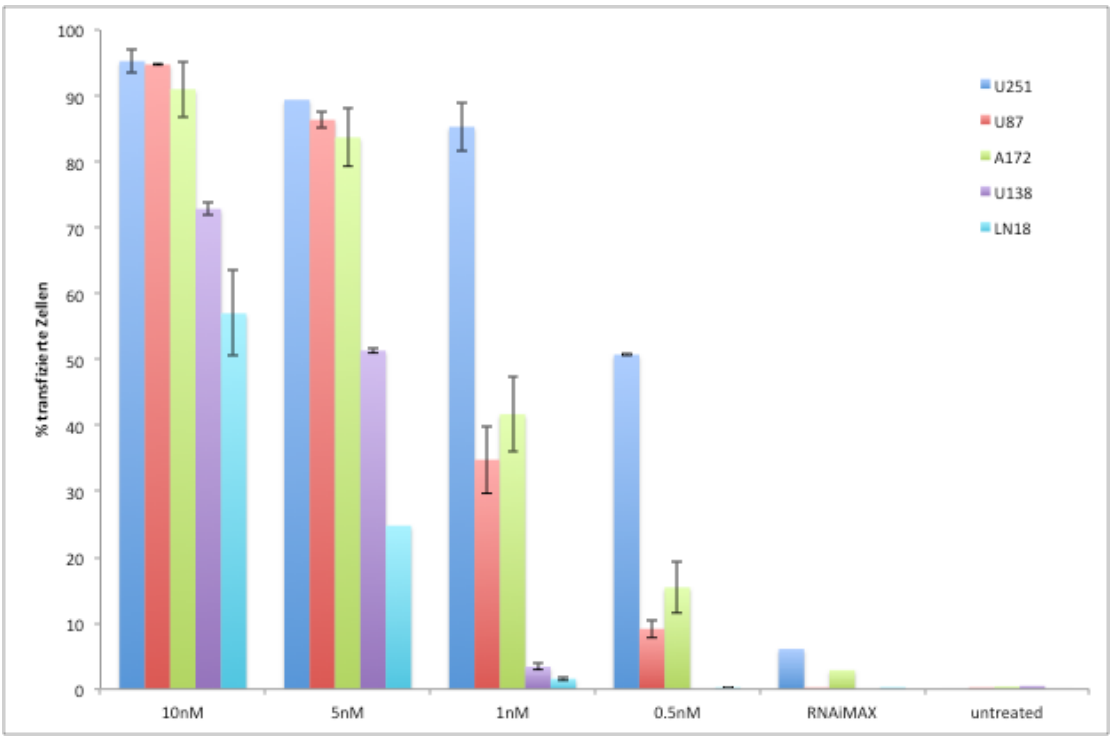

Figure 28: Results of the transfection of GBM cell lines using different siRNA concentration

The cell lines were transfected using RNAiMAX using different concentrations of the siRNA. The Y-axis shows the transfection efficiency as fraction of the living cells. The different transfection concentrations are depicted on the X-axis. Cells treated with transfection reagent alone and untreated cells were used as a control. The colors represent the transfected cell lines U138 (blue), U87 (red), A172 (green), U138 (purple) and LN18 (teal).

For further experiments, two cell lines (A172 and U138) were selected. Selection criteria were transfection efficiency, low karyotypic complexity and, if possible, absence of subclones. Additionally, different responses to radiation and TMZ treatments were considered. The levels of overexpression and knockdown, respectively, were characterized over a time period of 72 hours for the determination of the optimal concentration and time point of the siRNA transfection experiment. The cell lines A172 and U138 were transfected using 10 and 5 nM of let-7a-5p, let-7b-5p, miR-125a-5p and miR-615-5p mimic and inhibitor. The cells were harvested after 24, 48 and 72 hours. As controls, a siRNA that is not targeting any miRNA ('scramble'), a transfection control ('RNAiMAX') and untreated cells were

utilized. The resulting expression changes were normalized to the scramble control. The observed overexpression in both cell lines was highest after 24 hours and decayed over the following 48 and 72 hours (Figure 29, A and B, top panels). The highest overexpression generated by 10 nM mimic RNA reached expression differences of 80-800 times. For the knock down, the highest effect was observed using 10 nM inhibitor after 24 hours (Figure 29, A and B, bottom panels). The effect of the knock down weakened during the following 48 and 72 hours. In both cell lines, the strongest effect could be observed for the miR-125a-5p knock down. Notably, no effect of the knock down could be observed for miR-615-5p.

A

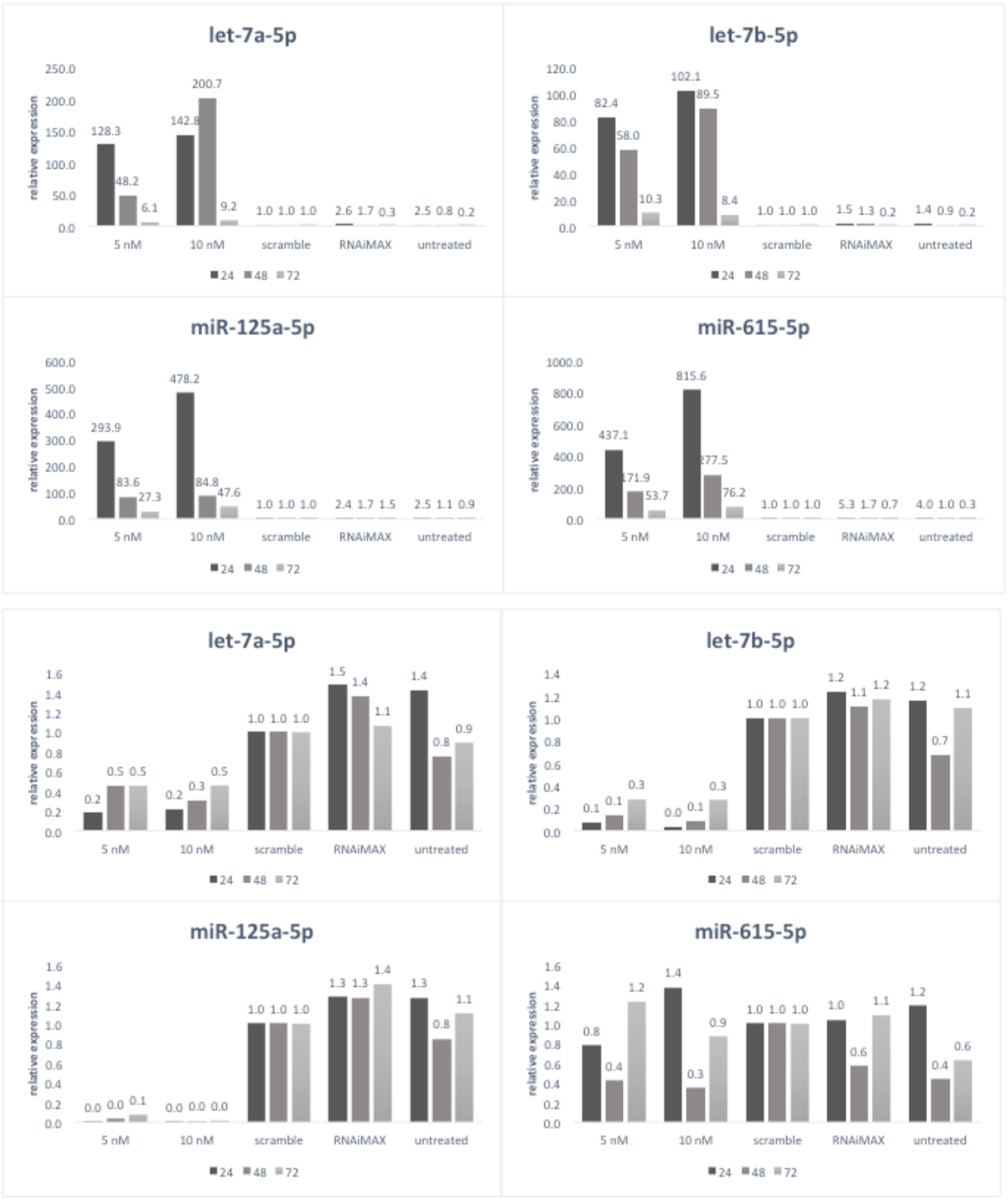
let-7a-5p
relative expression
250.0
200.0
150.0
100.0
50.0
0.0
128.3
48.2
6.1
142.8
200.7
9.2
1.0 1.0 1.0
2.6 1.7 0.3
2.5 0.8 0.2
5 nM
10 nM
scramble
RNAiMAX
untreated
24 48 72
let-7b-5p
relative expression
120.0
100.0
80.0
60.0
40.0
20.0
0.0
82.4
58.0
10.3
102.1
89.5
8.4
1.0 1.0 1.0
1.5 1.3 0.2
1.4 0.9 0.2
5 nM
10 nM
scramble
RNAiMAX
untreated
24 48 72
miR-125a-5p
relative expression
600.0
500.0
400.0
300.0
200.0
100.0
0.0
293.9
83.6
27.3
478.2
84.8
47.6
1.0 1.0 1.0
2.4 1.7 1.5
2.5 1.1 0.9
5 nM
10 nM
scramble
RNAiMAX
untreated
24 48 72
miR-615-5p
relative expression
1000.0
800.0
600.0
400.0
200.0
0.0
437.1
171.9
53.7
815.6
277.5
76.2
1.0 1.0 1.0
5.3 1.7 0.7
4.0 1.0 0.3
5 nM
10 nM
scramble
RNAiMAX
untreated
24 48 72
let-7a-5p
relative expression
1.6
1.4
1.2
1.0
0.8
0.6
0.4
0.2
0.0
0.2
0.5 0.5
0.2
0.3 0.5
1.0 1.0 1.0
1.5
1.4
1.1
1.4
0.8
0.9
5 nM
10 nM
scramble
RNAiMAX
untreated
24 48 72
let-7b-5p
relative expression
1.4
1.2
1.0
0.8
0.6
0.4
0.2
0.0
0.1
0.1
0.3
0.0
0.1
0.3
1.0 1.0 1.0
1.2
1.1
1.2
1.2
0.7
1.1
5 nM
10 nM
scramble
RNAiMAX
untreated
24 48 72
miR-125a-5p
relative expression
1.6
1.4
1.2
1.0
0.8
0.6
0.4
0.2
0.0
0.0 0.0 0.1
0.0 0.0 0.0
1.0 1.0 1.0
1.3 1.3
1.4
1.3
0.8
1.1
5 nM
10 nM
scramble
RNAiMAX
untreated
24 48 72
miR-615-5p
relative expression
1.6
1.4
1.2
1.0
0.8
0.6
0.4
0.2
0.0
0.8
0.4
1.2
1.4
0.3
0.9
1.0 1.0 1.0
1.0
0.6
1.1
1.2
0.4
0.6
5 nM
10 nM
scramble
RNAiMAX
untreated
24 48 72

B

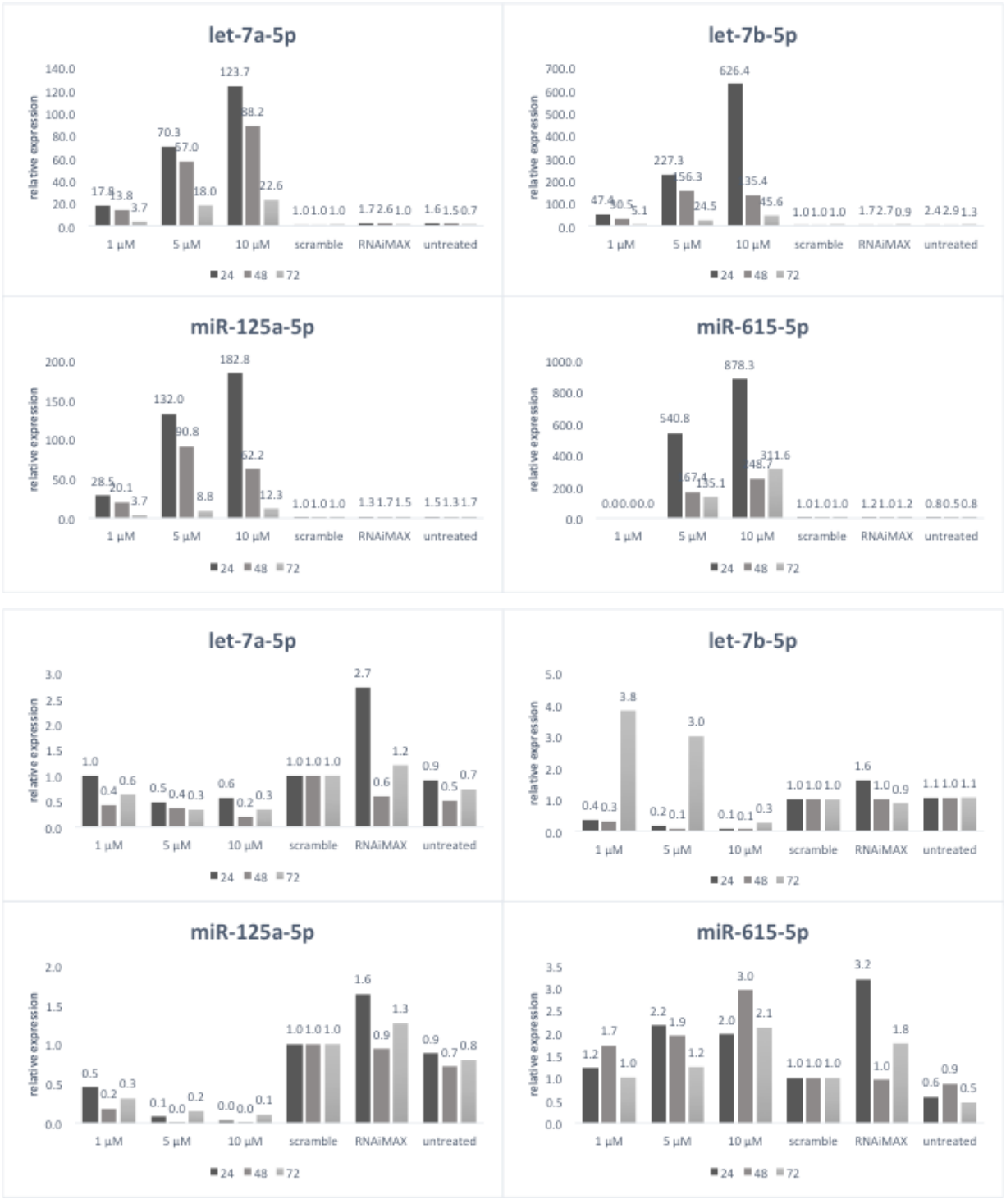
let-7a-5p
relative expression
1 µM
5 µM
10 µM
scramble
RNAiMAX
untreated
24
48
72
let-7b-5p
miR-125a-5p
miR-615-5p
let-7a-5p
let-7b-5p
miR-125a-5p
miR-615-5p

Figure 29: Results of the transfection of A172 and U138 cells using miRNA Mimics and Inhibitors

Transfection of the A172 cell line (A) and the U138 cell line (B). The cell lines were transfected using miRNA mimics (top panel) and miRNA inhibitors (bottom panel). The cells were transfected using 5 or 10 nM of the siRNA and the miRNA expression was analyzed every 24 hours for 72 hours by qRT-PCR. The resulting expression changes are shown on the Y-axis. The different transfection conditions are shown on the X-axis. For normalization of the expressions, a negative transfection control was utilized ('scramble'). Additionally, the cells were treated with the reaction reagent alone ('RNAiMAX') or were untreated. The resulting relative overexpressions are depicted in the numbers above the bars.

To characterize the effect on the transcriptome after miRNA inhibitor and mimic transfection, 3'-RNA sequencing was performed. Total RNA was isolated from A172 and U138-MG cells, 48 hours after transfection. The cells were transfected using 5 nM of the respective inhibitor or mimic and 'scramble' inhibitor or mimic was utilized as control. To analyze differentially expressed genes, the expression of the respective mimic and inhibitor transfections were compared to the expression in the 'scramble' controls. The top five up- and down-regulated genes with a FDR of less than 0.05 are depicted in Table 11 (A172) and Table 12 (U138-MG). A strong effect of differential gene expression was observed in A172 cells. The resulting log2 fold changes were in a magnitude of -40 to 50. Notably, four genes were discovered that had exactly opposing expressions in response to the let-7a-5p inhibitor and mimic transfection (HS3ST2, FAM3B, PCP4 and KCNF1; bold letters in the table), suggesting potential targets of the miRNA. Such clear effects were absent for the other miRNA transfections. Additionally, FAM3B, PCP4 and KCNF1 were highly up-regulated in the presence of let-7b-5p, miR-125a-5p and miR-615-5p mimic.

Table 11: Overview of deregulated genes in A172 cells after miRNA inhibitor and mimic transfection

	Inhibitor			Mimic		
	Gene	log2 FC	FDR	Gene	log2 FC	FDR
hsa-let-7a-5p	***HS3ST2***	***23.67***	***1.02976E-05***	***FAM3B***	***50.44***	***3.67309E-61***
	PTPRZ1	22.70	6.30014E-06	***PCP4***	***42.22***	***1.01461E-27***
	PNLIPRP3	20.23	0.011105951	***KCNF1***	***40.54***	***3.30229E-31***
	FOXI1	19.16	2.68066E-06	MAGEA4	24.13	8.77352E-10
	PTCHD1	19.00	3.69675E-07	SLC24A3	22.29	3.42141E-10
	MMEL1	-16.71	0.002470225	***HS3ST2***	***-22.50***	***4.53227E-05***
	TMPRSS4	-17.05	1.963E-06	MIA	-23.20	5.27223E-05
	FAM3B	***-17.70***	***4.45545E-06***	LIN28A	-28.91	8.63046E-05
	PCP4	***-18.20***	***0.000177231***	NCCRP1	-34.52	5.31621E-17
	KCNF1	***-20.74***	***1.99546E-07***	XAGE2	-39.48	9.43261E-09
hsa-let-7b-5p	CYP4X1	21.14	1.24213E-13	FAM3B	43.31	1.37642E-40
	PTPRZ1	21.00	0.000188777	PCP4	41.92	1.79778E-27
	PNLIPRP3	19.91	0.026040934	KCNF1	39.81	1.49592E-29
	FOXI1	16.14	0.002535677	TRIL	20.94	1.65834E-10
	PTCHD1	16.07	0.000729993	SLC24A3	20.45	2.12513E-08
	ANKRD1	-7.82	0.013896829	GFRA1	-20.00	0.209321165
	CD74	-7.86	0.04824074	APCDD1L	-20.08	4.45778E-19
	LPAR1	-21.09	9.80792E-21	IL1B	-22.65	4.84278E-11
	C5orf66-AS1	-22.48	4.01166E-12	LIN28A	-29.67	4.36989E-05
	ADA2	-28.25	0.018743528	NDN	-47.48	3.77155E-59
hsa-miR-125a-5p	FOXI1	22.65	9.69022E-10	FAM3B	43.75	3.19347E-42
	PTCHD1	18.97	1.94217E-07	PCP4	40.90	2.55002E-25
	CYP4X1	18.55	7.46548E-10	KCNF1	40.52	1.63986E-31
	HS3ST2	18.00	0.016203286	MAGEA4	22.16	5.1308E-08
	APOD	8.51	0.025681717	TRIL	17.17	4.53257E-06
	PDE2A	-6.65	0.03338845	ABCC11	-19.18	3.11705E-05
	ANKRD1	-8.12	0.004693111	SCNN1G	-21.10	0.00064104
	NFE4	-17.36	3.30407E-06	SHC3	-22.00	5.01429E-10
	APCDD1L	-22.52	2.6487E-24	NCCRP1	-35.08	1.29984E-17
	SPX	-36.52	2.81321E-26	XAGE2	-40.14	5.42512E-09
hsa-miR-615-5p	HS3ST2	23.43	1.3771E-05	FAM3B	44.05	4.83098E-44
	PNLIPRP3	23.11	0.000799727	PCP4	42.03	6.4233E-28
	CYP4X1	20.43	7.75756E-13	KCNF1	40.00	3.27525E-30
	PTPRZ1	19.47	0.000445397	SLC24A3	20.75	1.30115E-08
	PTCHD1	16.47	8.84034E-05	TRIL	20.52	6.49767E-10
	FBLN2	-21.26	1.13711E-05	ABCC11	-19.52	2.79656E-05
	ADA2	-28.52	0.007707694	TCN1	-21.42	1.50849E-21
	NCCRP1	-34.11	1.93466E-16	SCNN1G	-21.51	0.000624453
	SPX	-35.07	2.68692E-24	VAV1	-43.16	2.9684E-60
	LINC02434	-42.34	1.68097E-28	MMEL1	-43.19	6.39914E-28

Table 12: Overview of deregulated genes in U138-MG cells after miRNA inhibitor and mimic transfection

	Mimic		
	Gene	log2 FC	FDR
hsa-let-7a-5p	PRRG4	4.09	0.006968769
	PTPMT1	2.05	0.002917628
	HMOX1	2.03	0.009821705
	MET	1.78	4.46838E-08
	DPYSL3	1.51	2.78876E-06
	CPA4	-1.85	3.18271E-06
	MIER2	-1.92	0.001180775
	DICER1	-2.15	8.80187E-13
	PLAGL2	-2.29	0.000979854
	POU2F2	-2.35	4.30648E-07
hsa-let-7b-5p	KRT34	2.73	0.008894405
	HMOX1	2.13	0.006116614
	PTPMT1	2.09	0.002719916
	MET	1.94	9.28833E-10
	DPYSL3	1.29	0.000270753
	C18orf21	-2.26	0.012885386
	FKRP	-2.50	0.03711204
	LOXL3	-2.75	0.047404822
	E2F5	-2.88	0.012343437
	ACVR2B	-3.63	0.030468319
hsa-miR-125a-5p	MET	1.69	7.49606E-07
	DPYSL3	1.11	0.007375316
	PDCD6	1.09	0.001860794
	ANKRD52	0.98	0.023475619
	MCFD2	0.83	5.91564E-05
	EIF4EBP2	0.28	4.03283E-10
	ATOH8	0.58	0.013411369
	MTFP1	0.64	0.028642189
	KRTAP2-3	-6.14	0.044397781
	ENTPD1-AS1	-6.53	0.004303527
hsa-miR-615-5p	MET	1.51	5.90483E-05
	PDIA4	1.25	0.042458523
	ELOA	1.19	0.039372919
	DPYSL3	1.15	0.006201529
	PDCD6	1.01	0.006201529
	SBNO1	0.69	0.006201529
	MAP3K20	0.63	0.032217076
	MCFD2	0.62	0.023989317
	TRMT112	0.59	0.004444782
	MICAL2	-0.74	0.001619159

log2 FC: log2 fold change
FDR: false discovery rate
bold: genes that showed exactly opposing expressions between mimic and inhibitor transfections

In the U138-MG inhibitor transfection experiment, no differentially expressed genes could be found. Additionally, the effect of the mimic transfection was much smaller than in A172 cells. Notably, the genes MET and DPYSL3 were up-regulated in the presence of each miRNA mimic.

C.3 Knockout of miRNAs using CRISPR/Cas9

After transient knockdown and overexpression was established, the miRNAs let-7a-5p, let-7b-5p and miR-125a-5p were knocked out using the CRISPR/Cas9 system. Therefore, plasmids had to be transfected expressing Cas9 and the miRNA specific guide RNAs. Afterwards, knockouts were identified using a T7 endonuclease assay. To characterize the knockouts, single clones had to be generated. The cell lines were selected as described in C.2. Additionally, for the purpose of knocking out all alleles, low karyotypic complexity was required. In a first step, guide RNAs were designed targeting the miRNA precursor sequence. Those guide RNAs were received as oligos with 5'- and 3'-overlaps homologous to the upstream and downstream regions of the donor plasmid. For each guide RNA, forward and reverse oligos were annealed and cloned into the MLM3636 plasmid using Gibson cloning. The amount of oligo and plasmid was either in equimolar amounts (1:1) or in excess of the oligo (1:5). After transformation in bacteria, six colonies were picked and the plasmid was purified from the bacteria. For validation of the plasmids, PCR was performed that utilized the introduced guide sequence for binding of the reverse primer. Thus, creation of a PCR product was only possible if the guide RNA was correctly inserted. The PCR products were visualized using agarose gel electrophoresis (Figure 30).

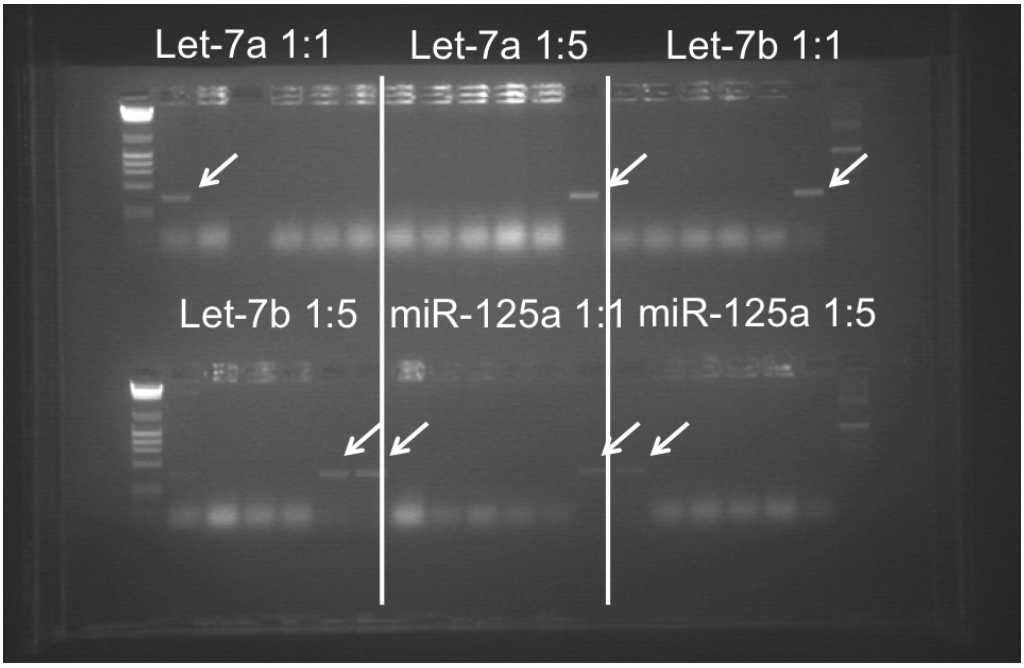

Figure 30: Agarose gel image visualizing the PCR products of the MLM3636 plasmid with guide RNAs

The plasmids were generated using Gibson cloning in equal amounts of insert and backbone (1:1) or in excess of the backbone (1:5). After transformation in competent bacteria, six colonies were picked and tested via PCR. The arrows are reflecting successful insert of the guide RNA.

Afterwards, the transfection efficiency of the cell lines U87-MG and U138-MG using plasmids was analyzed. Therefore, a GFP plasmid was transfected with different amounts of lipofectamine (Figure 31). The cells were harvested after 24 hours and GFP positive cells were analyzed using FACS. As shown in Figure 31, different lipofectamine amounts exhibited only minimal effects on the transfection efficiency. U138-MG cells showed a higher transfection rate (25%) than U87-MG cells (17%).

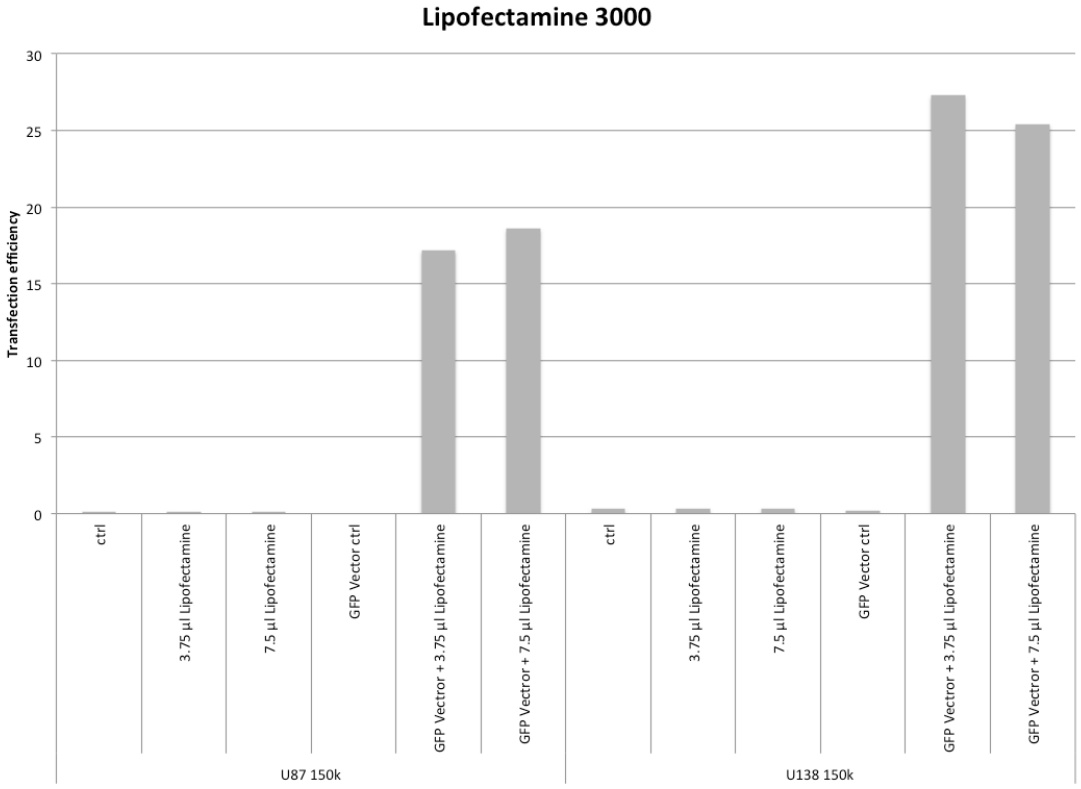

Figure 31: Results of the transfection of the plasmid pFG4-GFP

U87 and U138 were transfected with the plasmid pFG4-GFP using Lipofectamine 3000. The transfection efficiency is displayed on the Y-axis as a fraction of the amount of living cells. The different transfections are displayed on the X-axis. The cells were treated using different amounts (3.75 and 7.5 µl) of the transfection reagent ('Lipofectamine'). Additionally, as controls the cells were treated with the transfection reagent or the GFP plasmid alone.

To analyze whether knockouts after transfection of the CRISPR plasmids occurred, a T7 endonuclease assay was performed. Therefore, the plasmids carrying the guide RNAs were co-transfected with the Cas9 expressing plasmid VP12. Afterwards, the transfected cell pool was harvested and genomic DNA was purified from the cells. PCR analysis using primers that amplify the desired knockout site was performed. The PCR products were denatured and slowly re-annealed. In case of successful knockouts, heterodimers were formed that carry mismatches between the knockout and the wild type PCR fragments. T7 endonuclease cleaved the mismatched dimers and the resulting fragments were analyzed using agarose gel electrophoresis. As shown in Figure 32, only one visible band could be identified, meaning the CRISPR

knockout was not successful. After re-evaluation of the CRISPR system multiple challenges were identified. A major concern was that a knockout of the mature 5'-miRNA sequence also affects the expression of the complementary mature 3'-miRNA. A detailed discussion of miRNA knockout using CRISPR/Cas9 follows in the Discussion section.

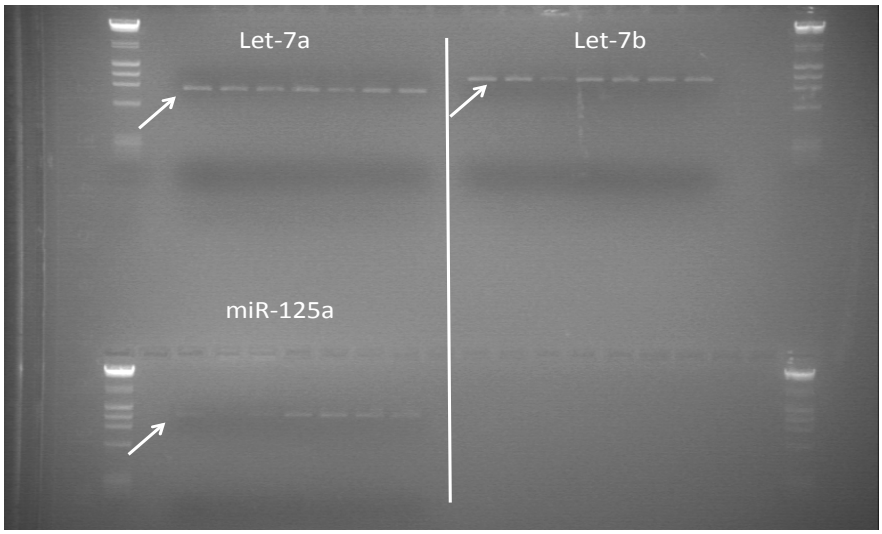

Figure 32: T7-endonuclease assay shows no effect of the transfected CRISPR-Cas9 system

U87-MG cells were transfected with the Cas9 plasmid (VP12) and a guide RNA expression plasmid targeting let-7a-5p, let-7b-5p or miR-125a-5p. The intended knockout positions were analyzed using the T7-endonuclease assay. Only one band is visible on the gel meaning the knockout did not succeed.

D Discussion

The aim of this thesis was to validate a prognostic 4-miRNA signature in GBM and to uncover the functional role of the miRNAs. The 4-miRNA signature was first discovered as a prognostic classifier by Niyazi et al., (2016) and allows the classification of GBM patients into high and low-risk groups that could be further sub-stratified into four risk groups by inclusion of the MGMT promoter methylation status. Generally, survival of GBM patients is poor due to the diffuse and infiltrative nature of the tumor and the appearance of treatment resistant clones after initial therapy (Delgado-López and Corrales-García, 2016). Thereby, there is medical need for an improvement and optimization of the standard-of-care therapy, which requires a stratification of GBM patients. Usually, miRNAs control a variety of genes and a functional characterization is needed for the determination of their biological role. Therefore, it is important to characterize the functional role of the four miRNAs of the signature in an in vitro cell culture model. For this example of a reverse translation from a patient derived observation into a cell culture a careful analysis of the model system is required in order to simulate actual tumor phenotypes. Seven established cell lines were thoroughly characterized. Special emphasis was put on the authentication of the cell lines and GBM-specific cytogenetic alterations. Furthermore, the cytogenetic complexity and the presence of cytogenetic subclones was analyzed. Also, the response to GBM standard-of-care treatment, which includes radiation response and TMZ sensitivity, was characterized. Additionally, molecular features of the cell lines were analyzed to assign the cell lines to GBM specific subtypes and to assort the GBM cell lines into patient-derived risk groups.

D.1 Cell line authentication and cytogenetic characterization

Cell lines models are a challenge in terms of cross-contamination, clonal evolution in vitro or confusion of samples during experiments. Therefore, scientific journals have started asking for obligatory cell line authentication data (Fusenig et al., 2017) and are establishing global quality measures. Thus, authentication and avoidance of confusion of cells lines is a prerequisite for their usage as model systems. Recently, it was shown that one of the most common GBM cell line U87-MG might not be authentic to the supposed tumor origin (Allen et al., 2016). The authors showed that the STR-profile of the commercially available U87-MG is not matching the STR-profile of the original cell line established in the 1960s. However, the authors also analyzed the mRNA expression profile and showed that the cell line is most likely of GBM origin. Despite this GBM-like phenotype, the usage of this cell line for preclinical GBM research remains questionable due to an overall uncertainty about its origin.

This example demonstrates the importance to verify of cell lines by STR-typing. Except for U87-MG, all characterized markers were matching to the respective database (www.dsmz.de) entries. In addition to STR-profiling, information was needed about the ploidy and genetic heterogeneity of all cell lines. Therefore, spectral karyotyping (SKY) was performed to investigate ploidy, subclones and clonal evolution. SKY analysis unveiled a high cytogentic variance and the presence of subclones in five out of seven cell lines. Four cell lines (LN18, U87-MG, U138-MG and U251-MG) showed a near-diploid or near-triploid karyotype, while three cell lines (A172, LN229 and T98G) exhibited a near-tetraploid or near-hexaploid karyotype. In GBM, karyotypic complexity is a common observation. Dahlback et al. (2009) showed that cell lines established from patient derived tumors usually exhibit abnormal karyotypes and a high cytogenetic complexity. Another study by Magnani et al., (1994) showed that GBM cells usually harbor near-diplod and near-triploid karyotypes. The most common cytogenetic marker of GBM is loss of heterozygosity on chromosome 10 (Thakkar et al., 2014). These alterations can either consist of the loss of a whole chromosome or parts of the short or long arm of the chromosome (Ohgaki and Kleihues, 2007).

In the cell line panel, only U87-MG showed loss of heterozygosity on chromosome 10 while the other cell lines either showed an amplification of chromosome 10 (A172, LN18, LN229 and T98G) or no alteration of chromosome 10 at all (U138-MG and U251-MG). Intra-tumor heterogeneity in the form of subclones is a common observation in GBM (Dahlback et al., 2009). Among the cell lines of the panel, subclones were identified in almost all cell lines, except for U138-MG and U251-MG. This observation might be in particular relevant for their usage in preclinical studies dealing with clonal approaches in order to determine radiotherapeutic and/or chemotherapeutic effects.

D.2 Radiation and TMZ sensitivity of the GBM cell lines

For therapeutic success, the response of tumor cells to specific treatments is crucial. Clonogenic survival assays are considered as “gold standard” to determine the treatment response to irradiation and chemotherapeutic treatment (Mirzayans et al., 2007) and were first described in 1956 (Puck and Marcus, 1956). The assay is primarily used for analyzing the colony formation ability of single cells and the survival fraction is a measure of radiation resistance. In our data no correlation between the ploidy and the resistance of the cells to radiation treatment could be observed in the cell line panel. The cell line with the lowest ploidy U87-MG (near-diploid) was the most resistant cell line, while LN229 cells harboring a near-tetraploid karyotype was the most sensitive cell line. Earlier studies have shown that the amount of lethal chromosomal damage increases with ploidy (Schwartz et al., 1999). However, the authors indicate that the survival of cells is also determined by other factors such as DNA damage response and subsequent DNA repair efficiency.

Differences in the survival between cells after a specific treatment are usually analyzed using a linear quadratic model that describes survival as a function of treatment response (Barendsen, 1982). The model divides the survival curves into a linear part (α value) and a quadratic part (β value). The α value is generally used to describe the survival at low doses and the β value represents the effectiveness of the

treatment at higher doses (Barendsen, 1982). The α/β ratio describes the dose at which the linear and quadratic part of the curve contribute equally to the survival of the cells (Franken et al., 2013). The linear term of this model is supposed to describe lethal DNA damage in the form of double strand breaks originating from single irradiation hits, while the quadratic term describes lethal double strand breaks from multiple independent irradiation hits (Unkel et al., 2016). For clinical applications, this approach supports the selection of optimal fractionation schedules in radiation oncology, by optimizing the dose per fraction, dose fractionation and dose rate in relation to tissue-specific α/β ratios (Franken et al., 2013). The α/β ratio is also utilized to describe radiosensitizing effects of treatments where an increase in the α/β ratio reflects higher sensitivity towards irradiation while a lower α/β ratio describes higher resistance to irradiation (Franken et al., 2013). There are scenarios for which the α/β ratio inadequately describes differences in radiation response. This could be the case if curves with a similar α/β ratio have a different steepness. Therefore, alternative approaches were suggested to determine the cellular response towards ionizing radiation. Principal component analysis may be used to describe radiosensitivity between cell lines of a specific data set. As described by Unkel et al., (2016), the first principal component of the analyzed surviving fractions represents a measure of the clonogenic survival over the whole dose range. Therefore, the authors suggest utilizing principal component scores for the description of the cellular response towards irradiation.

In this thesis, linear quadratic model dose-response curves were established for each GBM cell line to analyze differences in the sensitivity of the cell lines to radiation treatment. Statistical analysis of the survival curves using a F-test was carried out as described in Braselmann et al., (2015). In the dose range of 1-10 Gy T98G and U87-MG cells showed the most resistant radiation response while LN229 cells were most sensitive. In collaboration with Nikko Brix and Leon Schnöller from the Department of Radiotherapy and Radiation Oncology at the LMU University Hospital Munich, the survival data after irradiation treatment were independently repeated using the same GBM cell line panel for a dose range of 1-6 Gy. The resulting survival data was evaluated using a principal component analysis as described by Unkel et al., (2016).

To classify the cell lines into resistant and sensitive groups, reduction of data complexity of the survival data was done by cluster analysis and principal component analysis. For this purpose, survival data at each dose were linearly transformed into uncorrelated variables. Afterwards, the first principal component score was used for the determination of a radioresistance score. Classification of the cell lines into different radiation sensitivity groups was determined by combined consideration of the linear quadratic survival curves and the principal component scores. Due to the above-mentioned data transformation, the resulting principal component scores are only valid for a defined set of cell lines and scores might change if additional cell lines are added to the data set. Additionally, the correlation of an individual survival fraction to a specific dose is abolished. Nevertheless, this approach provided the best resolution of individual differences of radiation sensitivity between cell lines. Principal component analysis classified the cell lines T98G, U87-MG U251-MG and A172 as more resistant whereas U138-MG, LN18 and LN229 were more sensitive. Three groups became apparent that showed significant differences in the survival curves. The cell lines T98G and U87-MG showed the highest resistance to radiation while A172, LN18, U138-MG and U251-MG showed intermediate resistance and LN229 was most sensitive according to F-test analysis as described above. The cell lines with the most extreme response to irradiation (T98G, U87-MG and LN229) showed comparable results in both analyses while cell lines with a smaller difference in their response to irradiation exhibited varying results (A172, LN18, U138-MG and U251-MG). This indicates similar results with both approaches for cell lines with extreme radiation responses but distinct differences for cell lines with more similar responses to irradiation.

Accordingly, the colony formation assay was performed to determine the response of each cell line towards TMZ treatment. In comparison to a single dose irradiation treatment, the cells were incubated in the presence of TMZ for 24 hours. LN18, T98G, U138-MG and U251-MG cells were highly resistant to TMZ while A172, LN229 and U87-MG were sensitive to TMZ. In this context the expression and the promoter methylation status of the MGMT gene is important. MGMT removes the effect of

TMZ thus making cells resistant to the treatment (Brandes et al., 2008). Two of the most resistant cell lines (LN18 and U138-MG) showed no methylation of the MGMT promoter and no expression of the MGMT gene while the three most sensitive cell lines (A172, LN229 and U87-MG) were methylated. It is interesting to note that two of the more resistant cell lines (T98G and U251-MG) showed expression of the MGMT gene, however at low levels. Therefore, it can be concluded from these data that resistance to TMZ was better reflected by the MGMT gene expression than by MGMT promoter methylation status. The expression level of the MGMT gene is obviously of crucial impact. An explanation for this observation of a differentially expressed MGMT gene might be due to the differing ploidy of the cell lines, which generates a distinct heterogeneity for MGMT expression because a loss of the MGMT promoter methylation on some loci or genetic subclones modulate the expression of the gene.

D.3 Molecular subtypes of the GBM cell lines

A correlation analysis of gene expression patterns with clinical outcome is a common approach to define subgroups of patients and to achieve a stratification into different risk groups. As exemplified for breast cancer, the expression of the estrogen receptor and human epidermal growth factor receptor 2 could be associated with a more favorable clinical outcome because a targeted therapy for these two genes is here effective. On the other hand, tumors lacking the expression of both genes displayed a poorer prognosis (Desmedt et al., 2008). Another example in prostate cancer was the expression of MUC1 and AZGP1 which were highly predictive for tumor recurrence independent of tumor grade, stage, and preoperative prostate-specific antigen levels (Lapointe et al., 2004). Such observations render the question about different molecular subtypes in cancer. In GBM, four molecular subtypes were described using gene expression microarray data from the TCGA database: classical, mesenchymal, proneural and neural subtype (Verhaak et al., 2010). In a subsequent study the neural subtype was interpreted as not tumor specific because it could be associated with normal tissue (Wang et al.,

2017). The different subtypes were identified in a set of 200 GBM samples on three different microarray platforms. Clustering analysis of 1720 genes with the highest overall variance revealed four clusters with differential gene expression (Verhaak et al., 2010). Out of this larger gene set, 210 signature genes were identified for each subtype (Verhaak et al., 2010). Additionally, the expression of previously known GBM driver genes was analyzed in the subtypes (Verhaak et al., 2010). The subtypes differed in their clinical prognosis with the proneural subtype showing the worst survival (Verhaak et al., 2010). These subtypes may be utilized for targeting of subtype specific pathways and identification of personalized treatment options for GBM patients.

For this reason, the cell lines of this thesis were classified into classical, mesenchymal and proneural subtypes based on GBM-specific driver gene expressions. The most characteristic genes of the subgroups were EGFR amplification in the classical subgroup, NF1 deletion in the mesenchymal subgroup and PDGFRA amplification in the proneural subgroup. Cytogenetic features of the cell lines were combined with mRNA expression data to generate a scoring for each cell line. In this thesis the presence or absence of characteristic alterations were analyzed in order to calculate consensus scores for the classification of the cell lines into the molecular subtypes (Table 10, Results). According to this subtype classification, the majority of the cell lines were mesenchymal (A172, LN18, U87-MG, T98G and U138-MG) while the cell lines U251-MG and LN229 were classical. Molecular subtyping in established GBM cell lines is sparsely investigated. Xie et al., (2015) characterized a 48 GBM cell line panel that was created from GBM tumor samples. The authors showed that the majority of the cell lines resemble the mesenchymal subtype while classical and proneural subtypes occurred less frequently. Overall, the distribution of the subtypes described in this thesis reflected the observation by Verhaak et al., (2010), suggesting that cultured GBM cell lines belong primarily to the mesenchymal subtype.

D.4 Validation and assignment of cell lines to patient risk groups

To establish personalized treatment options for cancer patients, prognostic molecular markers are emerging that may be utilized in combination with new technologies like improved imaging and particle therapy (Baumann et al., 2016). For this purpose, stratification of patients into risk groups is a prerequisite for the identification of molecular markers. Such molecular classifiers consist of aberrant expression of genes and miRNAs that is correlated with clinical parameters in order to allow a prediction of the treatment response.

Recently, a prognostic 4-miRNA signature was described (Niyazi et al., 2016) that enabled a classification of standard-of-care treated GBM patients into low- and high-risk groups. The signature was identified in a retrospective set of 36 GBM patients. A forward selection approach was utilized for identification of significantly expressed miRNAs that had the largest impact on the survival of the patients. The resulting miRNA signature was the basis for a stratification into low- and high-risk groups. Patients belonging to the low-risk group showed an increased survival after standard-of-care treatment in comparison to patients belonging to the high-risk group. Additionally, the signature was independently validated in a subset of the TCGA GBM database using qRT-PCR. In a following study by Unger et al., (2020 *submitted*) the prognostic value of the miRNA signature was validated in a 106 GBM patient cohort from the LMU Munich (n=37), the University Hospital Düsseldorf (n=33) and The Cancer Genome Atlas (n=36). The tumors were all IDH1/2 wildtype with known MGMT promoter methylations. Overall survival (OS) of the patients was analyzed for combinations of risk score and MGMT promoter methylation. We could show that patients with a low-risk signature and methylated MGMT promoter had superior OS (median OS: 37,4 months) in comparison to patients with a low-risk signature and unmethylated promoter (median OS: 24,8 months). Accordingly, this could also be shown for patients with a high-risk signature and methylated MGMT promoter (median OS: 18,2 months) and patients with a high-risk signature and unmethylated MGMT promoter (median OS: 14,3 months). These data suggest that

the miRNA signature in combination with the MGMT promoter methylation status serves as a strong predictor for the clinical outcome of GBM.

To further characterize the risk groups and to create model systems for the different subgroups, the characterized cell line panel can be utilized. These model systems also offer the possibility to find correlations between phenotypical and molecular characteristics in specific risk groups. In the present thesis, the expression of the 4-miRNAs was analyzed in the GBM cell line panel using qRT-PCR to generate risk scores for each cell line. Based on the obtained risk score, the cell lines T98G, U87-MG and U251-MG were classified as low-risk while the cell lines A172, LN18, LN229 and U138-MG were assorted to the high-risk group. An association with radioresistance scores indicated a reverse correlation between risk score and radiation sensitivity (T98G and U87-MG were highly resistant to radiation). Additionally, no correlation could be observed between the risk factor and TMZ treatment. This is an unexpected finding and might be explained by several reasons. First of all, different treatments in the patient cohort and in the cell lines were applied. The standard-of-care treatment for patients consists of 30x 2 Gy radiotherapy in combination with adjuvant TMZ chemotherapy. The cell lines only received a single dose of radiation and TMZ treatment was performed independently. Furthermore, analysis of the let-7 miRNAs using qRT-PCR was challenging due to technical reasons related to the let7 family members. In humans, let-7c and let-7f only show one base pair difference in comparison to let-7a and let-7b (Lee et al., 2016). This suggests that primers amplifying let-7a and let-7b possibly amplify other let-7 miRNAs as well. Therefore, qRT-PCR measurement might not correctly reflect the expression of the miRNAs let-7a-5p and let-7b-5p in the cell lines. As a third factor for disagreement, subclones were identified in almost all cell lines that possibly influences expression of the miRNAs. Thus, microarray derived observations from patients might not be transferrable to expression data generated by qRT-PCR of in vitro cell culture systems. In GBM patients, a negative contribution to survival comes from the infiltrative nature of the tumor and the occurrence of treatment resistant cell clones shortly after initial therapy (Delgado-López and

Corrales-García, 2016). Those effects are absent in cell culture experiments. In conclusion, cell line models for specific patient risk groups could not be identified.

D.5 Selection of cell lines for functional studies of the 4-miRNAs

Although risk group specific cell line models are difficult to identify, the cell lines still allow a mechanistic investigation of the miRNAs of the signature. To characterize potential targets of the 4-miRNAs, suitable cell lines were selected for a modification of the 4-miRNA expressions. Based on the previous characterization, the cell lines A172 and U138-MG were chosen for further experiments. Both cell lines show less complex karyotypic changes and subclones were absent in the U138-MG cell line. Additional features of the cell lines were considered for the selection of the A172 and U138 cell line models: MGMT expression, methylation of the MGMT promoter, radiation response, GBM subtype and transfection efficiency. The remaining cell lines were not included because of either high ploidy and presence of subclones (LN229, T98G) or low transfection efficiency (LN18, U251-MG). The latter is of special interest because low amounts of transfected cells might not generate a significant phenotypic effect of the transfection.

D.6 Different approaches for modification of miRNA expression

A complete knockout of the mature miRNA by genome editing tools like the CRISPR/ Cas9 system is a major challenge for an experimental modification of miRNA expression. Stable knockouts usually require creation of plasmids and extensive target screening and validation experiments. Transient transfection using small RNAs provide a more rapid transfection process but the modification of the miRNA expression is only achieved for a limited time frame. Therefore, an identification of possible miRNA targets was carried out either by transient overexpression or by a stable knock down of the miRNAs in the selected cell lines. A transient modification was achieved by transfection of small RNA molecules that either have a similar

function as mature miRNAs (mimics) or inhibit endogenous miRNAs (inhibitors). A major challenge for the transfection of small RNAs lies in the possibility of introducing off-target effects by increasing or lowering the expression of other miRNAs with a high sequence similarity. Target recognition of the miRNA relies only on a small base pair sequence and high overexpression of the miRNAs and might lead to unwanted inhibition of mRNA targets (Lam et al., 2015). Additionally the external miRNAs compete with endogenously expressed miRNAs for regulatory proteins like RISC and other factors (Lam et al., 2015). Notably, studies have shown that oversaturation of miRNAs may even cause fatality in mice (Grimm et al., 2006). In conclusion, modification of miRNA expression by small RNAs provides a powerful tool for miRNA target identification but have possible off-target effects that might introduce bias into the data.

Another possibility to gain new insights into miRNA function is the investigation of stable, long-term knockouts of the miRNAs using the CRISPR/Cas9 system. The technology is suitable for a permanent inhibition of the miRNAs. Thereby, long-term effects of the miRNA knockout in in vitro and in vivo assays can be observed. Surprisingly, given the novelty and interest in CRISPR technology in the research community, only few research papers describe miRNA knockouts using CRISPR. Chang et al., (2016) reported a decrease of the expression of miRNAs by 96% using CRISPR. The authors constructed guide RNAs to target the stem-loop sequence of the miRNAs but it was not indicated whether the mature 5p-miRNA was knocked down or the 3p-miRNA or both. A loss in the complementarity of the miRNA stem-loop will inhibit its processing by RISC which will result in the loss of both active forms of the miRNA. Therefore, observed effects in the gene expression profile cannot be assigned to any of the mature miRNAs. Furthermore, Chang et al., (2016) observed that CRISPR-mediated knockout of miR-200c also inhibits the expression of another miRNA (miR-141). The authors found that repression of miR-200c triggers a negative feedback loop by upregulation of the gene ZEB1 that inhibits miR-141 expression. For the miRNAs from the prognostic signature, the miRNAs let-7a, let-7b and miR-125a are encoded on genomic clusters with other miRNAs. These clustered miRNAs are expressed on a single transcript (Lee et al., 2016) and modification of any of the miRNAs might also inhibit the expression of the others. Another technical

pitfall exists in working with cells that show high ploidy. For knockout of the miRNAs, the majority of the alleles had to be knocked out as the expression might be substituted by the miRNA expression of the other alleles. This poses even a further challenge for miRNAs like let-7a that are encoded on different positions of the genome with different pri-miRNA sequences but all expressing the same mature miRNA sequence (Lee et al., 2016). Repression of let-7a expression using CRISPR would not only require to knockout all alleles but all different pri-miRNA sequences as well. In conclusion, CRISPR offers a highly potential system for loss-of function studies targeting genes but for miRNA research certain limitations exist for knockout of specific mature miRNAs. Therefore, in this thesis miRNA modification was ultimately carried out by transient transfection of miRNA mimics and inhibitors.

D.7 Genes regulated by the 4-miRNAs

Global transcriptome measurements like microarrays or mRNA sequencing provide a powerful tool for analysis of miRNA mediated gene expression. As miRNAs repress the expression of their targets, the loss of miRNA function by miRNA inhibitors should lead to increased target expression (Hausser and Zavolan, 2014). Accordingly, gain of miRNA function by miRNA mimics should lead to a reduced target expression. Therefore, genes that show opposing effects after mimic and inhibitor transfection represent good candidates as potential miRNA targets.

In this thesis 3' RNA-sequencing was performed for the identification of miRNA targets. Differentially expressed genes were unveiled in A172 and U138-MG cells by characterization of the global gene expression using mRNA sequencing between miRNA inhibitor or mimic transfected cells and their respective 'scramble' controls. In the U138-MG cells no differentially expressed genes were found after transfection with the inhibitor, which is possibly due to technical reasons like a low transfection efficiency for one of the modulations. Nevertheless, in A172 cells strong effects of the miRNA inhibitor and mimic transfection could be observed. Thereby, four genes could be identified that show opposing expression in the presence of the let-7a-5p inhibitor and mimic: FAM3B, PCP4, KNCF1 and HS3ST2. The genes FAM3B, PCP4 and

KNCF1 showed strong up-regulation in the presence of the miRNA mimic while the genes were down-regulated in the presence of the inhibitor. These genes are possibly indirectly regulated by the let-7a-5p miRNA. In contrary, the HS3ST2 gene is down-regulated in the presence of the mimic and up-regulated in the presence of the inhibitor suggesting that this gene is supposed to be a direct target of the let-7a-5p miRNA.

The functional roles of the identified genes were previously described and all of the genes could be associated with cancer processes. Notably, FAM3B, KCNF1 and HS3ST2 have been reported to correlate with tumor invasiveness in colon, lung and breast cancer (Li et al., 2013; Baskaran, 2017; Kumar et al., 2014). FAM3B is a secreted cytokine that was first discovered in the Langerhans islets of the pancreas and is believed to play a role in the process of pancreatic β-cell apoptosis (Cao et al., 2003). More recently, FAM3B could be associated with increased invasion of colon cancer cells (Li et al., 2013). PCP4 plays an important role for synaptic function in the cerebellum (Wei et al., 2011). PCP4 knockout mice exhibit impaired locomotor learning (Wei et al., 2011). Additionally, it was reported that PCP4 regulates apoptosis in breast cancer (Hamada et al., 2014). The gene KCNF1 is sparsely investigated. Recently, KCNF1 was associated with cell proliferation and invasion in lung cancer, acting as tumor promoter (Baskaran, 2017). HS3ST2 is associated with Alzheimer disease and plays a role in the development of the disease-specific tau subtype (Sepulveda-Diaz et al., 2015). Additionally, the gene is involved in breast cancer cell invasion and chemosensitivity (Kumar et al., 2014). None of the genes have been associated with let-7a so far (http://mirtarbase.mbc.nctu.edu.tw), suggesting that these genes may be novel targets of the miRNA. Notably, by this approach only a fraction of the miRNA targets can be uncovered as two major pathways for miRNA induced target inhibition exist: miRNA-induced degradation of the mRNA and inhibition of translation (Huntzinger and Izaurralde, 2011). Target inhibition by repression of translation has only influence on protein expression but has no impact on the abundance of the mRNA (Olsen and Ambros, 1999). Therefore, those genes will not show differential gene expression using transcriptome analyses.

As shown in Table 11 no genes with opposing effects could be found for the miRNAs let-7b-5p, miR-125a-5p and miR-615-5p. Notably, the gene LIN28A was strongly

down regulated after let-7a-5p and let-7b-5p mimic transfections. LIN28 is a family of RNA binding proteins (Guo et al., 2006) that negatively regulate the expression of the let-7 precursor RNAs (Heo et al., 2008). Interestingly, the let-7 miRNAs are itself negatively regulating the expression of LIN28, thus creating a double negative feedback loop (Balzeau et al., 2017). Multiple studies have shown that expression of LIN28 and loss of let-7 expression leads to poor prognosis in cancer patients (Balzeau et al., 2017). It could also be shown that the expression of LIN28 was a predictor for clinical outcome in GBM patients (Qin et al., 2014). In conclusion, these observations might be an indication why the let-7 miRNAs of the signature were higher expressed in low-risk group comared to the high-risk group. Additionally, the genes FAM3B, PCP4 and KCNF1 were strongly up-regulated in the mimic transfection of the four miRNAs (Table 11). Likewise let-7a-5p these genes have not yet been associated with the expression of let-7b-5p, miR-125a-5p and miR-615-5p so far. On the one hand this could be an indicator that these genes are indirectly regulated by all miRNAs of the signature. On the other hand this observation could also be an artifact generated by the mimic transfection because it could not be validated by the transfection of the miRNA inhibitor. Therefore, further studies have to be performed to evaluate this observation.

In conclusion, in this thesis a seven GBM cell line panel was thoroughly characterized in order to find a suitable cell culture model for pre-clinical research. In, a first step a functional characterization of the prognostic 4-miRNA signature was achieved. The generated transcriptome data after miRNA mimic and inhibitor transfection offers an enormous resource for future studies that focus on identifying potential novel targets of the 4-miRNAs. Finally, further validation studies in the form of bioinformatic target validation and experimental approaches like qRT-PCR and western blots have to be performed to ultimately validate the discovered miRNA targets.

E Abstract

Glioblastoma (GBM) is the most frequent and the most aggressive type of primary brain tumors. It is characterized by a high degree of therapy resistance, invasiveness and a high recurrence rate after initial therapy. Currently, the standard therapy includes a combination of surgery and radiochemotherapy followed by maintenance chemotherapy with TMZ. Despite these aggressive treatment regimens, median overall survival times are limited to 15-18 months with large inter-individual differences. Current efforts in GBM research are aiming at advanced treatment modalities and implementing personalized treatment options requiring a stratification of patients into risk groups based on standard-of-care therapy. Recently, a 4-miRNA signature was discovered that allowed the stratification of GBM patients in high- and low-risk groups based on the expression of let-7a-5p, let-7b-5p, miR-125a-5p and miR-615-5p miRNAs. Yet, the cellular function of the miRNAs in GBM remains unclear. The aim of this thesis is to independently validate the 4-miRNA signature and to unveil the cellular role of the miRNAs by modification of the miRNA expression and characterization of the resulting transcriptomic changes in cell culture model systems.

Therefore, seven widely used GBM cell lines (A172, LN18, LN229, T98G, U87, U138, and U251) were analyzed for cytogenetic, phenotypic and transcriptomic properties. Cell line identity was confirmed by STR typing and the ploidy status and clonality were determined by SKY karyotyping. The ploidy among the cell lines panel ranged from near diploid to hexaploid. Additionally, subclones were present in the majority of the cell lines. Clonogenic survival assays were performed to characterize the cellular response towards irradiation or TMZ treatment, respectively. The response towards radiation treatment differed significantly among the cell line panel and the resistance towards TMZ was mainly reflected by expression of the MGMT gene. Global gene expression was determined by microarray analyses to classify the cell lines in GBM specific subtypes. The majority of the cell lines were assorted to the mesenchymal subtype. LN229 and U87-MG cell lines resembled the classical

subtype. Based on the cell line characterization, two cell lines (A172 and U138-MG) were chosen for modification of the miRNA expression based on their cytogenetic and phenotypic properties. Overexpression of the miRNA was achieved by miRNA mimic transfection and knockdown of the miRNAs was carried out by miRNA inhibitor transfection. The resulting changes in the transcriptome were analyzed by 3'-sequencing. Four genes were identified as potential targets of the let-7a-5p miRNA: FAM3B, PCP4, KCNF1 and HS3ST2. Most of the genes were previously associated with cancer by promoting invasiveness of the tumors. This is the first observation that these genes could be potential targets of the let-7a-5p miRNA. Additionally, the LIN28A was identified being negatively regulated by the let-7a-5p and let-7b-5p miRNAs. LIN28A was associated with poor prognosis in GBM patients whereas high expression of the let-7 miRNAs was observed in the low-risk patient group. Finally, the CRISPR/Cas9 system was evaluated for knockout of miRNAs but no effect was observed.

In conclusion, the present study provides a comprehensive characterization of a widely used panel of GBM cell culture models. Further, an independent validation and cellular characterization of a 4-miRNA signature in in vitro GBM cell culture models was achieved.

F Zusammenfassung

Glioblastome (GBM) sind die häufigste und aggressivste Form von primären Gehirntumoren. Das Merkmal von GBM ist eine hohe Resistenz gegenüber den Behandlungsmöglichkeiten sowie ein hohes Infiltrationspotential des Tumors. Für die Behandlung von GBM wird aktuell eine Kombination aus chirurgischer Entfernung des Tumors mit anschließender Strahlen- und Chemotherapie durchgeführt. Trotz der aggressiven Therapie liegt das klinische Überleben der Patienten im Median bei 15-18 Monaten. Das individuelle Überleben der Patienten unterliegt dabei starken Schwankungen. Neue Therapieformen zielen deshalb auf eine personalisierte Form der Behandlung ab. Eine Voraussetzung für eine personalisierte Therapie ist die Stratifizierung von die GBM Patienten. Mit Hilfe einer 4-miRNA (let-7a-5p, let-7b-5p, miR-125a-5p und miR-615-5p) Signatur kann ein Ansprechen auf die derzeitige Standardtherapie vorhergesagt werden. Damit könnte es möglich werden eine individuelle Anpassung der Behandlung durchzuführen und neuartige Therapieformen zu entwickeln.

Das Ziel dieser Arbeit ist es, die Signatur zu validieren und die zelluläre Funktion der miRNAs zu charakterisieren. Dafür soll die Expression der miRNAs modifiziert und die resultierenden Änderungen im Transkriptom analysiert werden. Um ein möglichst Tumor-nahes Modellsystem zu entwickeln, wurde eine Auswahl an sieben etablierten GBM Zelllinien (A172, LN18, LN229, T98G, U87-MG, U138-MG und U251-MG) charakterisiert und dabei zytogenetische, phänotypische und transkriptomische Eigenschaften der Zelllinien zu bestimmt. Die Identität der Zelllinien wurde mit STR-typing bestätigt und das Auftreten von Subklonen mit Hilfe von Karyogrammen bestimmt. Die Ploidie der Zelllinien schwankte von diploiden bis hin zu hexaploiden Genomen. Das Auftreten von Subklonen konnte in fünf der sieben Zelllinien nachgewiesen werden. Die Resistenz der Zelllinien gegenüber Bestrahlung und Behandlung mit Temozolomid (TMZ) wurde über das klonogene Überleben der Zellen bestimmt. Das Überleben der Zelllinien nach Bestrahlung schwankte stark in den analysierten Zelllinien und die Resistenz gegenüber TMZ war hauptsächlich von

der Expression des MGMT Gens abhängig. Das Transkriptom der Zelllinien wurde durch Microarrays charakterisiert und die Zelllinien konnten dadurch in GBM spezifische Subtypen eingeteilt werden. Mit Ausnahme von LN229 und U87-MG die dem klassischen Subtyp zugeordnet werden konnten, entstammten die Zelllinien dem mesenchymalen Subtyp. Aufgrund der phänotypischen und zytogenetischen Charakterisierung wurden die Zelllinien A172 und U138-MG für eine Modifikation der miRNAs ausgewählt. Eine Überexpression der miRNAs wurde durch Transfektion von miRNA ‚mimics' erzielt. Um die miRNAs in den Zellen zu reduzieren, wurden miRNA Inhibitoren eingesetzt. Die Veränderung der globalen Expression wurde mit 3'-mRNA Sequenzierung analysiert. Dabei konnten die Gene FAM3B, PCP4, KCNF1 und HS3ST2 als potentielle Ziele der miRNA let-7a-5p identifiziert werden. Diese Gene wurde bereits früher in Zusammenhang mit Krebs gebracht, indem sie das invasive Wachstum des Tumors verstärken. Diese Gene wurden bisher noch nicht als potentielle Zielgene der let-7a-5p miRNA beschrieben. Das Gen LIN28A, welches in früheren Arbeiten mit einer schlechten Überlebensprognose der GBM Patienten beschrieben wurde, zeigte eine starke Herrunterregulation nach Zugabe der let-7a-5p und let-7b-5p ‚mimics'. Dies könnte ein Hinweis darauf sein, warum die Patienten mit einem niedrigeren Risikofaktor eine höhere Expression dieser miRNAs zeigen. Zuletzt wurde das CRISPR/Cas9 System für die Herstellung von miRNA ‚knockouts' evaluiert, dabei konnte jedoch kein knockdown der miRNAs erzielt werden.

Zusammenfassend konnte in der vorliegenden Arbeit eine umfangreiche Charakterisierung von weit verbreiteten GBM Zellkultur Modellen erreicht werden. Zudem wurde eine prognostische 4-miRNA Signatur validiert und in GBM Zelllinien funktionell charakterisiert.

G Literature

Agrawal, N., Dasaradhi, P.V.N., Mohmmed, A., Malhotra, P., Bhatnagar, R.K., and Mukherjee, S.K. (2003). RNA Interference: Biology, Mechanism, and Applications. Microbiol. Mol. Biol. Rev. *67*, 657–685.

Allen, M., Bjerke, M., Edlund, H., Nelander, S., and Westermark, B. (2016). Origin of the U87MG glioma cell line: Good news and bad news. Science Translational Medicine *8*, 354re3-354re3.

Balzeau, J., Menezes, M.R., Cao, S., and Hagan, J.P. (2017). The LIN28/let-7 Pathway in Cancer. Front. Genet. *8*.

Barendsen, G.W. (1982). Dose fractionation, dose rate and iso-effect relationships for normal tissue responses. International Journal of Radiation Oncology*Biology*Physics *8*, 1981–1997.

Bartel, D.P. (2004). MicroRNAs: Genomics, Biogenesis, Mechanism, and Function. Cell *116*, 281–297.

Bartel, D.P. (2009). MicroRNAs: target recognition and regulatory functions. Cell *136*, 215–233.

Baskaran, A. (2017). KCNF1 is a Novel Regulator of NSCLC Cell Growth Independent of Its Potassium Ion Channel Function. Thesis.

Baumann, M., Krause, M., Overgaard, J., Debus, J., Bentzen, S.M., Daartz, J., Richter, C., Zips, D., and Bortfeld, T. (2016). Radiation oncology in the era of precision medicine. Nature Reviews Cancer *16*, 234–249.

Bigner, S.H., Mark, J., Burger, P.C., Mahaley, M.S., Bullard, D.E., Muhlbaier, L.H., and Bigner, D.D. (1988). Specific Chromosomal Abnormalities in Malignant Human Gliomas. Cancer Res *48*, 405–411.

Bohnsack, M.T., Czaplinski, K., and Gorlich, D. (2004). Exportin 5 is a RanGTP-dependent dsRNA-binding protein that mediates nuclear export of pre-miRNAs. RNA *10*, 185–191.

Bolotin, A., Quinquis, B., Sorokin, A., and Ehrlich, S.D. (2005). Clustered regularly interspaced short palindrome repeats (CRISPRs) have spacers of extrachromosomal origin. Microbiology *151*, 2551–2561.

Bousquet, M., Nguyen, D., Chen, C., Shields, L., and Lodish, H.F. (2012). MicroRNA-125b transforms myeloid cell lines by repressing multiple mRNA. Haematologica *97*, 1713–1721.

Brandes, A.A., Franceschi, E., Tosoni, A., Blatt, V., Pession, A., Tallini, G., Bertorelle, R., Bartolini, S., Calbucci, F., Andreoli, A., et al. (2008). MGMT promoter

methylation status can predict the incidence and outcome of pseudoprogression after concomitant radiochemotherapy in newly diagnosed glioblastoma patients. J. Clin. Oncol. *26*, 2192–2197.

Braselmann, H., Michna, A., Heß, J., and Unger, K. (2015). CFAssay: statistical analysis of the colony formation assay. Radiat Oncol *10*, 223.

Brennecke, J., Stark, A., Russell, R.B., and Cohen, S.M. (2005). Principles of microRNA-target recognition. PLoS Biol. *3*, e85.

Bumgarner, R. (2013). DNA microarrays: Types, Applications and their future. Curr Protoc Mol Biol *0 22*, Unit-22.1.

Cao, X., Gao, Z., Robert, C.E., Greene, S., Xu, G., Xu, W., Bell, E., Campbell, D., Zhu, Y., Young, R., et al. (2003). Pancreatic-Derived Factor (FAM3B), a Novel Islet Cytokine, Induces Apoptosis of Insulin-Secreting β-Cells. Diabetes *52*, 2296–2303.

Carthew, R.W., and Sontheimer, E.J. (2009). Origins and Mechanisms of miRNAs and siRNAs. Cell *136*, 642–655.

Chaichana, K.L., Jusue-Torres, I., Navarro-Ramirez, R., Raza, S.M., Pascual-Gallego, M., Ibrahim, A., Hernandez-Hermann, M., Gomez, L., Ye, X., Weingart, J.D., et al. (2014). Establishing percent resection and residual volume thresholds affecting survival and recurrence for patients with newly diagnosed intracranial glioblastoma. Neuro Oncol *16*, 113–122.

Chang, H., Yi, B., Ma, R., Zhang, X., Zhao, H., and Xi, Y. (2016). CRISPR/cas9, a novel genomic tool to knock down microRNA *in vitro* and *in vivo*. Scientific Reports *6*, 22312.

Choulika, A., Perrin, A., Dujon, B., and Nicolas, J.F. (1995). Induction of homologous recombination in mammalian chromosomes by using the I-SceI system of Saccharomyces cerevisiae. Molecular and Cellular Biology *15*, 1968–1973.

Cowden Dahl, K.D., Dahl, R., Kruichak, J.N., and Hudson, L.G. (2009). The epidermal growth factor receptor responsive miR-125a represses mesenchymal morphology in ovarian cancer cells. Neoplasia *11*, 1208–1215.

Dahlback, H.-S.S., Brandal, P., Meling, T.R., Gorunova, L., Scheie, D., and Heim, S. (2009). Genomic aberrations in 80 cases of primary glioblastoma multiforme: Pathogenetic heterogeneity and putative cytogenetic pathways. Genes Chromosom. Cancer *48*, 908–924.

von Deimling, A., Fimmers, R., Schmidt, M.C., Bender, B., Fassbender, F., Nagel, J., Jahnke, R., Kaskel, P., Duerr, E.M., Koopmann, J., et al. (2000). Comprehensive allelotype and genetic anaysis of 466 human nervous system tumors. J. Neuropathol. Exp. Neurol. *59*, 544–558.

Delgado-López, P.D., and Corrales-García, E.M. (2016). Survival in glioblastoma: a review on the impact of treatment modalities. Clin Transl Oncol *18*, 1062–1071.

Desmedt, C., Haibe-Kains, B., Wirapati, P., Buyse, M., Larsimont, D., Bontempi, G., Delorenzi, M., Piccart, M., and Sotiriou, C. (2008). Biological Processes Associated with Breast Cancer Clinical Outcome Depend on the Molecular Subtypes. Clin Cancer Res *14*, 5158–5165.

Dueck, A., Ziegler, C., Eichner, A., Berezikov, E., and Meister, G. (2012). microRNAs associated with the different human Argonaute proteins. Nucleic Acids Res. *40*, 9850–9862.

Edgar, R., Domrachev, M., and Lash, A.E. (2002). Gene Expression Omnibus: NCBI gene expression and hybridization array data repository. Nucleic Acids Res. *30*, 207–210.

Esau, C.C. (2008). Inhibition of microRNA with antisense oligonucleotides. Methods *44*, 55–60.

Fallon, K.B., Palmer, C.A., Roth, K.A., Nabors, L.B., Wang, W., Carpenter, M., Banerjee, R., Forsyth, P., Rich, K., and Perry, A. (2004). Prognostic Value of 1p, 19q, 9p, 10q, and EGFR-FISH Analyses in Recurrent Oligodendrogliomas. J Neuropathol Exp Neurol *63*, 314–322.

Franken, N.A.P., Oei, A.L., Kok, H.P., Rodermond, H.M., Sminia, P., Crezee, J., Stalpers, L.J.A., and Barendsen, G.W. (2013). Cell survival and radiosensitisation: modulation of the linear and quadratic parameters of the LQ model (Review). International Journal of Oncology *42*, 1501–1515.

Friedman, R.C., Farh, K.K.-H., Burge, C.B., and Bartel, D.P. (2009). Most mammalian mRNAs are conserved targets of microRNAs. Genome Res. *19*, 92–105.

Fusenig, N.E., Capes-Davis, A., Bianchini, F., Sundell, S., and Lichter, P. (2017). The need for a worldwide consensus for cell line authentication: Experience implementing a mandatory requirement at the International Journal of Cancer. PLOS Biology *15*, e2001438.

Garneau, J.E., Dupuis, M.-È., Villion, M., Romero, D.A., Barrangou, R., Boyaval, P., Fremaux, C., Horvath, P., Magadán, A.H., and Moineau, S. (2010). The CRISPR/Cas bacterial immune system cleaves bacteriophage and plasmid DNA. Nature *468*, 67–71.

Gasiunas, G., Barrangou, R., Horvath, P., and Siksnys, V. (2012). Cas9–crRNA ribonucleoprotein complex mediates specific DNA cleavage for adaptive immunity in bacteria. PNAS *109*, E2579–E2586.

Gibson, D.G., Young, L., Chuang, R.-Y., Venter, J.C., Hutchison, C.A., and Smith, H.O. (2009). Enzymatic assembly of DNA molecules up to several hundred kilobases. Nat. Methods *6*, 343–345.

Griffiths-Jones, S. (2004). The microRNA Registry. Nucleic Acids Res *32*, D109–D111.

Grimm, D., Streetz, K.L., Jopling, C.L., Storm, T.A., Pandey, K., Davis, C.R., Marion, P., Salazar, F., and Kay, M.A. (2006). Fatality in mice due to oversaturation of cellular microRNA/short hairpin RNA pathways. Nature *441*, 537–541.

Guo, Y., Chen, Y., Ito, H., Watanabe, A., Ge, X., Kodama, T., and Aburatani, H. (2006). Identification and characterization of lin-28 homolog B (LIN28B) in human hepatocellular carcinoma. Gene *384*, 51–61.

Ha, M., and Kim, V.N. (2014). Regulation of microRNA biogenesis. Nature Reviews Molecular Cell Biology *15*, 509–524.

Hamada, T., Souda, M., Yoshimura, T., Sasaguri, S., Hatanaka, K., Tasaki, T., Yoshioka, T., Ohi, Y., Yamada, S., Tsutsui, M., et al. (2014). Anti-apoptotic Effects of PCP4/PEP19 in Human Breast Cancer Cell Lines: A Novel Oncotarget. Oncotarget *5*, 6076–6086.

Hausser, J., and Zavolan, M. (2014). Identification and consequences of miRNA–target interactions — beyond repression of gene expression. Nature Reviews Genetics *15*, 599–612.

He, J., Mokhtari, K., Sanson, M., Marie, Y., Kujas, M., Huguet, S., Leuraud, P., Capelle, L., Delattre, J.Y., Poirier, J., et al. (2001). Glioblastomas with an oligodendroglial component: a pathological and molecular study. J. Neuropathol. Exp. Neurol. *60*, 863–871.

Hegi, M.E., Diserens, A.-C., Godard, S., Dietrich, P.-Y., Regli, L., Ostermann, S., Otten, P., Melle, G.V., Tribolet, N. de, and Stupp, R. (2004). Clinical Trial Substantiates the Predictive Value of O-6-Methylguanine-DNA Methyltransferase Promoter Methylation in Glioblastoma Patients Treated with Temozolomide. Clin Cancer Res *10*, 1871–1874.

Hegi, M.E., Liu, L., Herman, J.G., Stupp, R., Wick, W., Weller, M., Mehta, M.P., and Gilbert, M.R. (2008). Correlation of O6-methylguanine methyltransferase (MGMT) promoter methylation with clinical outcomes in glioblastoma and clinical strategies to modulate MGMT activity. J. Clin. Oncol. *26*, 4189–4199.

Heo, I., Joo, C., Cho, J., Ha, M., Han, J., and Kim, V.N. (2008). Lin28 mediates the terminal uridylation of let-7 precursor MicroRNA. Mol. Cell *32*, 276–284.

Huntzinger, E., and Izaurralde, E. (2011). Gene silencing by microRNAs: contributions of translational repression and mRNA decay. Nature Reviews Genetics *12*, 99–110.

Jansen, R., Embden, J.D.A. van, Gaastra, W., and Schouls, L.M. (2002). Identification of genes that are associated with DNA repeats in prokaryotes. Molecular Microbiology *43*, 1565–1575.

Jiang, L., Huang, Q., Zhang, S., Zhang, Q., Chang, J., Qiu, X., and Wang, E. (2010). Hsa-miR-125a-3p and hsa-miR-125a-5p are downregulated in non-small cell lung cancer and have inverse effects on invasion and migration of lung cancer cells. BMC Cancer *10*, 318.

Jinek, M., Chylinski, K., Fonfara, I., Hauer, M., Doudna, J.A., and Charpentier, E. (2012). A Programmable Dual-RNA–Guided DNA Endonuclease in Adaptive Bacterial Immunity. Science 1225829.

Kang, H., Kiess, A., and Chung, C.H. (2015). Emerging biomarkers in head and neck cancer in the era of genomics. Nature Reviews Clinical Oncology *12*, 11–26.

Kawamata, T., and Tomari, Y. (2010). Making RISC. Trends Biochem. Sci. *35*, 368–376.

Ketting, R.F., Fischer, S.E., Bernstein, E., Sijen, T., Hannon, G.J., and Plasterk, R.H. (2001). Dicer functions in RNA interference and in synthesis of small RNA involved in developmental timing in C. elegans. Genes Dev. *15*, 2654–2659.

Kleinstiver, B.P., Pattanayak, V., Prew, M.S., Tsai, S.Q., Nguyen, N.T., Zheng, Z., and Joung, J.K. (2016). High-fidelity CRISPR-Cas9 nucleases with no detectable genome-wide off-target effects. Nature *529*, 490–495.

Krol, J., Loedige, I., and Filipowicz, W. (2010). The widespread regulation of microRNA biogenesis, function and decay. Nature Reviews Genetics *11*, 597–610.

Kumar, A.V., Gassar, E.S., Spillmann, D., Stock, C., Sen, Y.-P., Zhang, T., Kuppevelt, T.H.V., Hülsewig, C., Koszlowski, E.O., Pavao, M.S.G., et al. (2014). HS3ST2 modulates breast cancer cell invasiveness via MAP kinase- and Tcf4 (Tcf7l2)-dependent regulation of protease and cadherin expression. International Journal of Cancer *135*, 2579–2592.

Lam, J.K.W., Chow, M.Y.T., Zhang, Y., and Leung, S.W.S. (2015). siRNA Versus miRNA as Therapeutics for Gene Silencing. Molecular Therapy - Nucleic Acids *4*, e252.

Lapointe, J., Li, C., Higgins, J.P., Rijn, M. van de, Bair, E., Montgomery, K., Ferrari, M., Egevad, L., Rayford, W., Bergerheim, U., et al. (2004). Gene expression profiling identifies clinically relevant subtypes of prostate cancer. PNAS *101*, 811–816.

Laws, E.R., Parney, I.F., Huang, W., Anderson, F., Morris, A.M., Asher, A., Lillehei, K.O., Bernstein, M., Brem, H., Sloan, A., et al. (2003). Survival following surgery and prognostic factors for recently diagnosed malignant glioma: data from the Glioma Outcomes Project. J. Neurosurg. *99*, 467–473.

Lee, H., Han, S., Kwon, C.S., and Lee, D. (2016). Biogenesis and regulation of the let-7 miRNAs and their functional implications. Protein Cell *7*, 100–113.

Lee, Y., Jeon, K., Lee, J.-T., Kim, S., and Kim, V.N. (2002). MicroRNA maturation: stepwise processing and subcellular localization. EMBO J. *21*, 4663–4670.

Lennox, K.A., and Behlke, M.A. (2011). Chemical modification and design of anti-miRNA oligonucleotides. Gene Therapy *18*, 1111–1120.

Li, Z., Mou, H., Wang, T., Xue, J., Deng, B., Qian, L., Zhou, Y., Gong, W., Wang, J.M., Wu, G., et al. (2013). A non-secretory form of FAM3B promotes invasion and metastasis of human colon cancer cells by upregulating Slug expression. Cancer Letters *328*, 278–284.

Lieber, M.R. (2010). The Mechanism of Double-Strand DNA Break Repair by the Nonhomologous DNA End-Joining Pathway. Annual Review of Biochemistry *79*, 181–211.

Lin, S., and Gregory, R.I. (2015). MicroRNA biogenesis pathways in cancer. Nature Reviews Cancer *15*, 321–333.

van Linde, M.E., Brahm, C.G., de Witt Hamer, P.C., Reijneveld, J.C., Bruynzeel, A.M.E., Vandertop, W.P., van de Ven, P.M., Wagemakers, M., van der Weide, H.L., Enting, R.H., et al. (2017). Treatment outcome of patients with recurrent glioblastoma multiforme: a retrospective multicenter analysis. J Neurooncol *135*, 183–192.

Liu, L., Nakatsuru, Y., and Gerson, S.L. (2002). Base excision repair as a therapeutic target in colon cancer. Clin. Cancer Res. *8*, 2985–2991.

Magnani, I., Guerneri, S., Pollo, B., Cirenei, N., Colombo, B.M., Broggi, G., Galli, C., Bugiani, O., DiDonato, S., Finocchiaro, G., et al. (1994). Increasing complexity of the karyotype in 50 human gliomas. Cancer Genetics and Cytogenetics *75*, 77–89.

Marraffini, L.A., and Sontheimer, E.J. (2008). CRISPR Interference Limits Horizontal Gene Transfer in Staphylococci by Targeting DNA. Science *322*, 1843–1845.

Mirzayans, R., Andrais, B., Scott, A., Tessier, A., and Murray, D. (2007). A sensitive assay for the evaluation of cytotoxicity and its pharmacologic modulation in human solid tumor-derived cell lines exposed to cancer-therapeutic agents. J Pharm Pharm Sci *10*, 298s–311s.

Monteys, A.M., Spengler, R.M., Wan, J., Tecedor, L., Lennox, K.A., Xing, Y., and Davidson, B.L. (2010). Structure and activity of putative intronic miRNA promoters. RNA *16*, 495–505.

Niyazi, M., Pitea, A., Mittelbronn, M., Steinbach, J., Sticht, C., Zehentmayr, F., Piehlmaier, D., Zitzelsberger, H., Ganswindt, U., Rödel, C., et al. (2016). A 4-miRNA signature predicts the therapeutic outcome of glioblastoma. Oncotarget *7*, 45764–45775.

Ohgaki, H., and Kleihues, P. (2007). Genetic Pathways to Primary and Secondary Glioblastoma. The American Journal of Pathology *170*, 1445–1453.

Olsen, P.H., and Ambros, V. (1999). The lin-4 regulatory RNA controls developmental timing in Caenorhabditis elegans by blocking LIN-14 protein synthesis after the initiation of translation. Dev. Biol. *216*, 671–680.

Ostrom, Q.T., Gittleman, H., Liao, P., Rouse, C., Chen, Y., Dowling, J., Wolinsky, Y., Kruchko, C., and Barnholtz-Sloan, J. (2014). CBTRUS Statistical Report: Primary Brain and Central Nervous System Tumors Diagnosed in the United States in 2007–2011. Neuro Oncol *16*, iv1–iv63.

Ozsolak, F., Poling, L.L., Wang, Z., Liu, H., Liu, X.S., Roeder, R.G., Zhang, X., Song, J.S., and Fisher, D.E. (2008). Chromatin structure analyses identify miRNA promoters. Genes Dev. *22*, 3172–3183.

Panaro, N.J., Yuen, P.K., Sakazume, T., Fortina, P., Kricka, L.J., and Wilding, P. (2000). Evaluation of DNA Fragment Sizing and Quantification by the Agilent 2100 Bioanalyzer. Clinical Chemistry *46*, 1851–1853.

Puck, T.T., and Marcus, P.I. (1956). Action of x-rays on mammalian cells. J. Exp. Med. *103*, 653–666.

Qin, R., Zhou, J., Chen, C., Xu, T., Yan, Y., Ma, Y., Zheng, Z., Shen, Y., Lu, Y., Fu, D., et al. (2014). LIN28 is involved in glioma carcinogenesis and predicts outcomes of glioblastoma multiforme patients. PLoS ONE *9*, e86446.

Quah, S., and Holland, P.W.H. (2015). The Hox cluster microRNA miR-615: a case study of intronic microRNA evolution. EvoDevo *6*.

Quah, S., Hui, J.H.L., and Holland, P.W.H. (2015). A Burst of miRNA Innovation in the Early Evolution of Butterflies and Moths. Mol. Biol. Evol. *32*, 1161–1174.

Quick, J., Gessler, F., Dützmann, S., Hattingen, E., Harter, P.N., Weise, L.M., Franz, K., Seifert, V., and Senft, C. (2014). Benefit of tumor resection for recurrent glioblastoma. J Neurooncol *117*, 365–372.

Reinhart, B.J., Slack, F.J., Basson, M., Pasquinelli, A.E., Bettinger, J.C., Rougvie, A.E., Horvitz, H.R., and Ruvkun, G. (2000). The 21-nucleotide let-7 RNA regulates developmental timing in Caenorhabditis elegans. Nature *403*, 901–906.

Robertson, B., Dalby, A.B., Karpilow, J., Khvorova, A., Leake, D., and Vermeulen, A. (2010). Specificity and functionality of microRNA inhibitors. Silence *1*, 10.

Ruby, J.G., Jan, C.H., and Bartel, D.P. (2007). Intronic microRNA precursors that bypass Drosha processing. Nature *448*, 83–86.

Sanai, N., Polley, M.-Y., McDermott, M.W., Parsa, A.T., and Berger, M.S. (2011). An extent of resection threshold for newly diagnosed glioblastomas. J. Neurosurg. *115*, 3–8.

Sanson, M., Marie, Y., Paris, S., Idbaih, A., Laffaire, J., Ducray, F., El Hallani, S., Boisselier, B., Mokhtari, K., Hoang-Xuan, K., et al. (2009). Isocitrate

Dehydrogenase 1 Codon 132 Mutation Is an Important Prognostic Biomarker in Gliomas. JCO *27*, 4150–4154.

Schroeder, A., Mueller, O., Stocker, S., Salowsky, R., Leiber, M., Gassmann, M., Lightfoot, S., Menzel, W., Granzow, M., and Ragg, T. (2006). The RIN: an RNA integrity number for assigning integrity values to RNA measurements. BMC Molecular Biology *7*, 3.

Schwartz, J.L., Murnane, J., and Weichselbaum, R.R. (1999). The contribution of DNA ploidy to radiation sensitivity in human tumour cell lines. British Journal of Cancer *79*, 744–747.

Sepulveda-Diaz, J.E., Alavi Naini, S.M., Huynh, M.B., Ouidja, M.O., Yanicostas, C., Chantepie, S., Villares, J., Lamari, F., Jospin, E., van Kuppevelt, T.H., et al. (2015). HS3ST2 expression is critical for the abnormal phosphorylation of tau in Alzheimer's disease-related tau pathology. Brain *138*, 1339–1354.

Stupp, R., Dietrich, P.-Y., Kraljevic, S.O., Pica, A., Maillard, I., Maeder, P., Meuli, R., Janzer, R., Pizzolato, G., Miralbell, R., et al. (2002). Promising Survival for Patients With Newly Diagnosed Glioblastoma Multiforme Treated With Concomitant Radiation Plus Temozolomide Followed by Adjuvant Temozolomide. JCO *20*, 1375–1382.

Stupp, R., Mason, W.P., van den Bent, M.J., Weller, M., Fisher, B., Taphoorn, M.J.B., Belanger, K., Brandes, A.A., Marosi, C., Bogdahn, U., et al. (2005). Radiotherapy plus concomitant and adjuvant temozolomide for glioblastoma. N. Engl. J. Med. *352*, 987–996.

Stupp, R., Hegi, M.E., Mason, W.P., van den Bent, M.J., Taphoorn, M.J., Janzer, R.C., Ludwin, S.K., Allgeier, A., Fisher, B., Belanger, K., et al. (2009). Effects of radiotherapy with concomitant and adjuvant temozolomide versus radiotherapy alone on survival in glioblastoma in a randomised phase III study: 5-year analysis of the EORTC-NCIC trial. The Lancet Oncology *10*, 459–466.

Thakkar, J.P., Dolecek, T.A., Horbinski, C., Ostrom, Q.T., Lightner, D.D., Barnholtz-Sloan, J.S., and Villano, J.L. (2014). Epidemiologic and Molecular Prognostic Review of Glioblastoma. Cancer Epidemiol Biomarkers Prev *23*, 1985–1996.

Torsvik, A., Stieber, D., Enger, P.Ø., Golebiewska, A., Molven, A., Svendsen, A., Westermark, B., Niclou, S.P., Olsen, T.K., Enger, M.C., et al. (2014). U-251 revisited: genetic drift and phenotypic consequences of long-term cultures of glioblastoma cells. Cancer Medicine *3*, 812–824.

Trivedi, R.N., Almeida, K.H., Fornsaglio, J.L., Schamus, S., and Sobol, R.W. (2005). The role of base excision repair in the sensitivity and resistance to temozolomide-mediated cell death. Cancer Res. *65*, 6394–6400.

Unkel, S., Belka, C., and Lauber, K. (2016). On the analysis of clonogenic survival data: Statistical alternatives to the linear-quadratic model. Radiation Oncology *11*, 11.

Verhaak, R.G.W., Hoadley, K.A., Purdom, E., Wang, V., Qi, Y., Wilkerson, M.D., Miller, C.R., Ding, L., Golub, T., Mesirov, J.P., et al. (2010). Integrated Genomic Analysis Identifies Clinically Relevant Subtypes of Glioblastoma Characterized by Abnormalities in PDGFRA, IDH1, EGFR, and NF1. Cancer Cell *17*, 98–110.

Wallner, K.E., Galicich, J.H., Krol, G., Arbit, E., and Malkin, M.G. (1989). Patterns of failure following treatment for glioblastoma multiforme and anaplastic astrocytoma. Int. J. Radiat. Oncol. Biol. Phys. *16*, 1405–1409.

Wang, H., La Russa, M., and Qi, L.S. (2016). CRISPR/Cas9 in Genome Editing and Beyond. Annual Review of Biochemistry *85*, 227–264.

Wang, Q., Hu, B., Hu, X., Kim, H., Squatrito, M., Scarpace, L., deCarvalho, A.C., Lyu, S., Li, P., Li, Y., et al. (2017). Tumor Evolution of Glioma-Intrinsic Gene Expression Subtypes Associates with Immunological Changes in the Microenvironment. Cancer Cell *32*, 42-56.e6.

Wang, Z., Gerstein, M., and Snyder, M. (2009). RNA-Seq: a revolutionary tool for transcriptomics. Nature Reviews Genetics *10*, 57–63.

Wei, P., Blundon, J.A., Rong, Y., Zakharenko, S.S., and Morgan, J.I. (2011). Impaired Locomotor Learning and Altered Cerebellar Synaptic Plasticity in pep-19/pcp4-Null Mice. Molecular and Cellular Biology *31*, 2838–2844.

Wen, P.Y., and Kesari, S. (2008). Malignant Gliomas in Adults. New England Journal of Medicine *359*, 492–507.

Wyvekens, N., Tsai, S., and Joung, J.K. (2015). GENOME EDITING IN HUMAN CELLS USING CRISPR/CAS NUCLEASES. Curr Protoc Mol Biol *112*, 31.3.1-31.318.

Xie, Y., Bergström, T., Jiang, Y., Johansson, P., Marinescu, V.D., Lindberg, N., Segerman, A., Wicher, G., Niklasson, M., Baskaran, S., et al. (2015). The Human Glioblastoma Cell Culture Resource: Validated Cell Models Representing All Molecular Subtypes. EBioMedicine *2*, 1351–1363.

(2011). NCI Dictionary of Cancer Terms.

Zuallererst möchte ich mich bei meinem Doktorvater Horst Zitzelsberger bedanken, für die ausgezeichnete Betreuung, für seine fachliche Expertise und nicht zuletzt für die vielen Arbeitsstunden und die unzähligen Verbesserungsvorschläge für diese Arbeit.

Gleicher Dank gebührt meinem Betreuer Kristian Unger für die unzähligen Arbeitsstunden die er in die Betreuung dieser Doktorarbeit investiert hat, für die Möglichkeit meine Forschung auf Fachkongressen und in wissenschaftlichen Veröffentlichungen präsentieren zu können, und dem ich nicht zuletzt einen tiefen Einblick in die bioinformatische Auswertung von Experimenten verdanke.

Weiterer Dank gebührt Julia Hess die mit ihrer Expertise viele Experimente in die richtige Richtung gelenkt hat und die immer Zeit für Ergebnisse und Auswertungen hatte.

Großer Dank gebührt Kirsten Lauber für die Möglichkeit einen Teil meiner Versuche in ihrem Labor durchzuführen sowie für die wertvollen Vorschläge bei der Planung und Auswertung von Experimenten und der Ausführung von Manuskripten.

Weiterhin möchte ich mich für die Unterstützung bei der Planung und Durchführung der Experimente bedanken bei: Isabella Zagorski, Laura Dajka, Steffen Heuer, Randy Caldwell, Theresa Heider, Peter Weber, Martin Selmansberger, Daniel Samaga, Herbert Braselmann, Aaron Selmeier, Claire Innerlohinger, Roland Wunderlich, Sebastian Kuger, und Michael Orth.

Außerdem möchte ich mich bei meinen PhD Kollegen Isolde Summerer, Valentina Leone, Agata Michna, Ludmila Schneider und Christina Wilke für die kollegiale Unterstützung bedanken.

Besonderer Dank gilt auch Doris Mittermeier, Marion Böttner und Giesela Dettweiler für die herzliche Zusammenarbeit sowie Christine Hunger für die Korrektur der Arbeit.

Abschließend gilt großer Dank meiner Familie, meinen Freunden und besonders meinen Eltern für die große Unterstützung während meiner Doktorarbeit.